NASA Contractor Report 4067

Passive Stabilization for Large Space Systems

J. R. Sesak, M. J. Gronet,
and G. M. Marinos

CONTRACT NAS1-17660
APRIL 1987

NASA

NASA Contractor Report 4067

Passive Stabilization for Large Space Systems

J. R. Sesak, M. J. Gronet,
and G. M. Marinos
Lockheed Missiles & Space Company, Inc.
Sunnyvale, California

Prepared for
Langley Research Center
under Contract NAS1-17660

National Aeronautics
and Space Administration

**Scientific and Technical
Information Branch**

1987

TABLE OF CONTENTS

Section 1

SUMMARY

The optimal tuning of multiple tuned-mass dampers for the transient vibration damping of large space structures is investigated. A multi-disciplinary approach is used. Structural dynamic techniques are applied to gain physical insight into absorber/structure interaction and to optimize specific cases. Modern control theory and parameter optimization techniques are applied to the general optimization problem. A design procedure for multi-absorber multi-DOF vibration damping problems is presented.

Classical dynamic models are extended to investigate the effects of absorber placement, existing structural damping, and absorber cross-coupling on the optimal design synthesis. An uncoupled dynamic optimization technique is developed which allocates the absorber mass budget over multiple absorbers in order to optimally damp the transient response.

The control design process for the general optimization problem is formulated as a linear output feedback control problem via the development of a feedback control canonical form. The design variables are expressed as control gains, and the analytical techniques of feedback control theory, both classical and modern, are applied to absorber design. A nonlinear parameter optimization method is developed and applied to an output feedback formulation of the vibration damping problem.

The techniques are applied to sample micro-g and pointing problems on the NASA dual keel space station. Damping levels in the range of 10 - 20% are achieved with two tuned-mass dampers. The potential damping performance gains obtained through the use of tuned-mass dampers on lightly-damped structures merits the further study of the hardware issues associated with these devices.

SECTION 2
INTRODUCTION

Many proposed future large space structure designs, including the NASA Space Station, may need to incorporate active and/or passive damping mechanisms in order to meet pointing, slewing, or microgravity acceleration requirements. Methods for implementing active and passive damping have been the subject of studies by many investigators [1-9]. Many of these studies have indicated the merits of passive damping, either in itself or in concert with active damping.

Incorporation of passive damping for vibration suppression in the design of large space-structures offers many benefits. Passive dampers require no power source, are inherently stable, and are potentially simple and reliable. Properly designed passive damping treatments can greatly reduce the settling time in transient response problems and reduce the peaks of steady state response problems.

The existence of small amounts of passive damping in an active control system can reduce active control effort such as actuator force, stroke, bandwidth, and system penalties such as the number of actuators, added mass, cost, and on-board power and microprocessing needs [5,6]. Increased performance over a larger bandwidth can be attained. In addition to improving system performance, the use of passive damping technology can be expected to ease the task of control system design. Proper implementation of passive damping in an active control system can result in a more robust, reduced-order control design with greater stability and reduced response to noise. Finally, passive damping devices provide an increased safety margin for active control systems.

Passive damping can be added to a structure through a variety of mechanisms including constrained layer treatments, impact/friction joints, discrete dampers, and tuned-mass dampers.

Each damping treatment performs best for certain classes of damping problems. The tuned-mass damper is especially well-suited for damping large structures which are characterized by low, highly distributed strain energy, e.g., the NASA Space Station. The NASA IOC Space Station response to orbiter docking exhibits small loads and only a few inches of deflection over the distance of a baseball field. The corresponding low strains may not be enough to efficiently "work" a distributed damping material, or a discrete damping material or device placed in the load path. The advantage of the tuned-mass damper is that it is "tuned" to draw energy from the main structure to a mechanism which works the damping material or damper (Figure 2-1). Some disadvantages of the tuned mass damper (also termed vibration absorber) are that it adds nonstructural mass and typically provides only modest levels of damping.

Tuned-mass dampers are used throughout industry in applications on ships, helicopters, cars, tall buildings, and rotating machinery. The classical two degree-of-freedom steady-state vibration absorber solution of Timoshenko [10] and Den Hartog [11] has been widely used to determine the optimal physical parameters (k,c,m) for absorber designs. Previous investigators have addressed the optimal placement and tuning of absorbers on beams and plates [7,8,9] and the use of absorbers for combined passive and active damping [3,4]. Some included hardware experiments with vibration absorbers [3,4]. Much of the emphasis has been placed on developing absorber designs for use in damping responses to steady-state excitation.

The present work concentrates on the application and extension of absorber design and optimization techniques to a multi-mode, multi-dof, large space structure, namely the NASA Space Station. The principal issue addressed is the optimal tuning of several absorbers for the transient response of a multi-dof system, including the effects of modal coupling, existing structural damping, absorber placement, and absorber mass. The Space Station

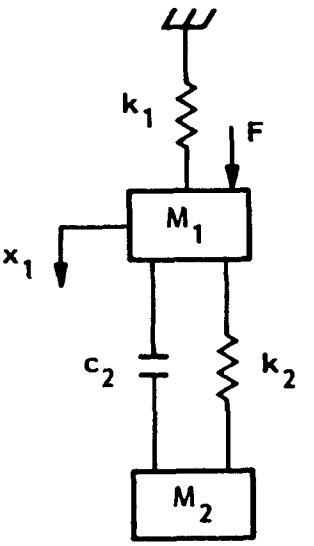

ABSORBER 2-DOF REPRESENTATION

M_1 = PLANT MODAL MASS

k_1 = PLANT MODAL STIFFNESS

Figure 2-1. Tuned-Mass Damper One-Mode, 2-DOF Representation

is subject to many transient disturbances such as docking, orbit reboost, crew motion, and payload slewing. A notable steady-state excitation source is the Science Research Centrifuge, which rotates at a frequency in the bandwidth of the primary structural modes. Because of the relatively advanced state of development of steady-state absorber design techniques, only the transient cases are considered in this study.

The remainder of the report is divided into four major sections. Section 3 reviews the classical two-dof problem and examines the two-dof transient response problem. The remainder of the section examines dynamic techniques for optimizing multi-mode problems with several absorbers. In Section 4, modern control techniques are employed to optimize the physical parameters of the absorbers. Section 5 applies both the dynamic and modern control techniques to Space Station pointing and microgravity responses and compares the results. A design procedure is presented in Section 6, based on the analysis and results of Sections 3 - 5. Finally, section 7 offers recommendations for further study.

SECTION 3
ABSORBER DYNAMIC ANALYSIS

3.1 Vibration Absorber Concept

Figure 2-1 illustrates the classical absorber problem where the absorber mass, spring, and damper (m2, k2, and c2) are attached to a single mode, represented by the modal mass M1, and modal stiffness K1. In this representation, the stiffness of the absorber mechanism and damping element are combined in k2, the structural and viscous damping of the absorber are combined in c2, and the frequency response of the damping element is assumed to be uniform. In this study, the damping element is treated generically, and could represent a variety of electromagnetic, fluidic, viscoelastic, or other types of passive devices. The structural damping of the single mode plant will initially be assumed to be zero.

The principle behind the vibration absorber is the tuning of the mass, M2, and the stiffness, k2, to a frequency that couples as much as possible with the mode to be damped. This maximizes the relative displacement across the damper c2, which is effectively amplified such that it is greater than the displacement of the plant mass M1. The concept can be likened to tuning a sprung payload to the peak of the transient relative shock spectrum (Figure 3-1) in order to maximize the energy transfer to the sprung mass, as opposed to tuning it to a valley, where energy transmission is minimized. The plant deflections, velocities, and accelerations at M1 can be amplified by factors of 8 to 10 at M2. For this reason, vibration absorbers are well-suited for problems with highly distributed strain energy, as energy is drawn to the site of the damping element or material. Once the absorber is tuned to interact with the desired mode, the damper strength c2 is tuned to maximize the energy dissipation.

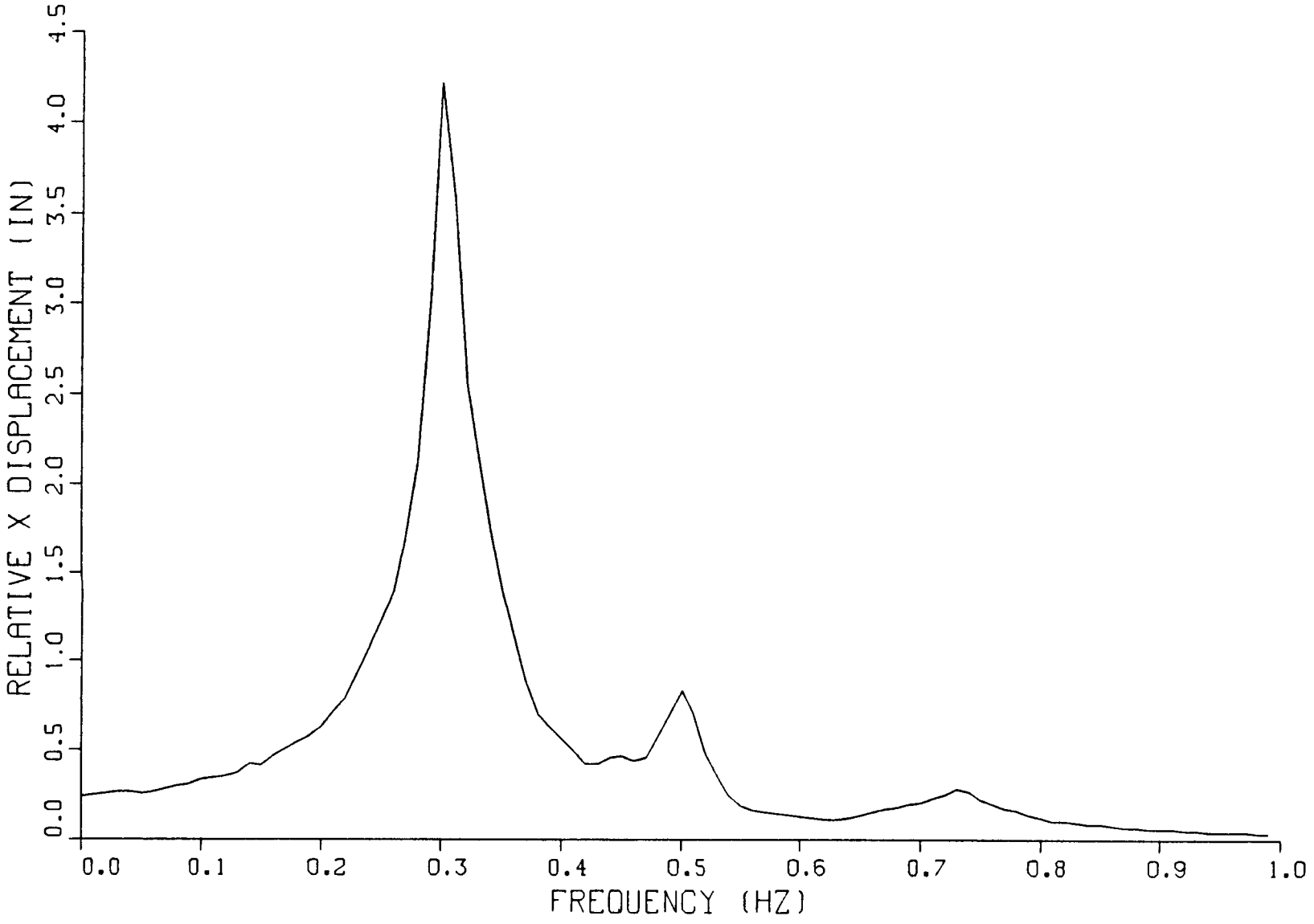

Figure 3-1. Space Station Payload Boom X-Direction Relative Shock Spectrum for Shuttle Dock Maneuver.

3.2 Classical Vibration Absorber Steady-State Solution

This discussion reviews the classical absorber solution presented in references [10] and [11], which is the foundation for the dynamic techniques presented in this section. The equations of motion for the system shown in Figure 1, assuming zero structural damping (c1=0) are:

$$m_1\ddot{x}_1 + c_2\dot{x}_1 + (k_1 + k_2)x_1 - c_2\dot{x}_2 - k_2x_2 = F \qquad (3\text{-}1a)$$

$$m_2\ddot{x}_2 + c_2\dot{x}_2 + k_2x_2 - c_2\dot{x}_1 - k_2x_1 = 0 \qquad (3\text{-}1b)$$

The classical steady state vibration absorber solution minimizes the peak response (x1) of the system to sinusoidal steady-state excitation. The approach describes the transfer function between the response of the structure (x1) and excitation (F) in terms of the physical parameters of the absorber. The damping performance is optimized by equating the two peaks of the transfer function. Adopting similar notation to that of reference [10], the non-dimensional transfer functions (plotted in Figure 3-2) can be written as:

$$\left|\frac{x_1}{x_o}\right|^2 = \frac{[4\mu^2\gamma^2 + (\gamma^2 - \delta^2)^2]}{4\mu^2\gamma^2[\gamma^2(1+\beta) - 1]^2\} + \{[\beta\delta^2\gamma^2 - (\gamma^2 - 1)(\gamma^2 - \delta^2)]^2} \qquad (3\text{-}2a)$$

where:

$$\beta = M_2/M_1 \qquad x_o = F/k_1 \qquad \omega_o = \sqrt{k_1/M_1} \qquad (3\text{-}2b)$$

$$\delta = \omega_A/\omega_o \qquad \text{thru}$$

$$\mu = c/2\,M_1\omega_o \qquad \gamma = \omega/\omega_o \qquad \omega_A = \sqrt{k_2/M_2} \qquad (3\text{-}2h)$$

The optimal solution is obtained through the selection of the non-dimensional absorber parameters: the mass ratio β, the damping

$\beta = 0.02 \qquad \delta = 0.98$

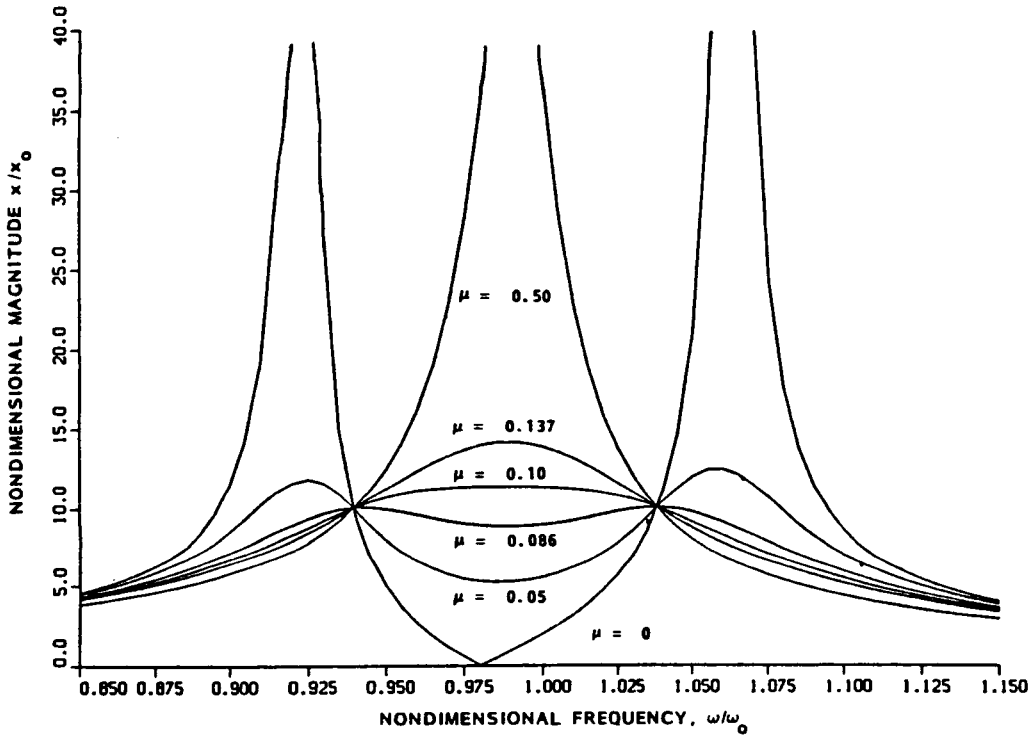

- AS $\mu \to \infty$,
  MASSES M_1, M_2 ARE LOCKED
  GET ONE UNDAMPED POLE

- AS $\mu \to 0$,
  GET TWO UNDAMPED POLES WITH
  A ZERO AT ω_o; "NOTCH FILTER"

$$\left|\frac{x_1}{x_o}\right|^2 = \frac{[4\mu^2\gamma^2 + (\gamma^2 - \delta^2)^2]}{4\mu^2\gamma^2[\gamma^2(1+\beta) - 1]^2\} + \{[\beta\delta^2\gamma^2 - (\gamma^2 - 1)(\gamma^2 - \delta^2)]^2}$$

Figure 3-2. Nondimensional Transfer Functions at M1 for Various Damper Strength Values.

ratio μ, and the frequency ratio, δ . Examination of the equation for the maximum plant response,

$$\left(x_1/x_o\right)_{MAX} = \sqrt{(2 + \beta)/\beta} \qquad (3\text{-}3)$$

yields that the performance of the absorber increases with the weight of the sprung mass m2. Thus, the absorber mass optimization for a single mode problem drives the sprung mass to its maximum allowable value [1]. Therefore, a suitable mass value can be chosen a priori based on trade studies, or set at the maximum value allowed by the mass budget.

The optimal frequency tuning for a selected mass ratio is:

$$\delta = 1/1 + \beta \qquad (3\text{-}4)$$

and the optimal non-dimensional damper setting is:

$$\mu^2_{OPT} = \frac{N - Q'X_1/X_o)^2}{P(X_1/X_o)^2 - M} \qquad (3\text{-}5a)$$

where

$$M = \frac{4\left[1 + \sqrt{\frac{\beta}{2+\beta}}\right]}{1+\beta} \qquad N = \left[\frac{\beta + (1+\beta)\sqrt{\frac{\beta}{2+\beta}}}{(1+\beta)^2}\right]^2$$

$$P = \frac{4\beta\left[1 + \sqrt{\frac{\beta}{2+\beta}}\right]}{(1+\beta)^2(2+\beta)} \qquad Q = \left[\frac{\beta\left[(2+\beta)\sqrt{\frac{\beta}{2+\beta}} + 1 + \beta\right]}{(1+\beta)^2(2+\beta)}\right]^2 \qquad (3\text{-}5b) \text{ thru } (3\text{-}5e)$$

A series of curves representing the transfer functions for a sprung mass ratio of β=.02 is shown in Figure 3-2. Note that for μ=0, the optimal frequency ratio (δ_{opt}) results in two modes (poles) equally spaced about a zero near the initial plant modal frequency. This case corresponds to the classical "Undamped Vibration Absorber"

[12] wherein practically all of the energy is transferred to the absorber when the system is forced at the initial plant frequency. At this point, the sprung mass has been tuned to maximize absorber/structure interaction, and maximize the relative motion across the damper. In fact, previous investigators [4] have shown that the optimal value of δ maximizes the relative motion across the damper on average in both modes, as the relative motion in both modes is approximately equal.

As the damping ratio μ is increased from zero, the overall magnitude of the transfer function decreases until the optimum ratio of μ=.086 (for β=.02) is reached, and the peak response of both modes is minimized. As the value of μ is increased further, the absorber performance is reduced. The reason for this is that the damper force is too high and restrains the relative motion between the two masses. As the damper ratio is increased still further, the two masses become "locked" together and the resulting transfer function appears to contain only a single mode.

In the case where it is desired to tune the absorbers to minimize acceleration, the transfer function can be normalized such that:

$$\left| \frac{\ddot{x}_1}{x_0 \omega_0^2} \right|^2 = \frac{[4\mu^2 \gamma^2 + (\gamma^2 - \delta^2)^2]}{4\mu^2 \gamma^2 [\gamma^2(1+\beta) - 1]^2\} + \{[\beta\delta^2 \gamma^2 - (\gamma^2 - 1)(\gamma^2 - \delta^2)]^2} \quad (3\text{-}6)$$

and the same results are obtained.

The concept of an optimum damper value or loss factor bears resemblance to other techniques such as the modal strain energy method which are used to optimize the damping coefficient in other types of damping devices.

3.3 Optimization of Two-DOF Model for Transient Response

This section reviews the classical techniques for optimal tuning of the 2-DOF absorber, and details the development of techniques for optimization of multiple passive vibration absorbers

for multi-DOF large space structures. The dynamics of the absorber-structure interaction are examined, optimality criteria for the impulse response problem are evaluated and the effects of existing structural damping and absorber placement are investigated. A technique for the optimization of the mass distribution among the absorbers is developed under the assumption that coupling effects between vibration modes are insignificant when the vibration absorbers are attached. Finally, the quantification of coupling effects through the absorbers is discussed.

3.3.1 Characterization of Space Station Disturbances

Because of the many different Space Station disturbances and the continuing evolution of the IOC design in the Phase B program (there were three significant configuration changes during the course of this study), it was decided to model the transient disturbances using initial conditions corresponding to a unit impulse (unit initial velocity). This simplification is justified by the relatively short duration of the transient pulses in comparison with the long periods of the dominant structural modes of the Space Station (2.0 - 4.0 sec). This is evident in Figure 3-3 which shows an FFT of the NASA 500 lb., 1 sec orbiter docking input. An FFT of the crew motion input is shown in Figure 3-4. Note that there are several "notches" in the FFT, where specific Space Station modes may not be excited. Small changes in the design evolution of the Space Station could easily change the mix of modes which are excited. Because the impulse input excites all modes, some of the dependence of the study conclusions on a specific Space Station evolutionary model is removed, and the results can be applied to a more general class of broad-band excitation problems. Henceforth, the remainder of the study optimizes the absorber parameters for the case of unit impulse input and all the results are normalized to that condition. Because the system linear, the results can be multiplied by an impulse strength of 500 or 25, for the orbiter docking and crew motion impulses, respectively.

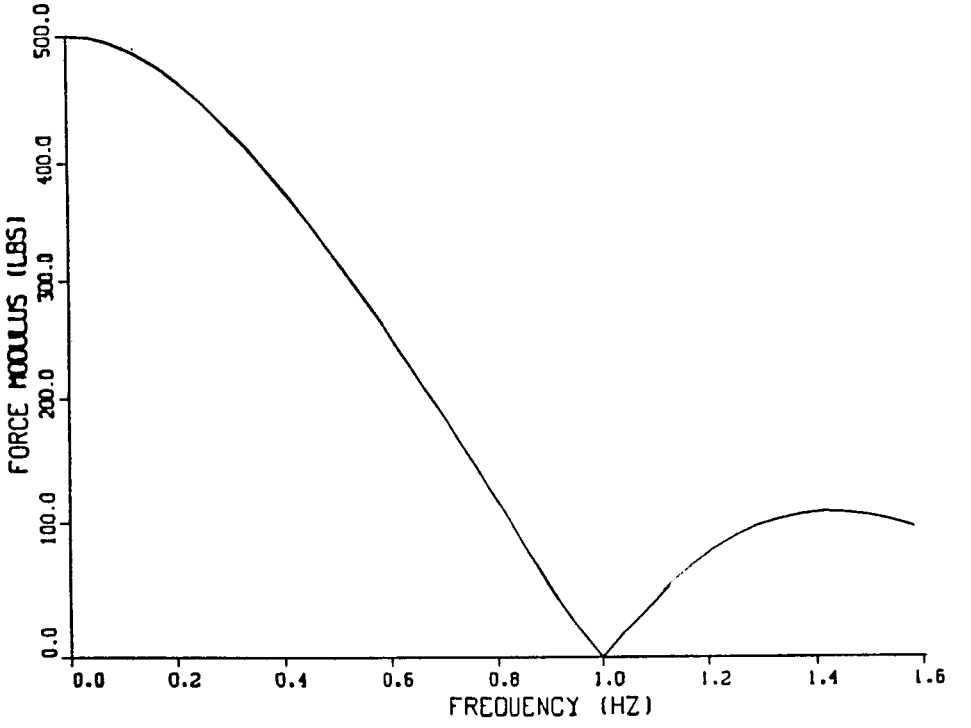

Figure 3-3. FFT of 500 lb, 1 Sec. Shuttle Docking Force Input.

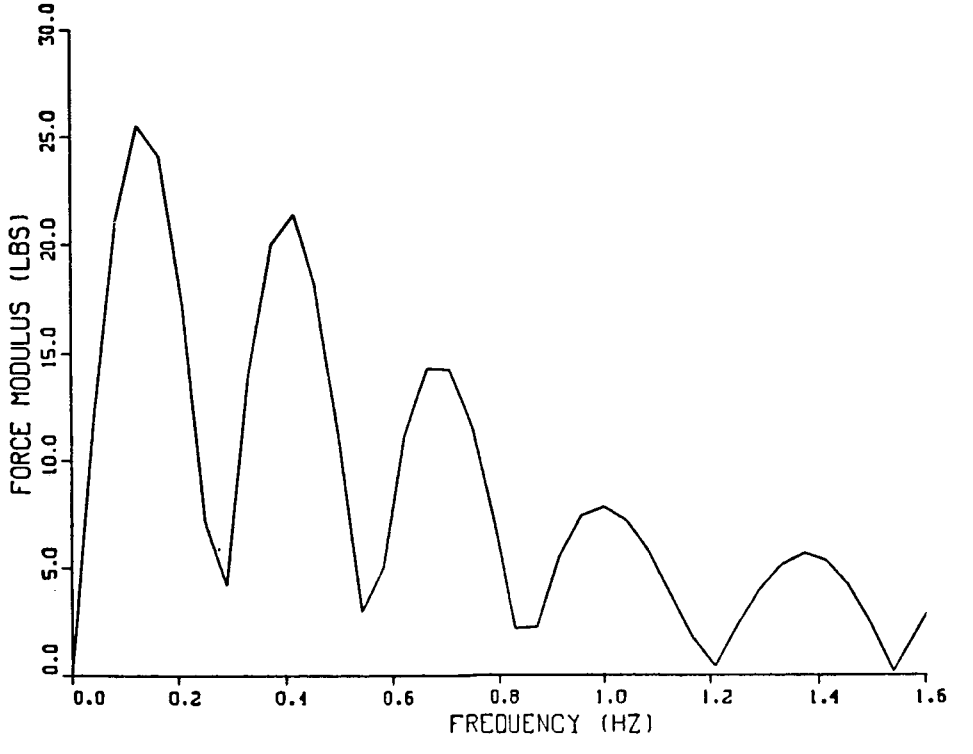

Figure 3-4. FFT of 5 Sec. Crew Motion Input.

3.3.2 Impulse Response Formulation

The general formulation for the impulse response of the system in Figure 3-5 has not been solved in a closed form in terms of the absorber parameters. The method discussed here follows that in in reference [13]. The following equations are solved for the initial conditions of unit velocity:

$$m_1\ddot{x}_1 = -k_1x_1 - c_1\dot{x}_1 + k_2(x_2 - x_1) + c_2(\dot{x}_2 - \dot{x}_1) \tag{3-7a}$$

$$m_2\ddot{x}_2 = -k_2(x_2 - x_1) - c_2(\dot{x}_2 - \dot{x}_1) \tag{3-7b}$$

The solution is assumed to have the form

$$x_1(t) = C_1e^{st} \tag{3-8a}$$

$$x_2(t) = C_2e^{st} \tag{3-8b}$$

and thus the derivatives have the form

$$\{\dot{x}(t)\} = \{sC\}e^{st} \tag{3-9a}$$

$$\{\ddot{x}(t)\} = \{s^2C\}e^{st} \tag{3-9b}$$

Substitution of Eqs. (3-8) and (3-9) into the equations of motion, Eqs. (3-7), yields a matrix equation in the unknowns C1 and C2. In order for nontrivial solutions to exist, the determinant of the matrix D must vanish:

$$[D]\{C\} = \begin{bmatrix} d_{11} & d_{12} \\ d_{21} & d_{22} \end{bmatrix} \begin{Bmatrix} C_1 \\ C_2 \end{Bmatrix} = 0 \tag{3-10}$$

$$d_{11} = m_1s^2 + (c_1 + c_2)s + k_1 + k_2 \qquad d_{21} = c_2s - k_2$$

$$d_{12} = c_2s - k_2 \qquad d_{22} = m_2s^2 + c_2s + k_2$$

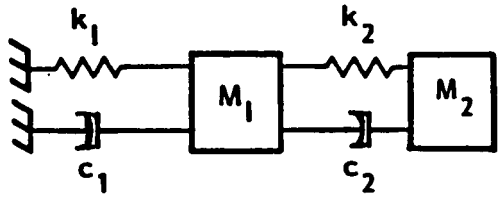

$$c_1 = 2M_I\omega_o\zeta_{ST}$$

Figure 3-5. 2-DOF Absorber Model with Additional Damper to Model Existing Structural Damping.

The resulting fourth-order equation

$$M_1M_2s^4 + [M_1c_2 + M_2(c_1 + c_2)]s^3 + [M_1k_2 + M_2(k_1 + k_2) + c_1c_2]s^2 + (k_1c_2 + k_2c_1)s + k_1k_2 = 0 \qquad (3\text{-}11)$$

is analogous to the characteristic determinant of an undamped system. Unless there is a double pole, the four roots of Eq. (3-11) occur as two pairs of complex conjugates:

$$s_{1,2} = -\zeta\omega_{n1} \pm \omega_{d1} \qquad s_{3,4} = -\zeta\omega_{n2} \pm \omega_{d2} \qquad (3\text{-}12)$$

The displacement solutions can be expressed in the form:

$$x_1 = \frac{A_1}{\omega_{d1}} \exp(-\zeta_1\omega_n t) \sin(\omega_{d1}t + \phi_1) + \frac{A_2}{\omega_{d2}} \exp(-\zeta_2\omega_{n2}t) \sin(\omega_{d2}t + \phi_2) \qquad (3\text{-}13)$$

where the amplitude and phase coefficients are determined by the initial conditions. Note that for the unit initial velocity case, the values of A1 and A2 are unity, and the amplitude coefficients are the inverse of the damped natural frequency. A simple Fortran algorithm is applied to solve the quadratic and obtain the displacement solution. The acceleration solution is found by differentiating Eq. (3-13) twice. For more general absorber analyses, the ALADIN multi-step integrator code is used, which employs the ADAMS method for integration.

The above equations are used to generate Figure 3-6, which may be viewed as the transient response analog to Figure 3-2. For clarity, the impulse response envelopes (which connect the peaks of the magnitude of the sinusoidal transient response) of the plant-absorber system are shown. The mass ratio β and the optimal frequency ratio δ are .02 and .98 respectively, while the damping ratio μ is varied. The discussion of the effect of varying the damper strength in Section 3.2 also applies here. A low damper strength does not provide sufficient damping performance while an overly large damper strength locks the damper, and results in

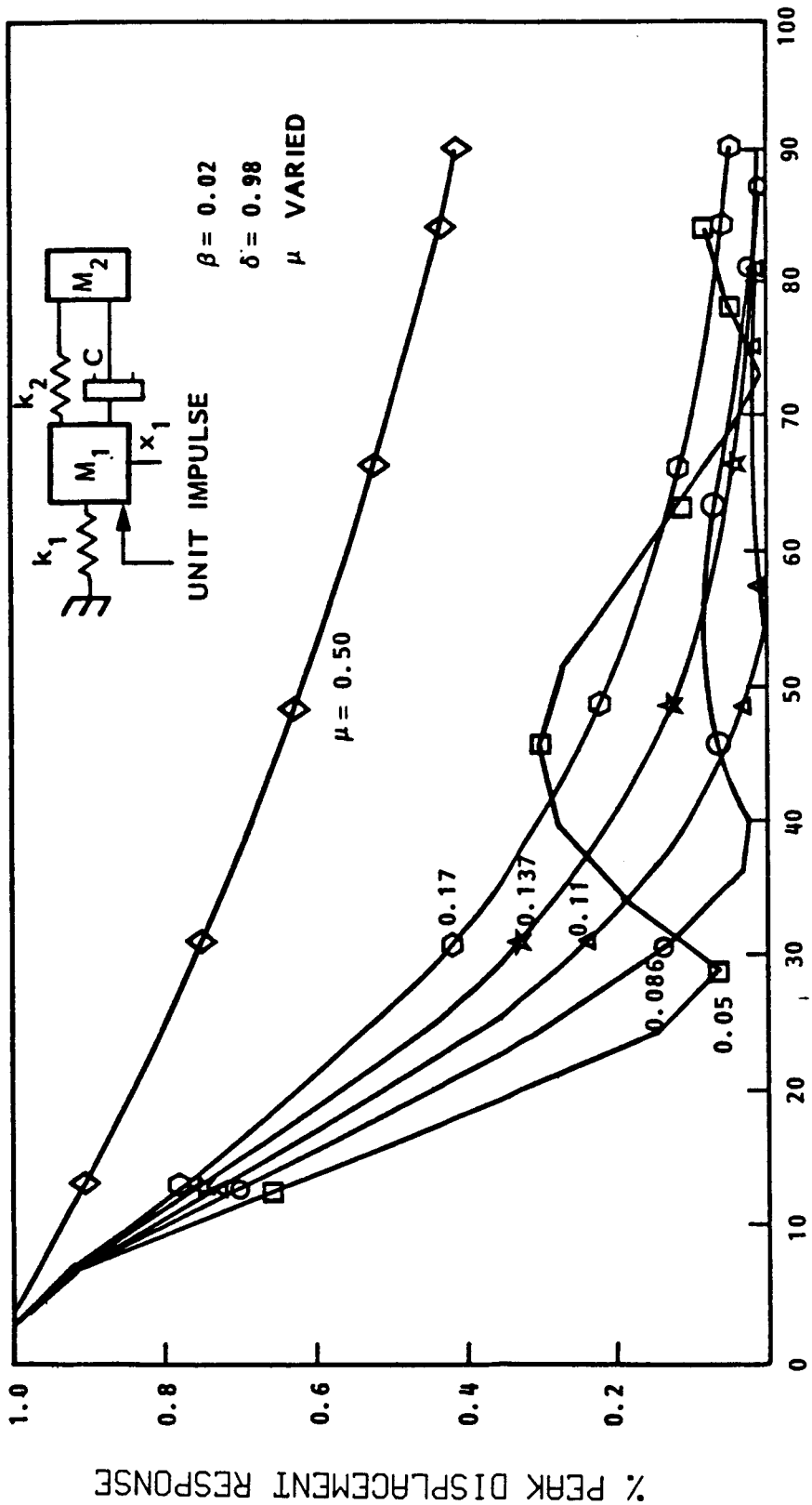

Figure 3-6. Normalized Impulse Response Envelopes for Various Damper Strength Values.

sub-optimal damping performance. Note that for small amounts of modal damping, the ordinate in Figure 3-6 could also be labelled:

$$\omega_0 x_1(t) \tag{3-14}$$

as an alternate way of normalizing the data.

3.3.3 Examination of Criteria for Optimization of the Transient Response

The next sections examine the effect of different optimality criteria on the tuning of the absorbers and the minimization of the transient response. Prior investigations [3,4] have discussed pole placement and minimum quadratic cost methods for tuning absorbers to optimize the transient response, in addition to the steady-state solution. In this comparative discussion, the structural damping of the plant (c1) is assumed to be zero.

The optimal pole placement solution maximizes the rate of modal energy dissipation. As with the classical steady-state solution, the mass ratio β is selected first, based on a trade study of performance vs. available mass budget. Then, the absorber parameters δ and μ are adjusted to locate the two plant and absorber poles as far left as possible in the S-plane. This maximizes the modal damping and typically decreases the system response time. Derivations in reference [4] show that application of the pole placement criterion results in a double pole at the extreme left of the root locus (Figure 3-7). For comparison, the pole locations of the steady-state solution are also shown. The pole placement solution exhibits higher modal damping ratios for both poles. Although it is not clearly discernible in this region of the root locus, both poles in either the pole placement solution or the steady state solution have the same modal damping (phase angle in the S-plane).

The value of δ which creates a double pole is identical to that of the steady-state minimize solution (Eq. 3-4):

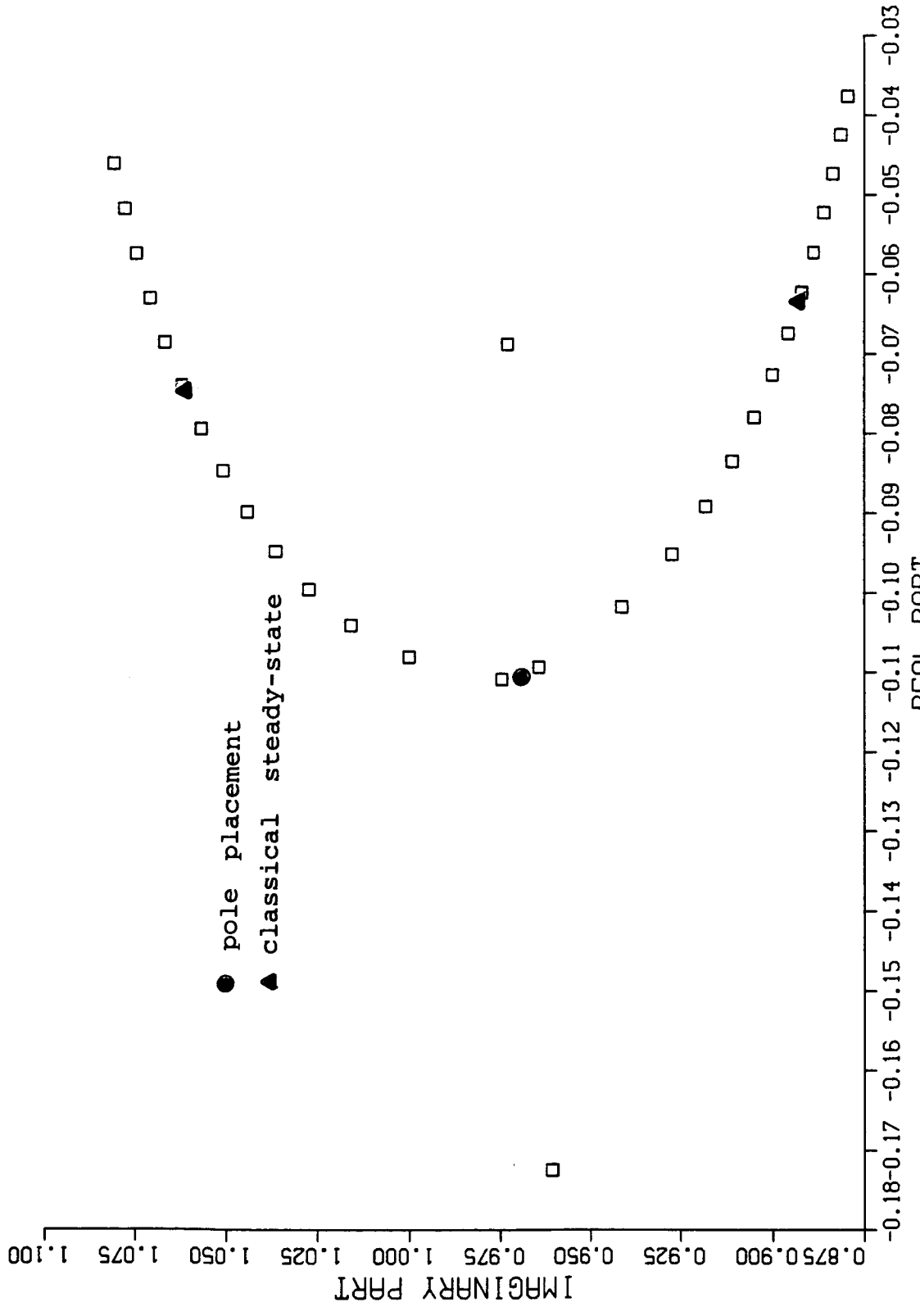

Figure 3-7. Root Locus for 2-DOF System Where the Damper Strength is Varied.

$$\delta = 1/1 + \beta \tag{3-15}$$

Substitution of this value of δ_{opt} in the characteristic equation and solving for the pole locations and damping yields [4]:

$$Re(S) = -1/2 \sqrt{\beta/(1 + \beta)} \tag{3-16a}$$

$$Im(S) = \pm 1/2\sqrt{(4 - \beta)/(1 + \beta)} \tag{3-16b}$$

$$\mu^2_{opt} = \beta/[(1 + \beta)^3] \tag{3-16c}$$

Figure 3-8 shows the impulse response of the two-dof system with a 5% modal mass absorber optimally tuned using the pole placement criterion.

Another optimal design technique found in the literature is the minimum quadratic cost solution [3,4]. Again, the first step is to choose the desired mass ratio, β and then proceed to optimize the other two absorber parameters, δ and μ. This criterion minimizes a cost function which penalizes the total energy in the system, and thereby maximizes the flow of energy out of the system. The quadratic cost function of the system states is

$$J = 1/2 \int_0^\infty x^T Q x \, dt \tag{3-17}$$

where the matrix Q is formed such that the quadratic terms are equated with the system's total non-dimensional energy. Evaluation of the above integral yields

$$J = 1/2 \; x_0{}^T P x_0 \tag{3-18}$$

where P is the solution of the Lyapunov equation for the equations of motion given the initial state of vector x_0 corresponding to unit initial velocity. Numerical search or carpet-map techniques can be used to find the optimal values of δ and μ which minimize the cost (J) for a fixed mass ratio (β). Figure 3-9 shows the resulting impulse response for a two-dof system with a 5% modal

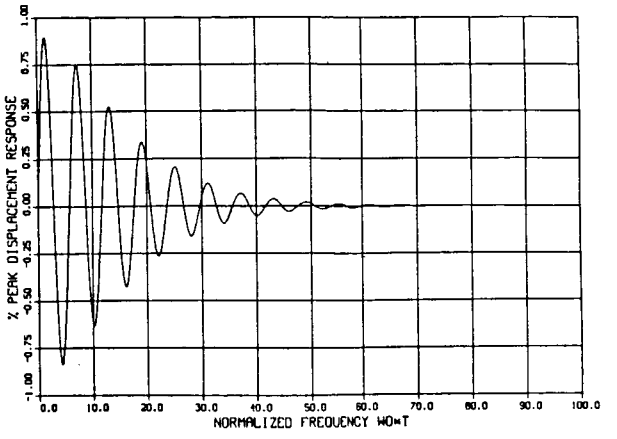

Figure 3-8. Impulse Response of 2-DOF System with a 5% Modal Mass Absorber Tuned Using the Pole Placement Criterion.

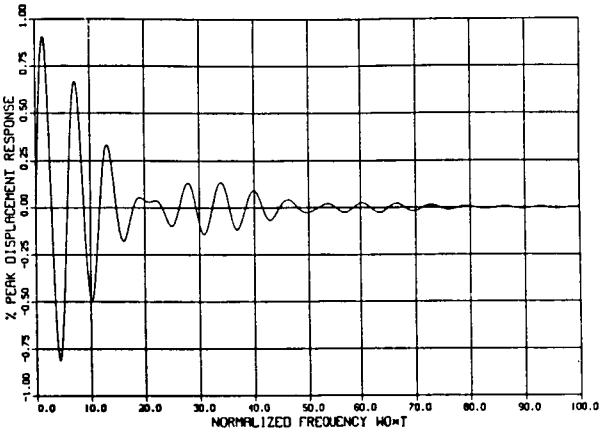

Figure 3-9. Impulse Response of 2-DOF System with a 5% Modal Mass Absorber Tuned Using the Quadratic Cost Criterion.

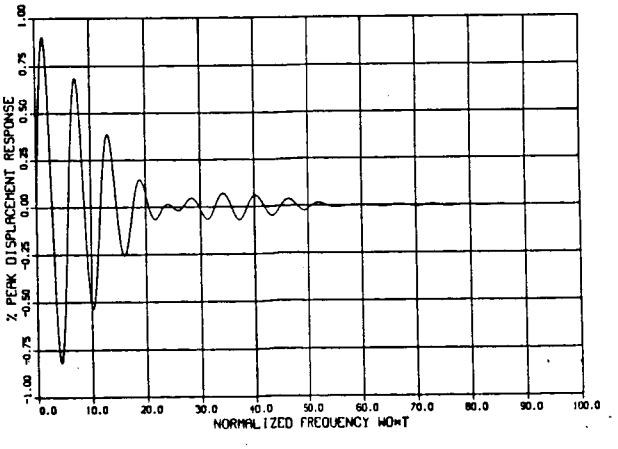

Figure 3-10. Impulse Response of 2-DOF System with a 5% Modal Mass Absorber Tuned Using the Classical Steady-State Criterion.

mass absorber optimally tuned by this criterion. Figure 3-10 shows the resulting impulse response for a two-DOF system with a 5% modal mass absorber optimally tuned using the classical steady-state criterion.

Insight can be gained by comparing the impulse responses of the one-mode system with absorbers tuned using the three different optimization techniques: classical steady-state, pole placement, and quadratic cost. Figure 3-11 compares the envelopes of the absolute value of the responses of Figs. 3-8, 3-9, and 3-10. Note that the pole placement solution does not exhibit the pronounced "beating" effect of the other two solutions. Ultimately, the selection of the "best" transient response criterion may depend on specific requirements. Although all of the responses are similar, the classical steady-state solution appears to be the best. It is rather unusual that a steady-state optimization technique should provide the best transient response solution. This issue is examined further in the next section.

3.3.4 Derivation of Energy Dissipated Through the Absorber

The rate of change of mechanical energy through the absorber can be written as [14]

$$dE/dt = -c_2(x_2 - x_1)^2 \tag{3-19}$$

and is always negative because the system is passive and can only dissipate energy. Since

$$\dot{x}_{rel} = \dot{x}_2 - \dot{x}_1 \tag{3-20}$$

and the damping force is

$$F_d = c_2\dot{x}_{rel} \tag{3-21}$$

Eq. (3-19) can be rewritten as

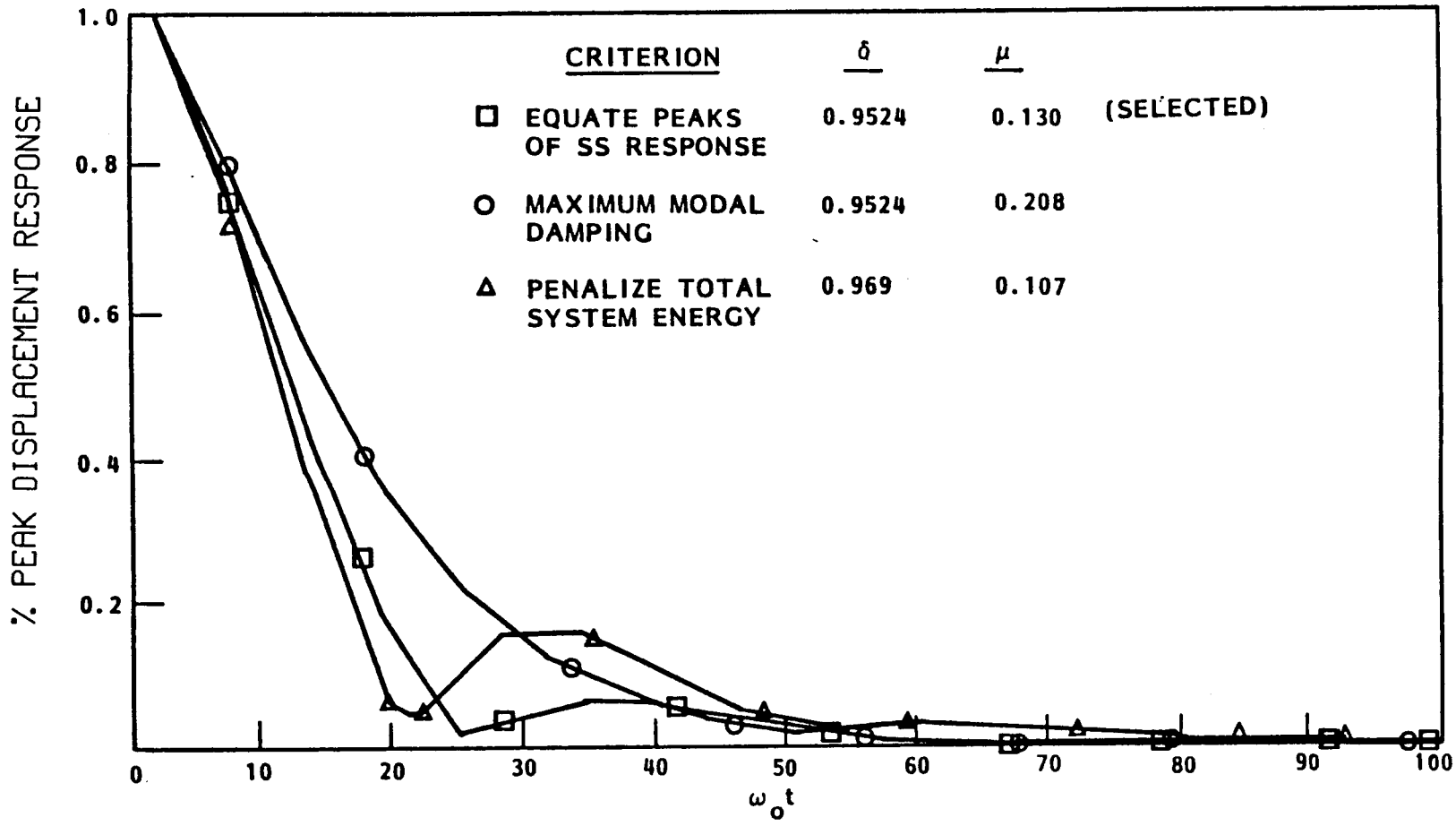

Figure 3-11. Comparison of the Envelopes of the Impulse Responses of 2-DOF Systems with a 5% Modal Mass Absorber Tuned Using the 3 Different Optimality Criteria.

$$dE/dt = F_d \dot{x}_{rel} \tag{3-22}$$

Further understanding of the results of the previous section can be gained by looking at the energy dissipated through the absorber during the impulse response. Figure 3-12a shows the instantaneous power dissipated through the damper for a system tuned using the classical steady-state optimization criterion. Figure 3-12b shows the running integral of the function in Figure 3-12a, which is the total energy dissipated through the damper at a given time. The envelopes of the corresponding curves for the pole-placement solution are also shown on both plots. Comparison of these curves reveals that the pole placement solution does initially provides the maximum rate of energy dissipation. However, the "beating" effect of the classical steady-state solution soon overtakes it. The net result is that the energy dissipated by the absorber tuned using steady-state design technique converges to the total energy in the system faster. In the next section, a fourth optimality criterion for minimizing the transient response is formulated.

3.3.5 Development of a Cost Criterion for the Impulse Response Case

The selection of the proper cost function for use in later optimization work on multi-dof systems and in later parameter optimization schemes is further investigated in this section. Further research in this area resulted in a fourth technique, based on a minimum area criterion. A performance index is postulated which penalizes the absolute value of the state deflection vector, $x_1(t)$. This performance index is expressed in the form of the cost function

$$J = \int_0^\infty \left| x_1(t) \right| dt \tag{3-23}$$

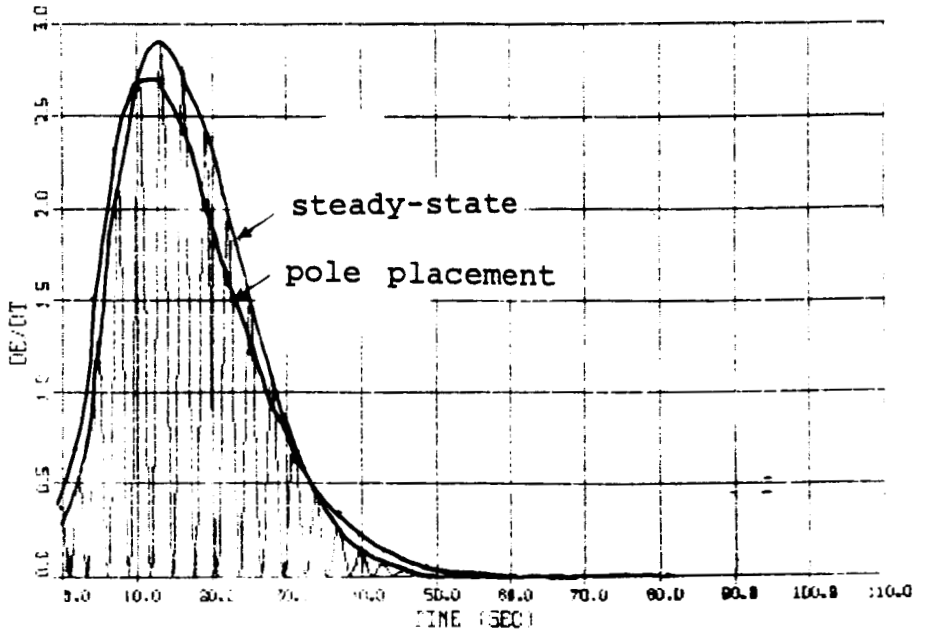

Figure 3-12a. Comparison of Instantaneous Power Dissipated Through Absorber During Impulse Response.

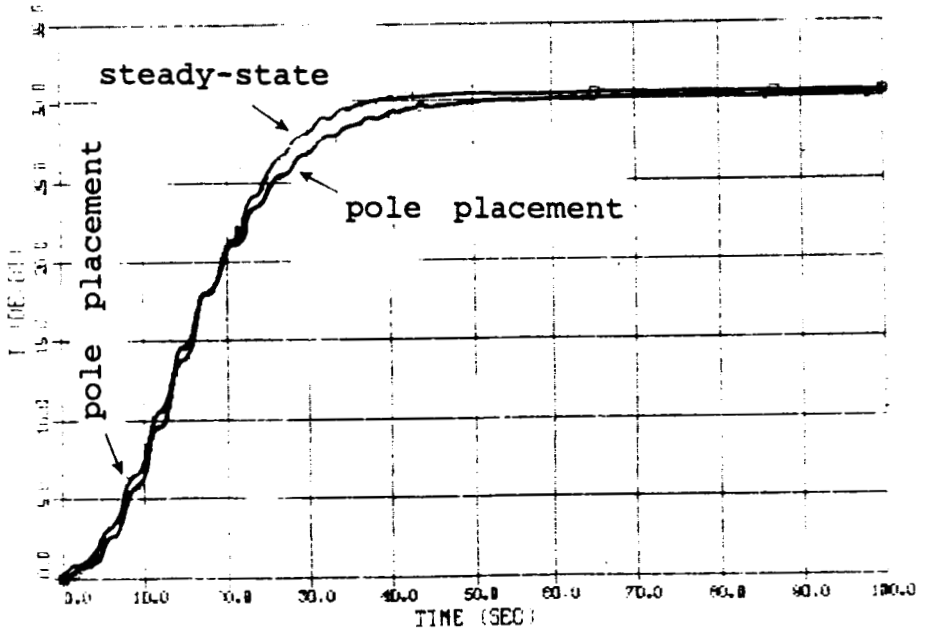

Figure 3-12b. Comparison of the Running Integral of the Instantaneous Power Dissipated During the Impulse Response.

Insight into the nature of the performance index is gained by numerical evaluation of the cost function and examination of the surface contours. The absolute value of the impulse response solution (Eq. 3-13) is integrated numerically over a large time interval such that convergence of the area to that of the infinite interval occurs. Given the analytic form of the impulse response solution, these trade studies do not require a great deal of computation time. Figure 3-13 shows the surface contours (the area under the displacement curve) for various values of δ and μ. Although enlarged for clarity, each contour had a single minimum. The figure shows that for a mass ratio of β=.02, the optimum values of δ and μ are .98 and .090 respectively. The point on the graph indicates the values for the classical steady-state criterion, .98 and .086 respectively, which are very close to the minimum of the cost J. The points for the pole placement and quadratic cost solutions are further away from the minimum to such an extent that they are off the plot in Figure 3-13. This explains the result mentioned in section 3.3.3, where the steady-state design technique resulted in a better response than the other transient optimization methods.

Figure 3-14 compares the root loci for the solutions using the steady-state criterion and the minimum area criterion (μ=.98 and μ=.90 respectively). The roots of the two solutions are very close. The difference in the solutions can be examined in terms of the modal damping. The roots of the steady-state solution have equal modal damping. Because there is a slight difference in frequency between the two poles, the amplitude of the impulse response of the higher frequency pole is slightly lower and damps out slightly faster. Therefore small performance gains can be acquired by shifting the root locus to give the lower frequency pole more damping (a slightly larger phase angle in the S-plane). Thus, the minimum area criterion locates the poles in a position which maximizes the modal damping and the beating effects collectively.

Because the separation between the poles increases with increasing values of the mass ratio β, the difference between the

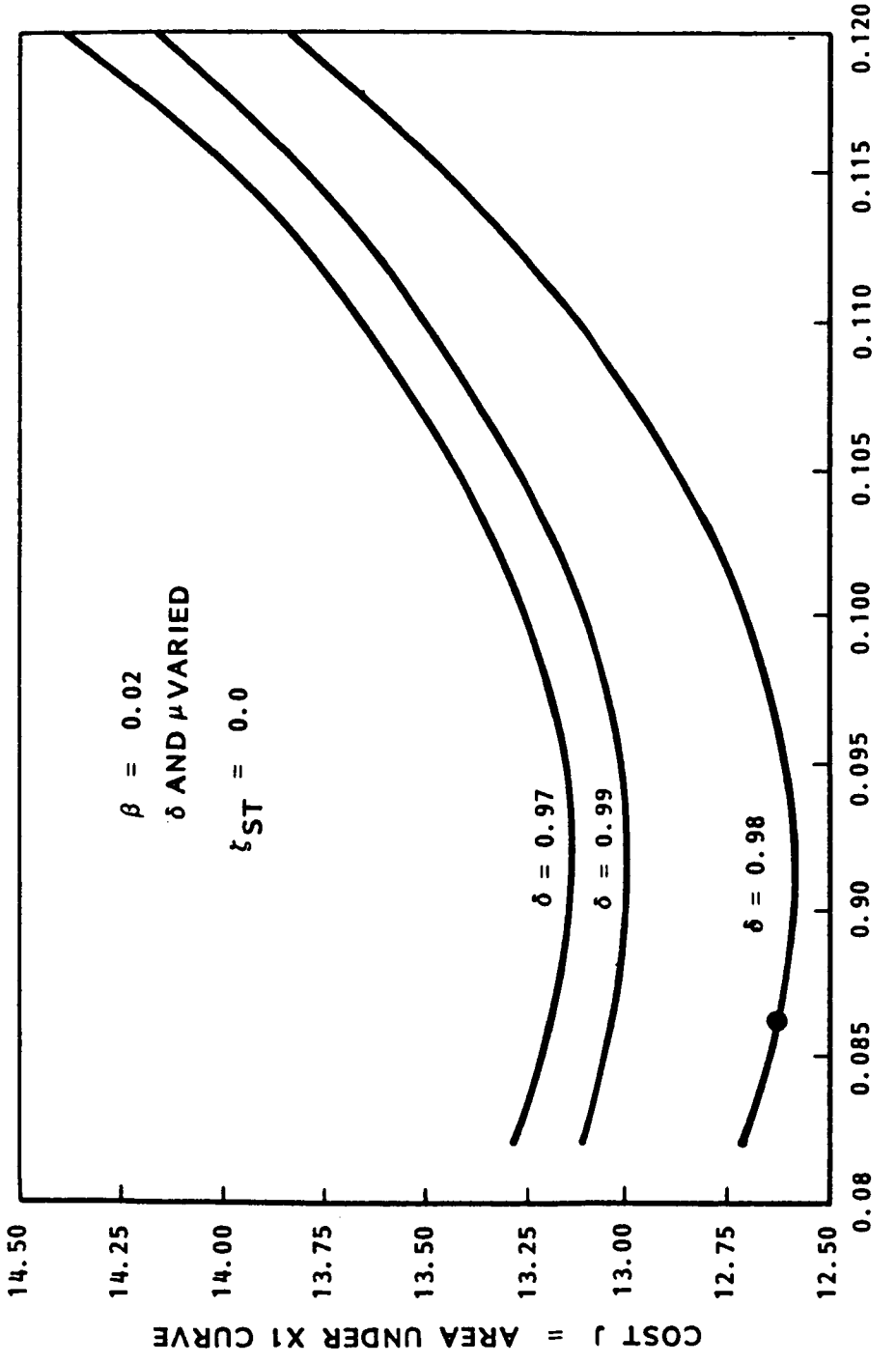

Figure 3-13. Surface Contours of the Cost Function for the Minimum Area Criterion. The Point on the Graph Marks the Values for the Classical Steady-State Design Criterion Which Are Very Close to the Optimum or Minimum Cost Design.

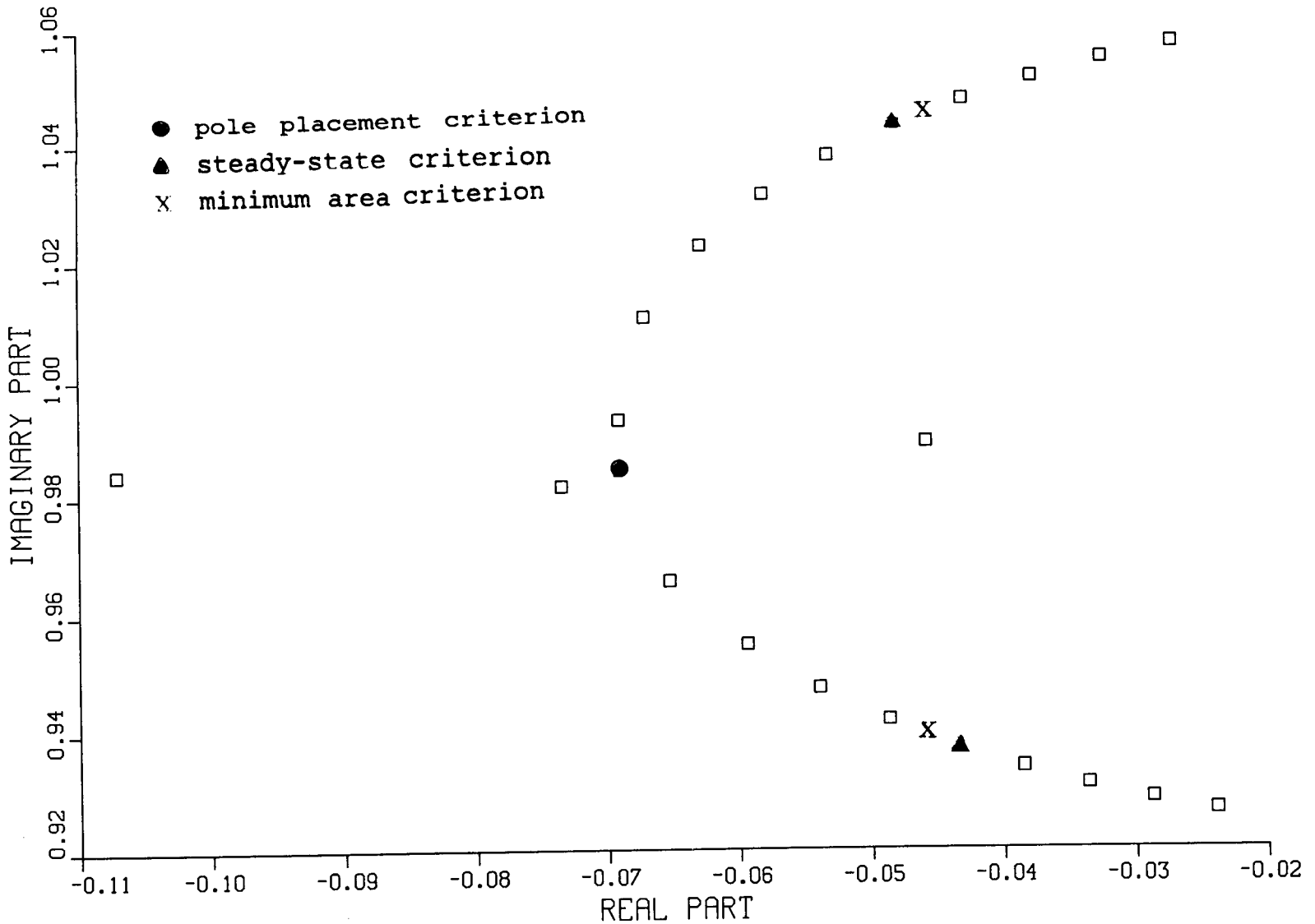

Figure 3-14. Root Locus Comparison of Different Optimality Criteria.

minimum area solution and the classical steady-state optimal solution will also increase. However, the difference between the frequencies of the two poles increases from 10% at a mass ratio of β=.02 to a modest 20% for a mass ratio of β=.20. The error is small enough that for all practical purposes, the designer can adopt the classical steady-state tuning equations to design an absorber which meets the criterion of minimizing the cost (Eq. 3-23). The notion of using the classical steady state equations to arrive at a solution very close to the minimum of the desired cost function J is instrumental in developing the multi-mode optimization technique in Section 3.6. In addition, the cost function (Eq. 3-23) which penalizes the displacement response is also adopted for use in the parameter optimization procedure described in Section 4.

In an analogous manner, the acceleration impulse response can be minimized by implementing a minimum area under the acceleration curve criterion. The cost function is expressed:

$$J = \int_0^\infty \left|\ddot{x}_1(t)\right| dt \qquad (3\text{-}24)$$

Figure 3-15 shows the contours describing the area under the acceleration response vs. μ. The conclusions drawn from the previous discussion on minimizing the displacement impulse response apply for this case as well.

3.4 Effect of Structural Damping on Absorber Optimization.

The effect of structural damping on the optimal tuning of vibration absorbers is investigated in this section. Structural damping is properly added to the two-dof model by using a non-zero value for c1 in Figure 3-15,

$$c_1 = 2M_1\omega_0\zeta_{st} \qquad (3\text{-}25)$$

where ζ is the percent critical structural damping. Figure 3-16 was created in the same manner as Figure 3-13, i.e., by evaluating

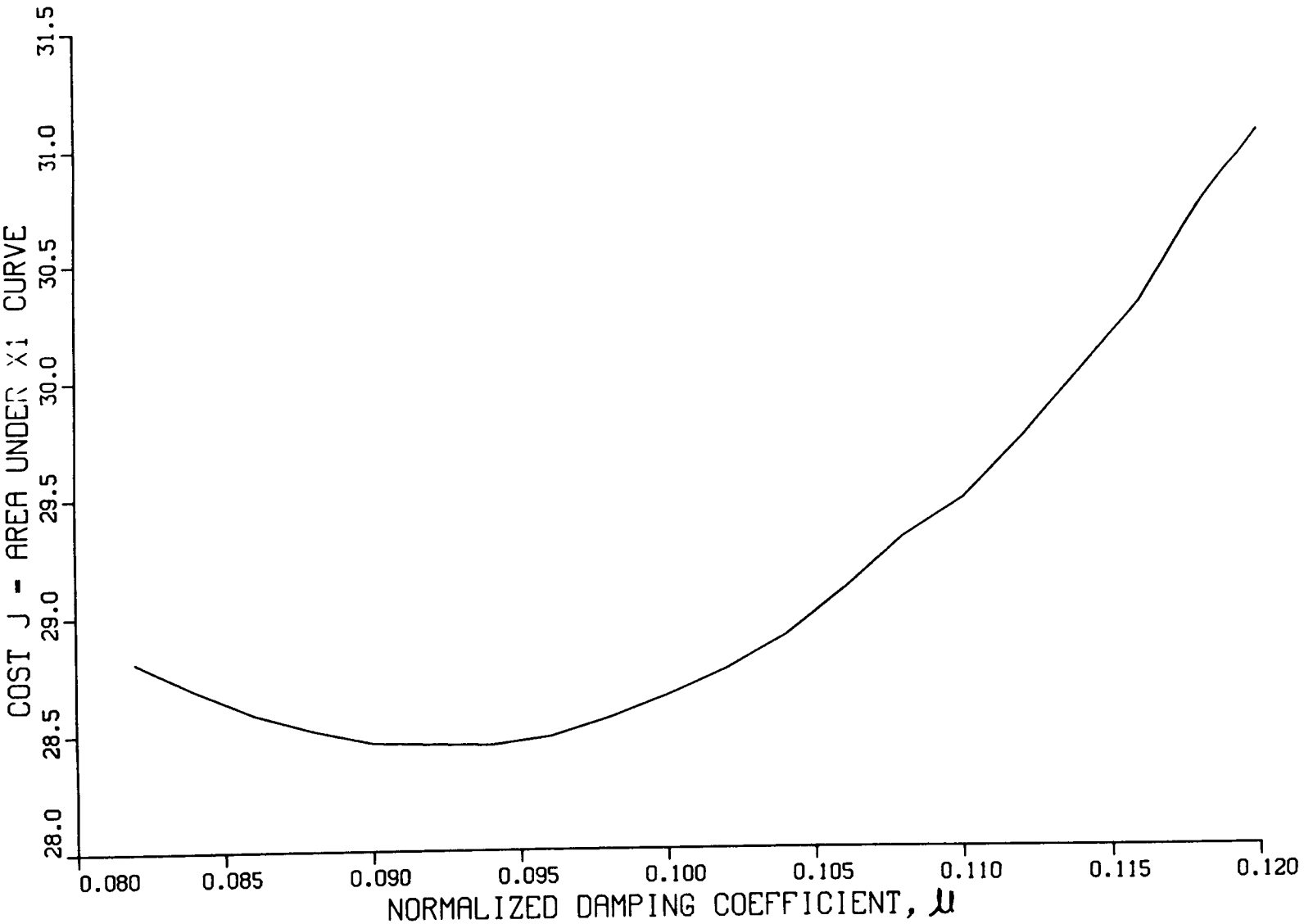

Figure 3-15. Surface Contour of the Cost Function for the Minimum Area Criterion for Accelerations.

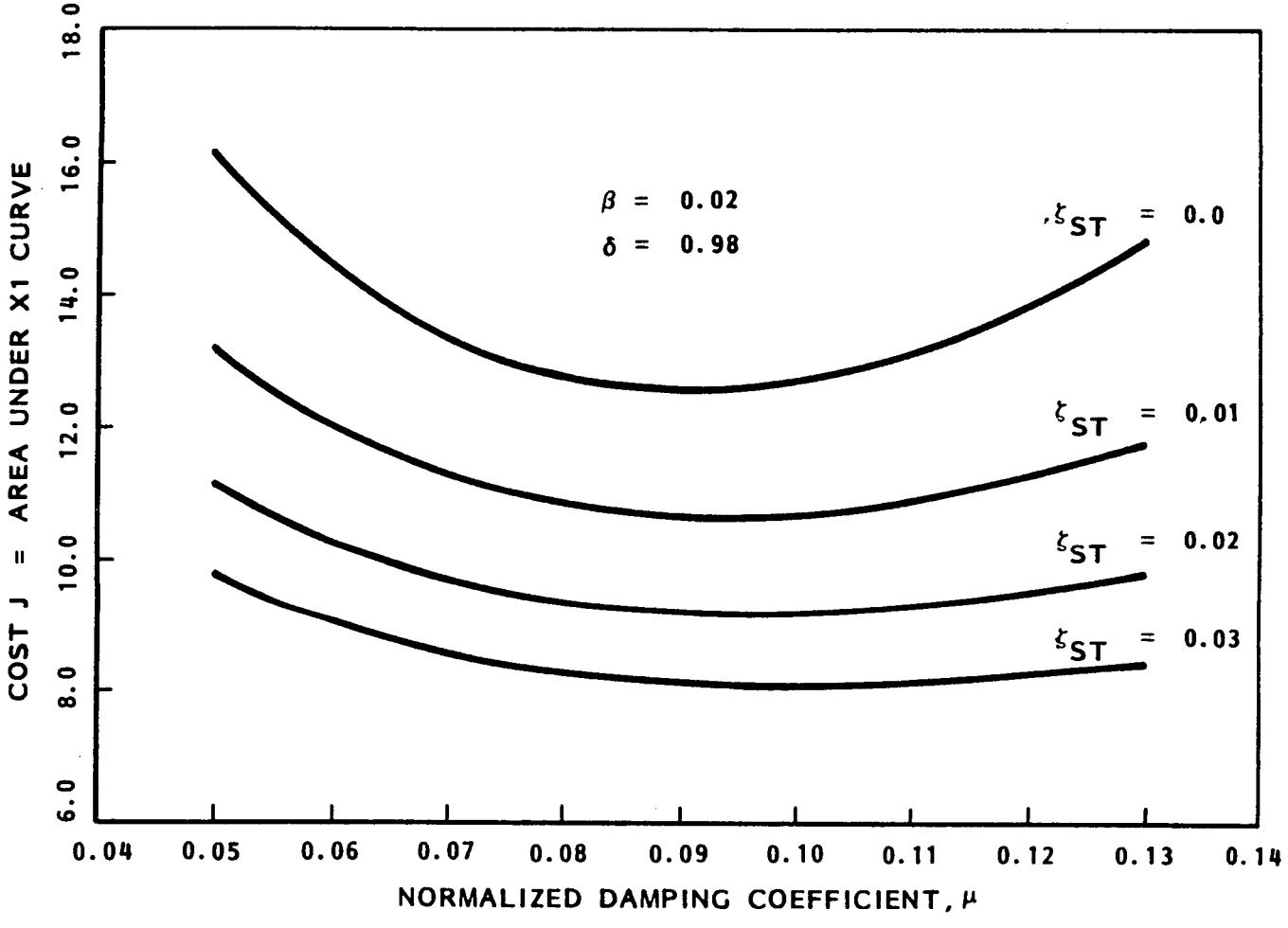

Figure 3-16. Surface Contours of the Cost Function for the Minimum Area Criterion for Various Values of Inherent Structural Damping. The Value of the Normalized Damping Coefficient Which Minimizes the Cost is Nearly Unaffected by Small Amounts of Inherent Structural Damping.

the impulse response (Eq. 3-13) and integrating it numerically to find the area under the absolute value of the response. The plot shows the effect of structural damping on the location of the minimum cost. Note that as the amount of structural damping is increased, the impulse response is improved and the contours flatten out. The absorber μ value for minimum cost is near enough to the classical steady-state design that it can be concluded that small amounts of structural damping do not perturb the optimal design synthesis.

Additional conclusions can be drawn by examination of the effect of structural damping on absorber optimal design from the viewpoint of the response settling time. Figure 3-17 depicts the settling time to 20% of the original impulse response peak versus the plant structural damping for a mass ratio β of 2%. The upper curve shows the same response time for the system without the absorber. The results indicate that a 2% modal mass absorber can significantly improve the settling time of systems with less than about 5% structural damping. Beyond the 5% structural damping level, the structure itself is dissipating energy so well that the absorber has little effect. Examination of the figure yields that for a 2% modal mass absorber, the response time to 20% peak is equivalent to that for the same plant without an absorber but with a structural damping level of 6%. Successive curves for larger absorber mass ratios than 2% would lie below the 2% curve as shown, having a shorter settling time.

3.5 Tuning Laws for Multi-DOF Structures

This section examines the tuning laws for a multi-dof structures. Analyses of an early Dual Keel configuration space station model support the tuning laws presented in this section. The discussion of this model is kept to a minimum as the results of examples employing a later model are given in Section 5. Assuming a structural damping value of 1/2%, the response is calculated at the upper payload boom and the lab module due to a unit x-direction impulse input at the berthing node. A 2% modal mass absorber is

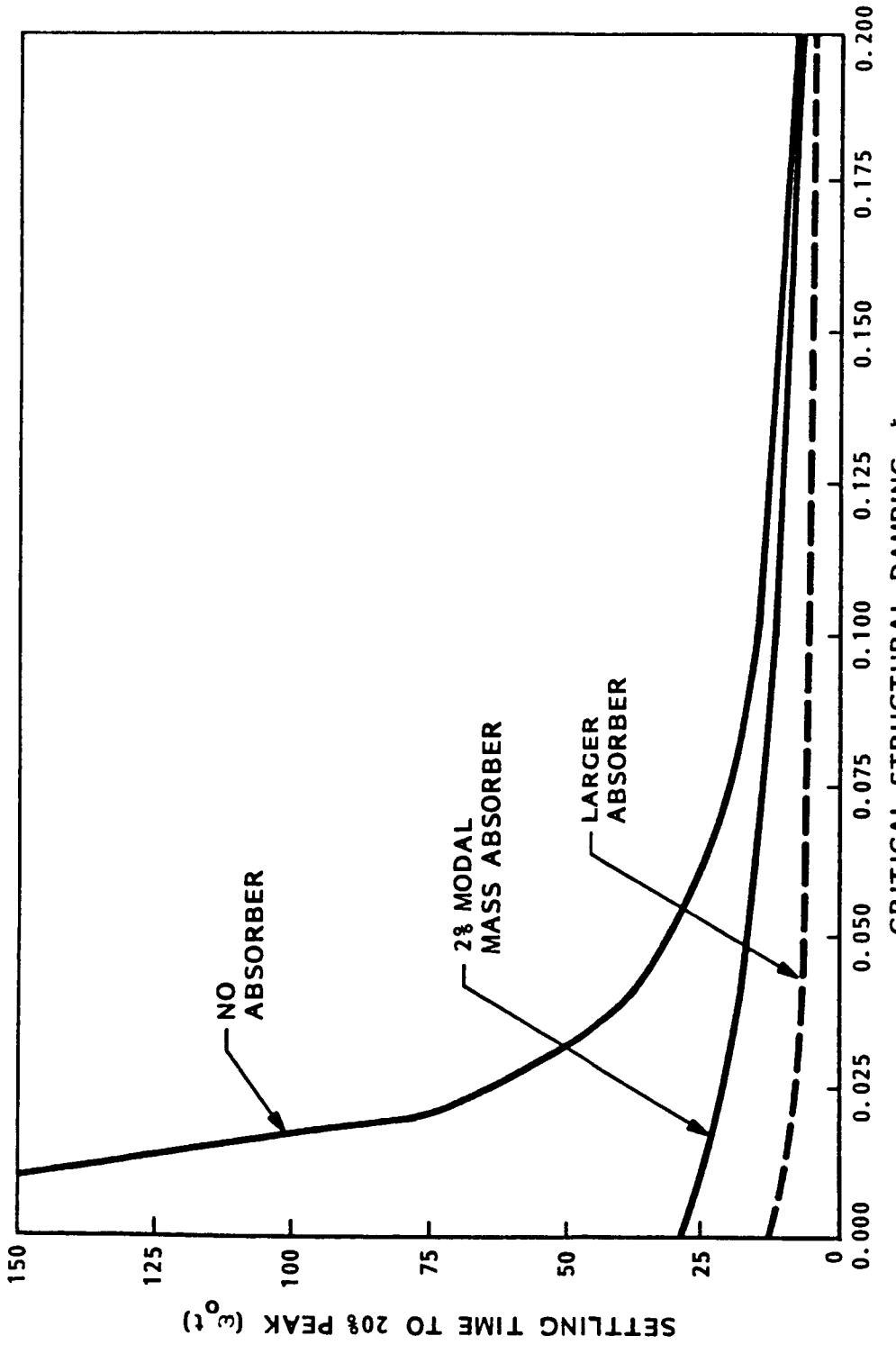

Figure 3-17. Comparison of the Settling Time to 20% of the Peak of the Impulse Response for Systems With and Without an Absorber. For Typical, Smaller Values of Inherent Structural Damping, Large Performance Gains can be Attained Through the Addition of an Absorber.

used, tuned to the single mode of importance at the payload boom. The ALADIN code, based on the multi-step ADAMS integration technique, is used to generate the impulse response for the "closed-loop" (structure and absorber) case. Figure 3-18 compares the responses at the payload boom before and after the absorber was added. Figure 3-19 compares the spectra of the two responses in Figure 3-18, where the FFT was obtained over the same 50-second time period. Figures 3-20 and 3-21 illustrate the respective results for the same analysis at the lab module response location. The results indicate that, in this case, the absorber did not couple the primary modes, and that the net solution was the linear sum of the two-dof response corresponding to the primary mode with an absorber on it, and the other higher frequency modes.

In the process of conducting these analyses, two simple tuning laws were established for tuning absorbers to a single mode of a multi-dof structure. One tuning law describes the performance of the absorber at a particular location on a particular mode by introducing the notion of an effective absorber mass ratio

$$\beta_{eff} = \varphi_{n1}{}^{2}\beta \tag{3-26}$$

where the eigenvectors are normalized such that the maximum value of each mode is 1.0. This can be rewritten using modes normalized to the mass matrix by

$$\beta_{eff} = \varphi_{i}{}^{2}M_{a} \tag{3-27}$$

where M_a is the mass of the absorber. Eqs. (3-26, 3-27) exhibit the sensitivity of absorber performance to location, which appears to be generally greater than the sensitivity to different tuning techniques. Embedded in the equation is the fact that a misplaced absorber is also tuned incorrectly, as the mass ratio β_{eff} is a variable in all the classical steady-state tuning laws. Note that these statements do not include the effect of the added mass on the mode shape (i.e., the addition of the tuning mass alters the mode shape so that the absorber is no longer located at a maximum).

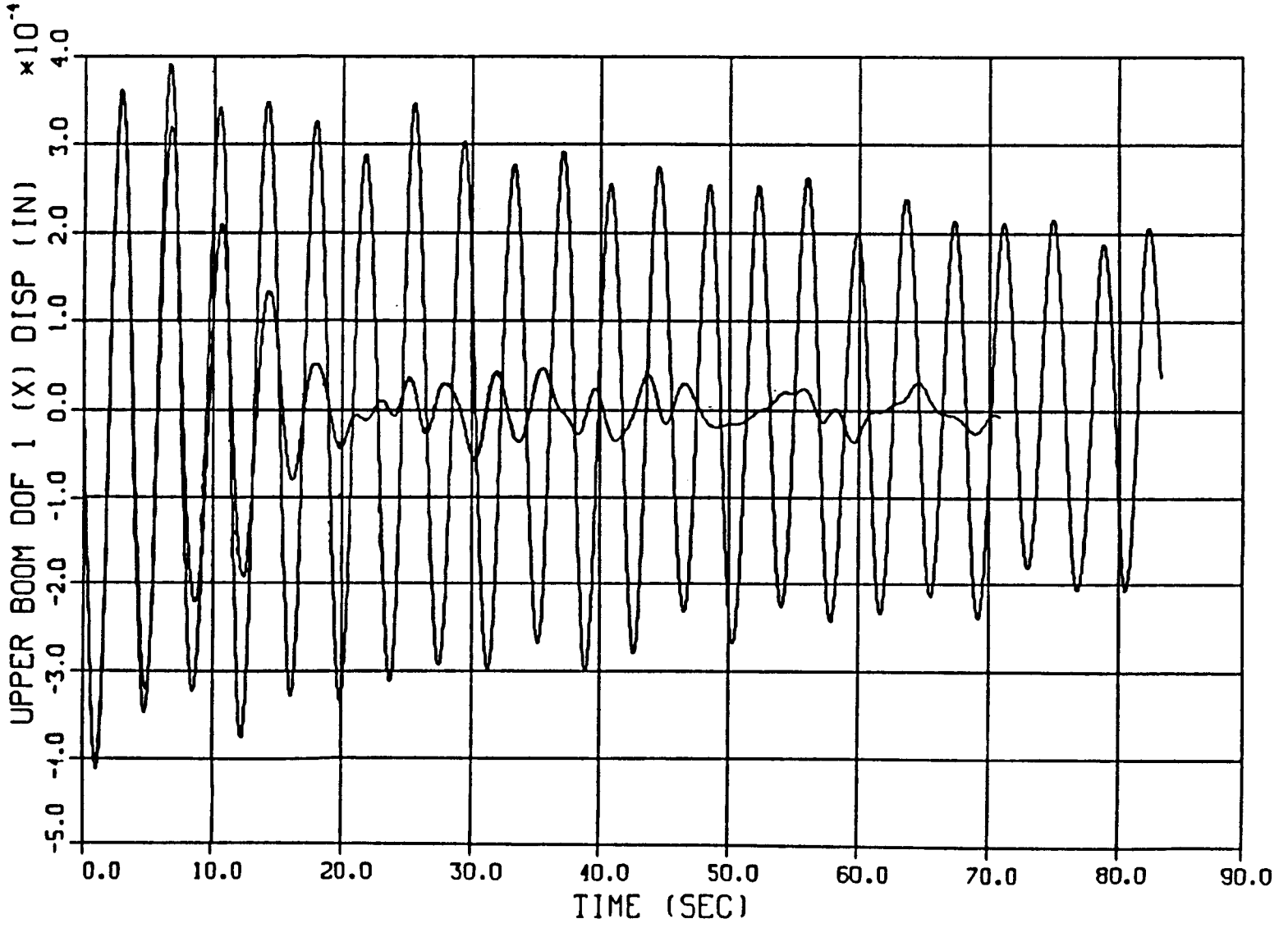

Figure 3-18. X-Direction Responses at the Payload Boom With and Without a 2% Modal Mass Absorber. The Force Input is a Unit Impulse at the Shuttle Docking Node.

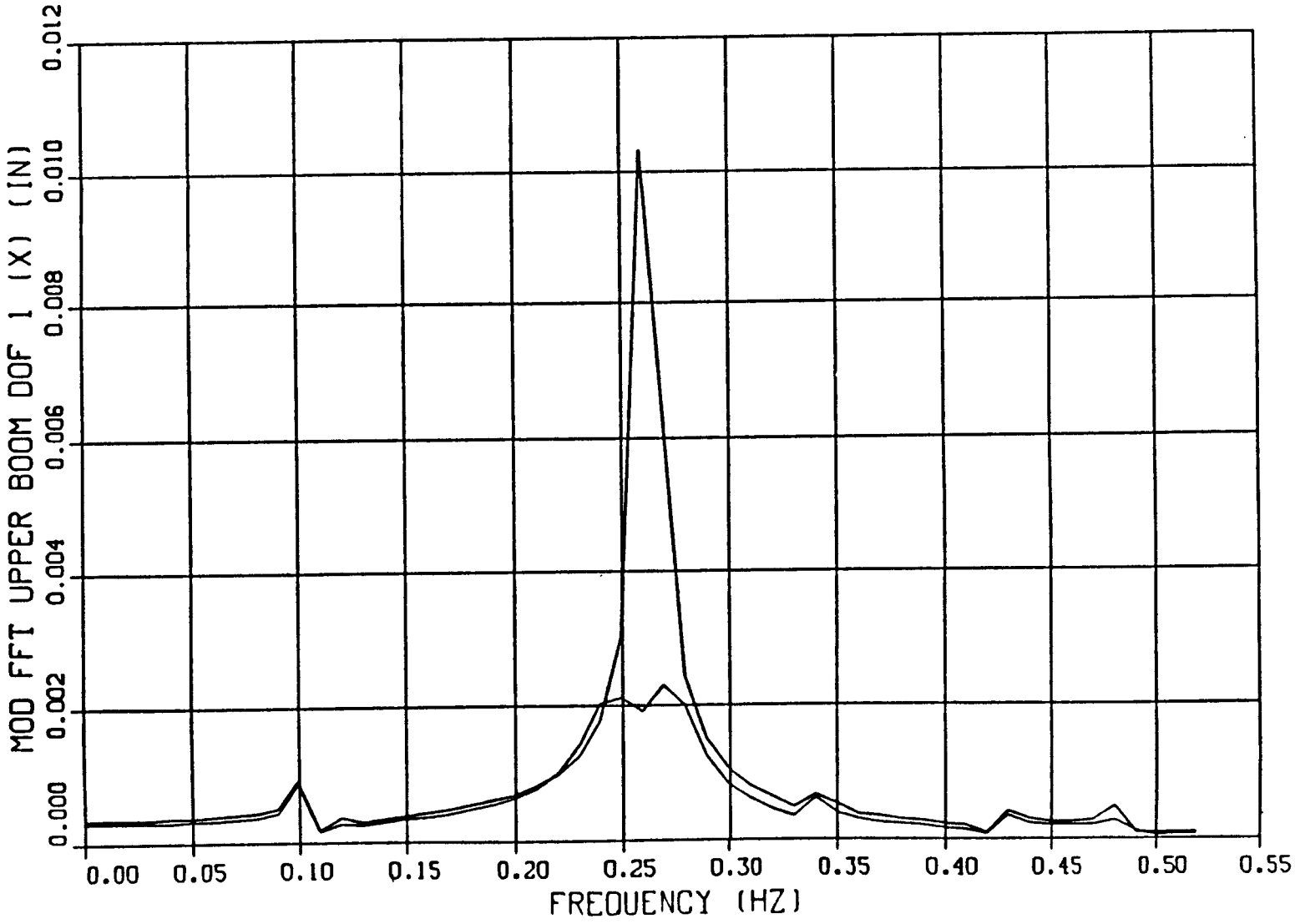

Figure 3-19. FFT of the Responses at the Payload Boom With and Without a 2% Modal Mass Absorber.

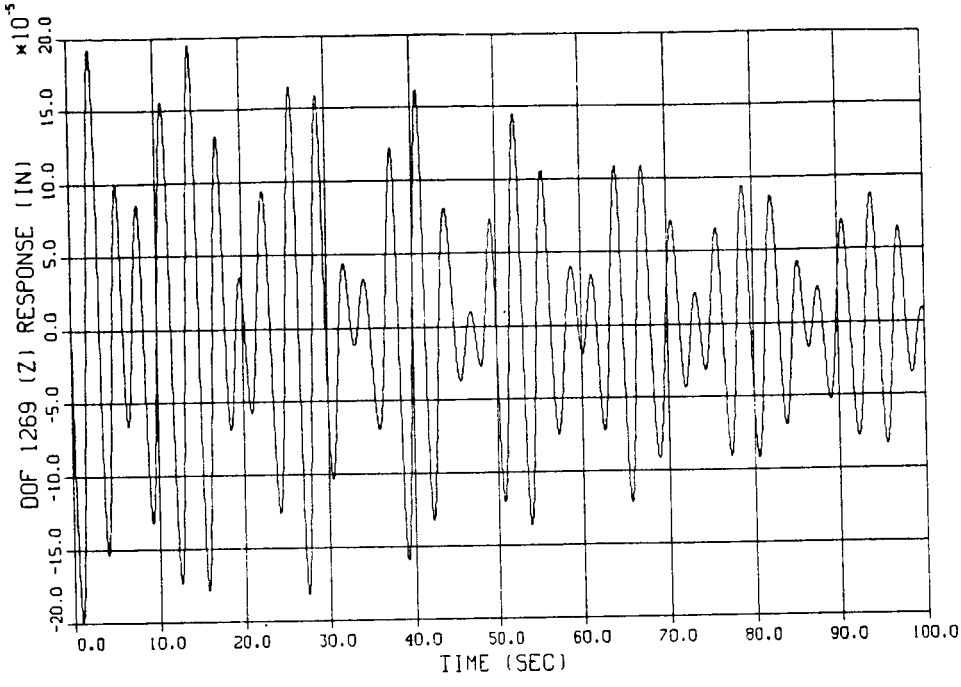

(a) No Absorber

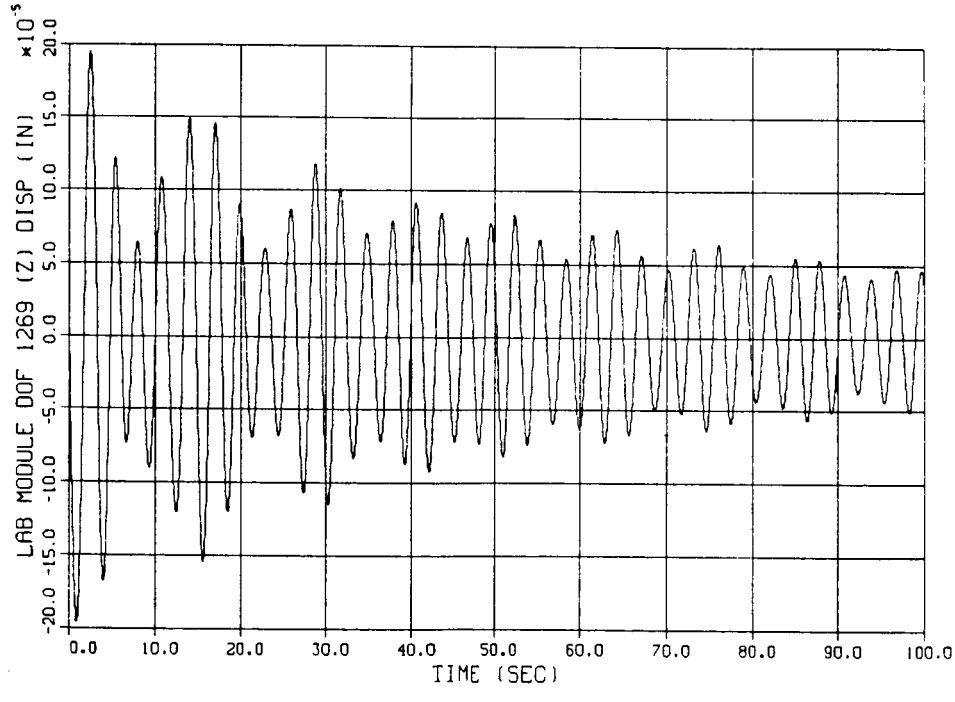

(b) With 2% Modal Mass Absorber

Figure 3-20. Z-Direction Response at the Lab Module due to a Unit Impulse at the Docking Node.

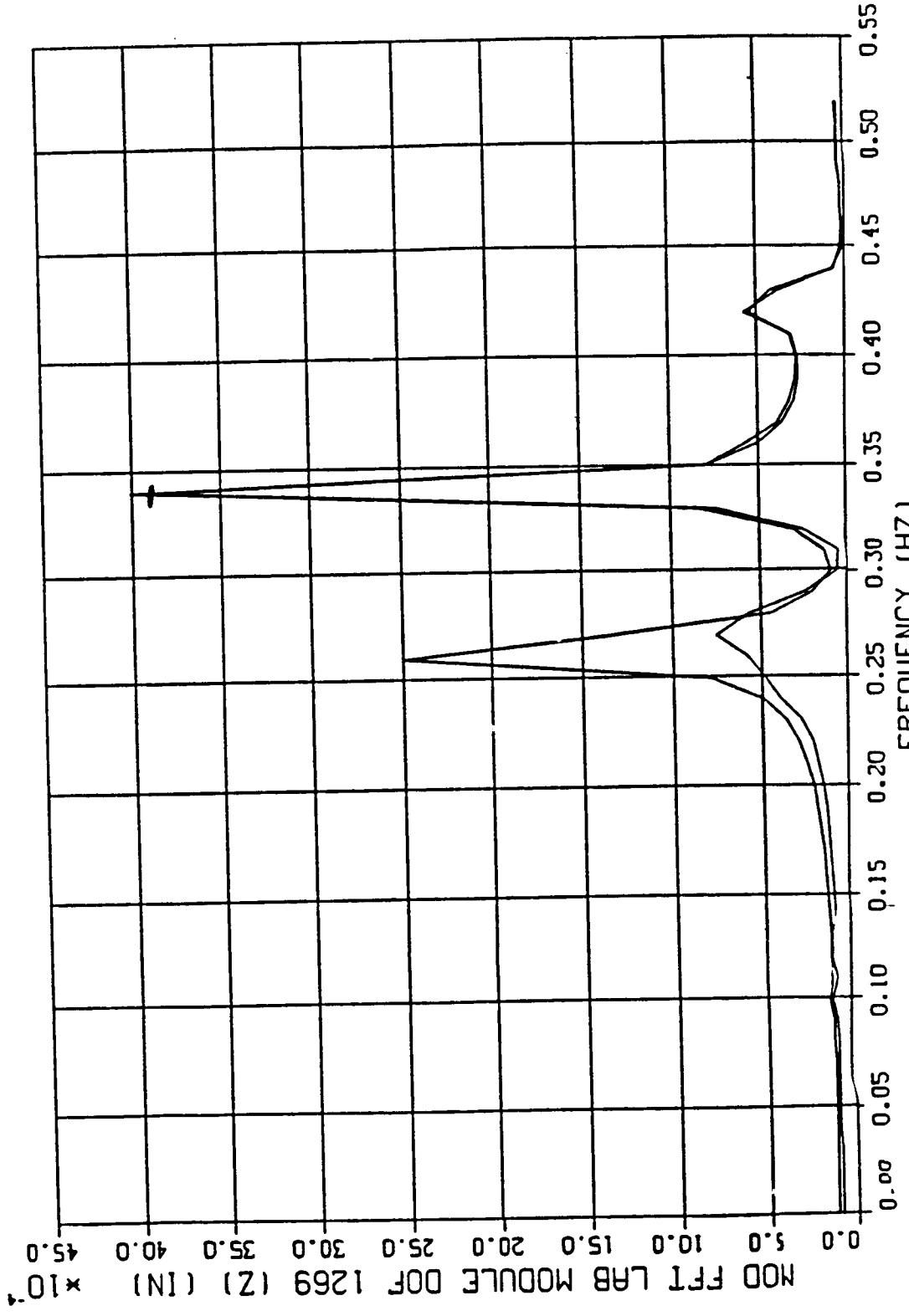

Figure 3-21. FFT of the Responses at the Lab Module With and Without a 2% Modal Mass Absorber.

However, the effect is negligible for reasonably small absorber mass ratios, and for most large space structure absorber applications, the above equations will suffice.

Another tuning law describes the tuning of several absorbers to the same mode. The question is whether there is a theoretical performance advantage to using a single absorber or several smaller ones? Analyses bear out that for n absorbers at n locations with equal modal displacements, the absorbers should be tuned by the simple relations:

$$m_i = M/n \tag{3-28a}$$

$$c_i = C/n \tag{3-28b}$$

$$k_i = K/n \tag{3-28c}$$

Thus, two absorbers tuned according to the above relations will have the same effect as a single absorber whose optimally tuned parameters are M, C, and K. However, it is important to note that if both absorbers aren't placed at equal maxima locations for the same mode (e.g. the two tips of a free-free beam), there will be a reduction in performance because the net β_{eff} for that mode will be lowered. Thus, aside from physical design constraints, it seems desirable to use a small number of absorbers. Ultimately, the design constraints associated with the use of certain spring and damper materials may dictate the number of absorbers which should be placed on a particular mode (e.g., for large n, the spring constants k_i may become so low that it would be impossible to manufacture them.)

3.6 Multi-Mode, Multi-Absorber Optimization

The nature of the results shown in Figs. 3-18 - 3-21 indicates that for cases involving structures where the primary modes of interest are uncoupled, the tuning of absorbers to each of the primary modes can be treated independently. In addition, section

3.3.5 shows that the classical steady state solution and the optimal impulse response solution (Eq.3-23) yield nearly the same result. Consequently, by adopting the classical steady-state tuning laws, the absorber k and c (Eqs. 3-4 and 3-5) for each primary mode can be described solely as a function of the absorber mass ratio for that mode (β_i). This suggests that a multi-mode optimization could be conducted by deciding how much absorber mass should be placed on each significant mode, and then tuning each of the absorbers using the classical steady-state criterion. Assuming an absorber was placed on each mode, the result is essentially the sum of n two-dof impulse responses corresponding to n modes. Since this technique assumes that the absorber does not couple the modes, the appropriate barometer of what constitutes coupling of the modes by the absorber is discussed in the next section.

With this mass optimization technique in mind, it is desired to formulate the damping performance of a particular absorber tuned to a particular mode (by the classical steady-state criterion) in terms of the mass ratio, β. The cost function (adopted in Section 3.3.5) minimizes the sum over the modes of the impulse responses at a particular response location:

$$J = \int_0^\infty \sum_{\text{modes}} |x_1(t)| \, dt \tag{3-29}$$

Thus, one can proceed to formulate the area under the absolute value of the impulse response curve as a function of the absorber mass ratio, β and any other pertinent systems parameters. To simplify the analysis, it is assumed that the area under the impulse response for each mode adds linearly to the total area under the collective modes (this assumption is justified in later examples). The integral in Eq. (3-29) can be expanded:

$$\text{Min } J_T = J_{\text{mode 1}} + J_{\text{mode 2}} + \cdots J_{\text{mode n}} \tag{3-30}$$

Given the form of the impulse response solution in Eq. (3-13),

$$x_1 = \frac{\varphi_i \varphi_j}{\omega_d} e^{-\zeta \omega_n t} \sin \omega_d t \tag{3-31}$$

the sum can be expanded in terms like:

$$\int_0^\infty |x_1| \, dt = \varphi_i \varphi_j \; 1/(\zeta \omega_n) \; * \; [....] \tag{3-32}$$

The key to this method is that for a particular level of structural damping, the function for the area under the absolute value of the impulse response of a particular pole

$$J = \int_0^\infty \left| 1/\omega_d \exp(-\zeta \omega_n t) \sin \omega_d t \right| dt \tag{3-33}$$

depends only on ζ for ω_n approximately equal to ω_d. Furthermore, Eq. (3-3) can be equated with the steady-state dynamic magnification factor

$$\left(x_1/x_o \right)_{MAX} = 1/(2\zeta) = \sqrt{(2 + \beta)/\beta} \tag{3-34a}$$

to yield

$$\zeta = 1/2 \sqrt{\beta/(2 + \beta)} \tag{3-34b}$$

Given these equations, a unique expression for the displacement area under each "2-dof mode" (the cost J) can be determined using a linear fit on a plot of the cost J versus the reciprocal of ζ:

$$\int_0^\infty |x_1| \, dt = \phi_i \phi_j \sqrt{\frac{2 + \beta}{\beta}} + 1.2 \tag{3-35}$$

And likewise for the area under the acceleration impulse response:

$$\int_0^\infty |\ddot{x}_1| \, dt = 2.5 \; \phi_i \phi_j \sqrt{\frac{2 + \beta}{\beta}} \tag{3-36}$$

Figure 3-22 compares the fit of the actual area under the two-dof displacement response curve as a function of β with Eq. (3-35). Note that 1/2% structural damping is assumed. Also shown is the same fit for the acceleration case. The result is not surprising when one considers that all the absorber parameters and the

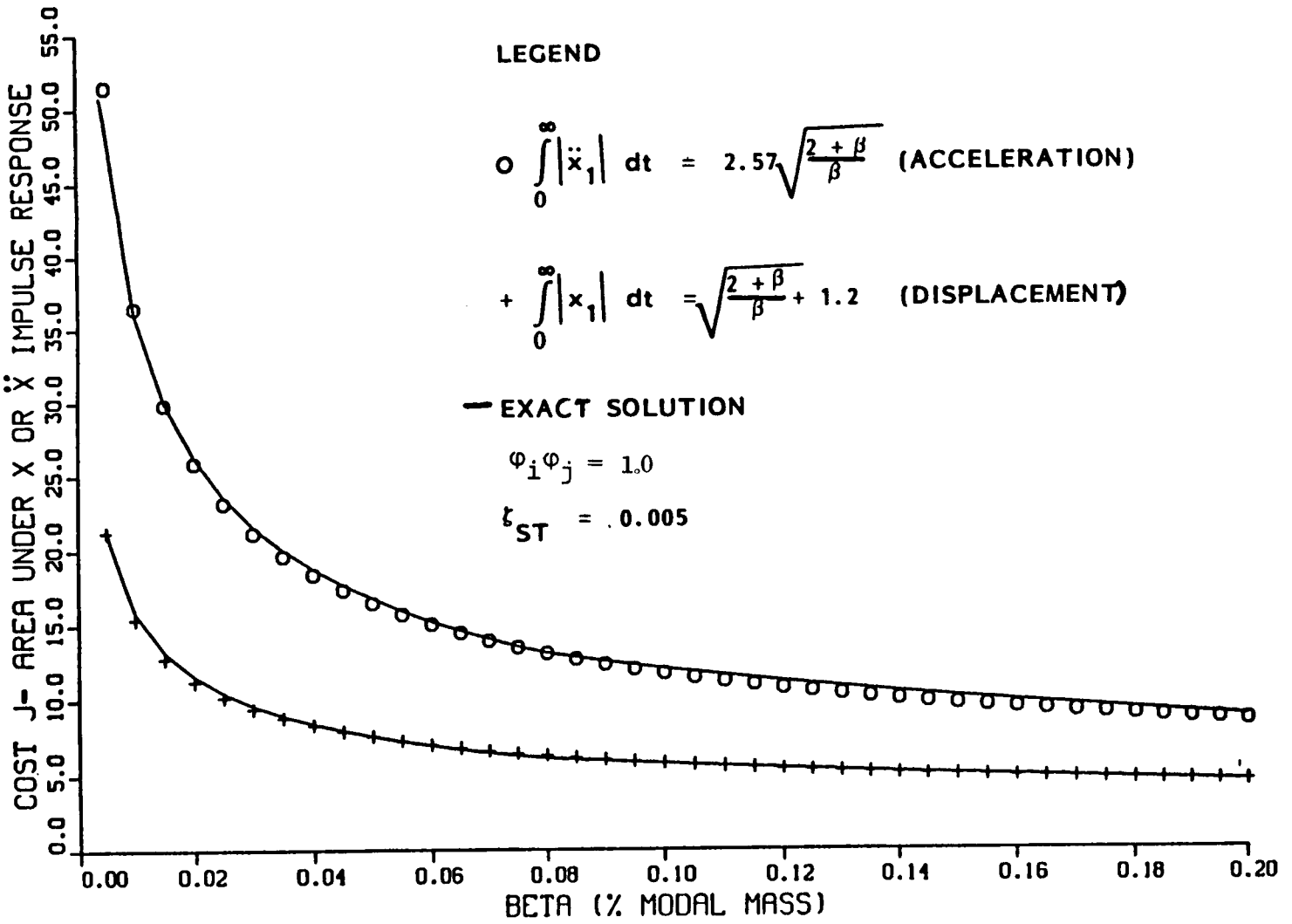

Figure 3-22. Comparison of the Fitted Equation and the Exact Solution for the Cost J for a Single Mode with an Absorber Tuned to it. The Good Fit for Both the Displacement and Acceleration Equations Indicates That the Cost is Solely a Function of the Inherent Structural Damping and the Absorber Modal Mass Ratio.

expression for modal damping (Eq. 3-34 above) are functions of only β.

Given these unique functions, a global optimization over n primary modes can be conducted under the constraint of the total absorber mass available:

$$\text{Min } J_T = J(\beta_1)_{\text{mode 1}} + J(\beta_2)_{\text{mode 2}} + \ldots J(\beta_n)_{\text{mode n}} \tag{3-37}$$

subject to constraint,

$$M_{aT} = \beta_1 M_1 + \beta_2 M_2 + \ldots \beta_n M_n \tag{3-38}$$

Invoking constrained multivariate optimization techniques, n equations in n unknowns can be solved for β_i by finding the zeros of the matrix equation:

$$\frac{\alpha J_T}{\alpha \beta_i} - \frac{\alpha J_T}{\alpha \beta_1} \frac{\alpha M_{A_T} / \alpha \beta_i}{\alpha M_{A_T} / \alpha \beta_1} = 0 \ (i = 2, \ldots n) \tag{3-39}$$

$$M_{A_T} - (\beta_1 M_1 + \beta_2 M_{11} + \ldots \beta_n M_n) = 0 \tag{3-40}$$

Software routines capable of finding the zeros of matrix equations can be found in IMSL, SLATEC, and other standard math libraries. For cases involving just two primary modes, a graphical technique can be used to examine the contours of the cost function (see Figures 3-13, 3-16). Once the mass ratio for each mode is known, the absorber k_i and c_i for each mode can be determined based on the classical steady-state tuning laws. The technique is referred to as the "uncoupled dynamic optimization". It is applied to coupled and uncoupled Space Station examples in Section 5, and the results are compared with nonlinear techniques developed in Section 4.

3.7 Coupling of Impulse Response by Absorbers in Multi-DOF Space Structures.

The addition of absorbers can introduce coupling between the otherwise orthogonal modes of a large space structure in two ways. The first is through spatial coupling, whereby the location of an absorber at the maxima of one mode also affects another mode. The effect is especially significant if the absorber is located at a location which is the maxima of both modes. The spatial coupling effect can be described in terms of an effective mass ratio:

$$\beta_{eff} = \phi_n^2 \, M_a/M_n \tag{3-41}$$

where n is the index for the mode without an absorber which couples to another mode with an absorber of mass M_a.

The absorbers also introduce coupling through closely spaced modal frequencies. The tendency for frequency coupling increases with increasing values of the cross-mass ratio, β_{eff}. Figure 3-23 shows the results of a parametric study that investigates the coupling effect (by measure of the cost J) of an absorber that is tuned to another mode but possibly coupled to the mode of interest. The curves were generated by using the two-dof system (Figure 2-1), parametrically mistuning the value of the plant frequency, and evaluating the area under the curve. Note that no structural damping was assumed in the generation of this curve. The plot is interpreted using the following steps: 1) the value of β_{eff} is determined based upon Eq (3-41), 2) the ratio of the frequency of the mode of interest to that of the mode with an absorber attached is selected on the abcissa, and 3) the corresponding area under the response is found on the ordinate. The plot is cut off at a maximum area of 126.0, which represents the area corresponding to the impulse response of the plant with 1/2% structural damping. Thus, if the point cannot be found on the graph which matches both ω/ω_1 and β_{eff}, there is no coupling. Modes with points falling within the interior of the parabola are coupled, and the effect of

$$\beta_{eff} = \phi^2 M_A \quad \text{WHERE } \phi^T M \phi = I$$

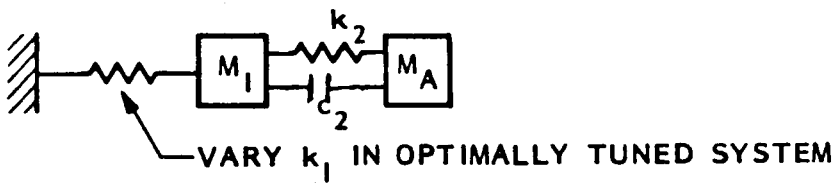

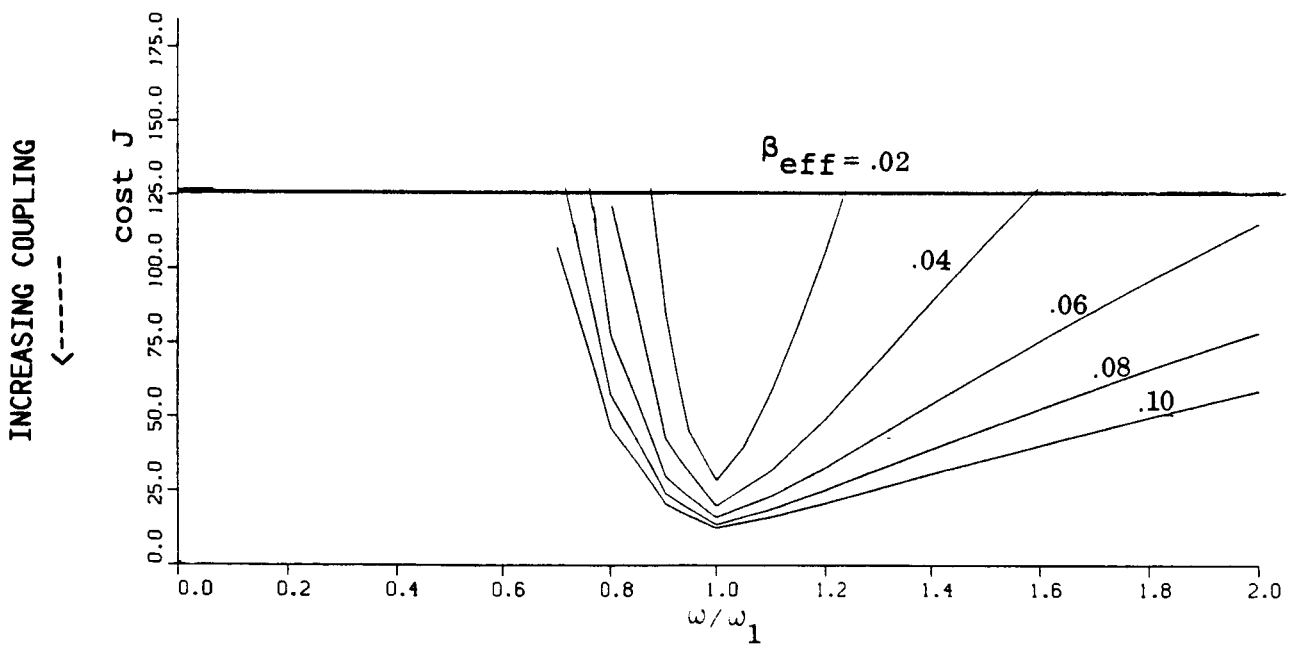

Figure 3-23. Characterization of Net Effect of Absorber Spatial and Frequency Coupling.

the coupling on damping the mode of interest can be ascertained by noting the magnitude of the area under the response (cost).

Figure 3-24 shows Figure 3-23 replotted on a log base 10 scale. Several trends and conclusions can be drawn from this figure. First, the larger the effective mass ratio, β_{eff}, the greater the tendency there is to couple the damping effect of an absorber tuned to one mode with another. Second, the "parabolas" are asymmetric, indicating that the mode of interest couples more strongly with a lower frequency mode that is damped by an absorber than a higher frequency one. This trait is confirmed by other investigators who showed that to damp the steady-state response of two modes, the absorber should first be tuned to the lower mode and then the damper value adjusted to optimally damp both modes.

Figure 3-24 also can be interpreted from the point of view of "mistuning" the absorber. The figure shows that the sensitivity of the absorber performance to tuning errors decreases as the absorber mass ratio increases. Additionally, the sensitivity to tuning errors is greater if the absorber is mistuned above the optimal frequency as opposed to below.

Typically, the designer would attempt to size and locate the absorbers in such a way that the coupling between the modes was increased, thereby increasing the damping performance of a single absorber over many modes. However, in certain situations, it is possible that the maximization of coupling could result in reduced damping performance. Therefore, a fully-coupled analysis is necessary to analyze absorber locations for problems involving large amounts of coupling. The methods described in this section apply to uncoupled or lightly coupled modes, but can also be used to provide location and mass distribution input for the fully coupled parameter optimization. The application of modern control theory and parameter optimization techniques to the vibration absorber problem takes into account coupling effects, and is discussed in Section 4. Section 5 compares the results of the dynamics and controls techniques applied to two Space Station vibration damping cases, one uncoupled and the other highly coupled.

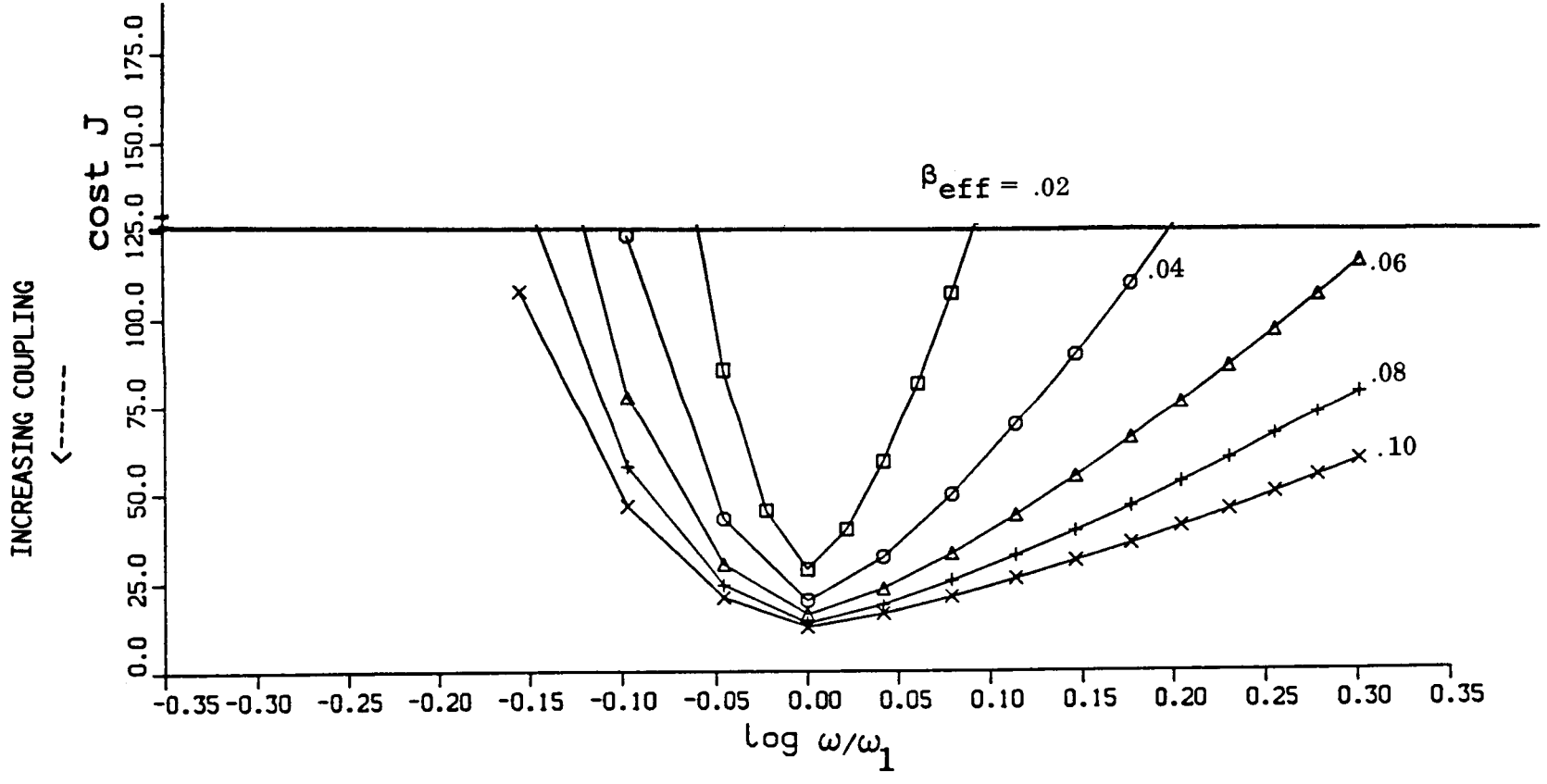

Figure 3-24. Characterization of Net Effect of Absorber Spatial and Frequency Coupling. The Asymmetry of the Curves on this Log Plot Indicate Stronger Absorber Coupling with Modes that are Higher in Frequency than the Absorber.

SECTION 4
CONTROL THEORETIC APPROACH TO ABSORBER DESIGN

This section presents a control theoretic approach to vibration absorber design. The design process is formulated as a linear output feedback control problem via the development of a feedback control canonical form. The design variables are expressed as control gains, and the analytical techniques of feedback control theory, both classical and modern, are applied to absorber design. Although active control algorithms are used in the design process, the final design remains passive; i.e., we are not designing active systems. The constrained nature of the feedback gain matrix makes the application of established output feedback solution methods difficult; therefore, a nonlinear parameter optimization method is developed and applied to the output feedback formulation of the vibration damping problem. The optimization algorithm is applied to the simple 2-DOF system for comparison with known solutions to the 2-DOF problem.

4.1 Conceptual Development

The motivation for a new approach to absorber design stems from the complexity of the Large Space Structure (LSS) vibration damping problem. These structures have many closely spaced vibration modes and many candidate locations for placement of vibration absorbers. This multi-input problem (many different vibration sources) and multi-output problem (many different absorber locations), coupled with large numbers of vibration modes requiring damping, leads to a complex regime of damping problems that require new approaches to absorber design.

The multi-input/multi-output (MIMO) nature of these problems lends itself to the analytical methods of multivariable feedback control theory. These feedback methods are well developed and an extensive body of knowledge and engineering experience exists concerning the effects of feedback gains on system performance, damping levels, and frequency response. The expression of the

absorber design process in feedback control format permits use of these analytical techniques and provides convenient methods to evaluate system performance in terms of accepted control system terms and concepts. Although some of these concepts may be unfamiliar to the structural dynamics community, their use in absorber design allows development of design procedures specifically tailored for LSS vibration absorbers that must cope with the new regime of complexity imposed by large space structures.

The key concepts that allow application of feedback control techniques to absorber design are the placement of the design problem in a linear format, and the recasting of the combined structure-absorber dynamic equations in a feedback canonical form. This linear form is useful because most of the control-theoretic results apply to linear systems and the linear format greatly simplifies analysis and design. The feedback canonical form allows expression of the absorber parameters as controller gains and provides a convenient method for the evaluation of absorber performance. This formulation also provides needed visibility into the absorber design process.

4.1.1 Linear Format

Consider the development of a linear formulation. It is well known that absorber design becomes highly nonlinear when the calculation of all design parameters (mass, damper constant, spring constant and location) are performed under one optimization process [1-4]. However the design process can be performed under a linear regime if recent research results are applied such that absorber masses and absorber locations are determined outside the primary design process. The logic supporting this procedure is as follows:

Absorber Mass: The rationale for determination of absorber mass outside the main optimization process is based on research results that show that as the optimization proceeds, the optimum value of absorber mass tends to large values that uniformly

approach 50% of the main system mass [2]. Thus unconstrained optimization procedures tend to large mass values that cannot be applied to LSS design. Typically the LSS requires that non structural mass be restricted to a small percentage of the total system mass. Because of the uniform nature of absorber mass variation as it approaches the optimum, imposition of mass constraints generally results in the optimization procedure riding the constraint boundaries in an attempt to drive the absorber mass toward higher values. The smoothness of the optimization curve and its known tendencies toward large mass values provide the rationale for setting the absorber mass at its maximum allowable value. The problem of optimum mass distribution between two or more absorbers is considered in Section 3.6.

Absorber Placement: The problem of absorber placement can also be addressed outside the main optimization process: One simply determines the troublesome modes that require damping and locates absorbers at positions of maximum modal gain. This procedure is based on knowledge that absorber must experience velocity in order to function properly. Places of maximum velocity occur at station points where the eigenvector has maximum values. From a control perspective, one locates the absorbers at points of maximum modal gain and thus assures maximum excitation of the absorber.

The removal of absorber mass and location from the primary design process leaves the parameters of damper value and spring constant to be determined. These parameters can be determined by feedback control algorithms.

4.1.2 Control Canonical Form

The control canonical form for absorber design is developed in a three step process. First the dynamic equations for a two degree of freedom absorber system are formulated in both scalar and matrix form. Second these equations are placed in block diagram form and the variable parameters are isolated as feedback gain matrices. And finally, block diagram reduction is employed to develop the

absorber canonical form. The development of this form rests on judicious handling of the coupling terms between the dynamic equations of the absorber and the damped structure, and the successful resolution of problems that result from single gain elements appearing in multiple feedback loops.

Step 1. Equation Formulation: The dynamic equations for the absorber and the system may be formulated as shown in Figure 4-1. These equations take the form of coupled second-order differential equations. System I denotes the main system, or the structure to be damped. System II denotes the absorber dynamics for the coupled equations. The main system variables and parameters are denoted by the subscripts 1, and the absorber variables and parameters by the subscripts 2. The symbol, P, represents an external force applied to the system.

Additional insight into the nature of the problem is gained if the combined system dynamics are expressed in matrix form as shown in Figure 4-1. The two second-order differential equations of Systems I and II are expressed as four first-order equations. States 1 and 2 are associated with System I, and states 3 and 4 are associated with System II, the absorber. This decomposition emphasizes the coupling between the two systems: System II, the absorber, drives System I via the Y_2 vector. The isolation and careful handling of these coupling vectors and their corresponding matrices is a key concept for the development of the control canonical form. The entries of each coupling matrix involve k_2 and c_2 multiplied by an appropriate scalar. The significance of this symmetry becomes more pronounced as the development proceeds.

Step 2. Block Diagram Formulation: The system dynamics can be represented in block diagram form as shown in Figure 4-2. The blocks that contain (1/s) represent integrators. Four such integrators are present, one for each of the first-order dynamic equations. The subscripts are associated with parameters and variables as defined previously.

Examination of the block diagram yields several important properties of the damper problem. First it is observed that each

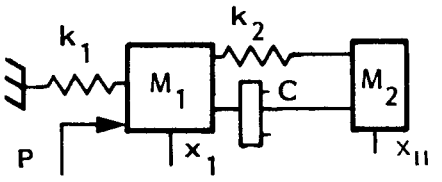

$$\frac{P}{M_1} = \ddot{X}_I + \frac{C_2}{M_1}\dot{X}_I + \frac{K_1 + K_2}{M_1} X_I - \frac{C_2}{M_1}\dot{X}_{II} - \frac{K_2}{M_1} X_{II} \qquad \text{SYSTEM I (MAIN)}$$

$$0 = \ddot{X}_{II} + \frac{C_2}{M_2}\dot{X}_{II} + \frac{K_2}{M_2} X_{II} - \frac{C_2}{M_2}\dot{X}_I - \frac{K_2}{M_2} X_I \qquad \text{SYSTEM II (ABSORBER)}$$

IN MATRIX NOTATION (SYSTEM I)

$$\begin{bmatrix} \dot{X}_1 \\ \dot{X}_2 \end{bmatrix} = \begin{bmatrix} 0 & \\ \frac{-(K_1 + K_2)}{M_1} & -\frac{C_2}{M_1} \end{bmatrix} \begin{bmatrix} X_1 \\ X_2 \end{bmatrix} + \begin{bmatrix} 0 & 0 \\ \frac{1}{M_1} & 1 \end{bmatrix} \begin{bmatrix} P \\ Y_2 \end{bmatrix}; \quad Y_1 = \begin{bmatrix} \frac{K_2}{M_1} & \frac{C_2}{M_1} \end{bmatrix} \begin{bmatrix} X_1 \\ X_2 \end{bmatrix}$$

SYSTEM II

$$\begin{bmatrix} \dot{X}_3 \\ \dot{X}_4 \end{bmatrix} = \begin{bmatrix} 0 & 1 \\ \frac{-K_2}{M_2} & \frac{-C_2}{M_2} \end{bmatrix} \begin{bmatrix} X_3 \\ X_4 \end{bmatrix} + \begin{bmatrix} 0 \\ 1 \end{bmatrix} Y_1 ; \quad Y_2 = \begin{bmatrix} \frac{K_2}{M_2} & \frac{C_2}{M_2} \end{bmatrix} \begin{bmatrix} X_3 \\ X_4 \end{bmatrix}$$

Figure 4-1. Dynamic Equations for 2-DOF Absorber System.

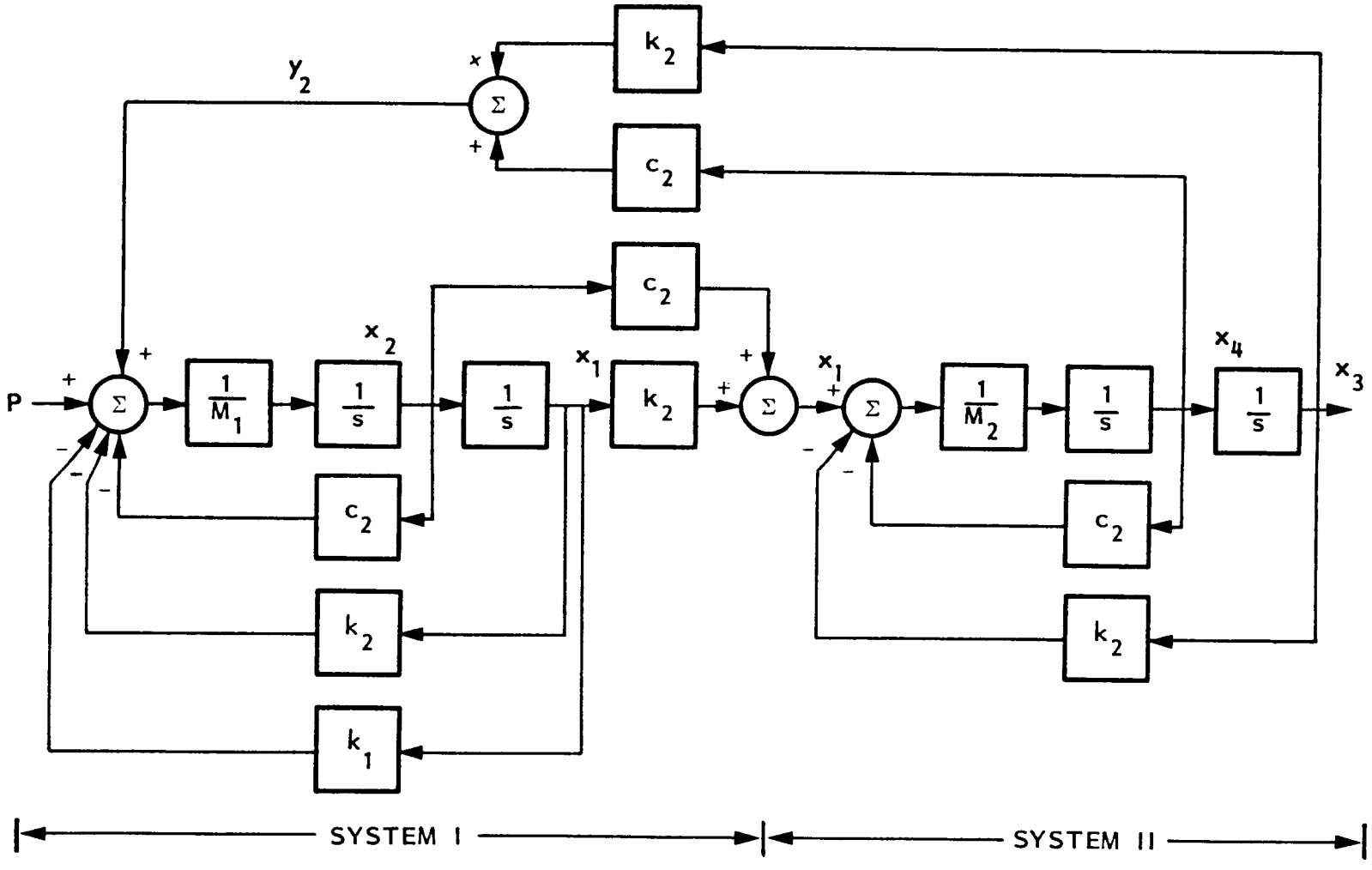

Figure 4-2. Block Diagram of 2-DOF Absorber System Dynamics.

spring constant, k_2, is associated with a deflection and each damper constant, c_2, is associated with a velocity. This structure suggests a well known feedback form ($k_2 + sc_2$) where, s, represents differentiation. This form is representative of output feedback systems having a position loop and a velocity loop.

Additional examination of block diagram signal paths and connection matrices reveals a significant property: All connection elements and feedback elements, with the exception of k_1 are identical. The absorber parameters, c_2 and k_2, form identical feedback structures for both System I and System II. Similarly the feed-forward coupling terms associated with each system are identical. Although these parameters seem to be independent and appear in different system loops, in actuality they are the same parameter appearing simultaneously. This implies that parametric adjustment in one loop yields simultaneous adjustment in every loop containing that parameter.

The multipath gain characteristics are emphasized by the generalized block diagram of Figure 4-3. This form demonstrates the multipath nature of the control problem. The control design gain, K, appears in two inner feedback loops, and forms the coupling matrix between the two systems. The outer feedback loop is positive in nature. Positive feedback loops are generally avoided in practice because of reduced stability margins that can cause system-wide instability. However, stability constraints are not a concern in this design process, for the entire system is guaranteed to remain stable as the passive nature of the absorber guarantees stability. The system dynamic equations are inherently stable for all physically realizable parameter values.

Examination of Figure 4-3, with attention to the outer loop, shows that the gain appears in both the feed forward path and the feedback path. This implies that the gain will appear in the problem formulation as a squared quantity; thus, potential nonlinearity, has reentered the formulation. However, as shown in Step 3, the positive outer loop when combined with Mason's block diagram reduction techniques removes the nonlinearity.

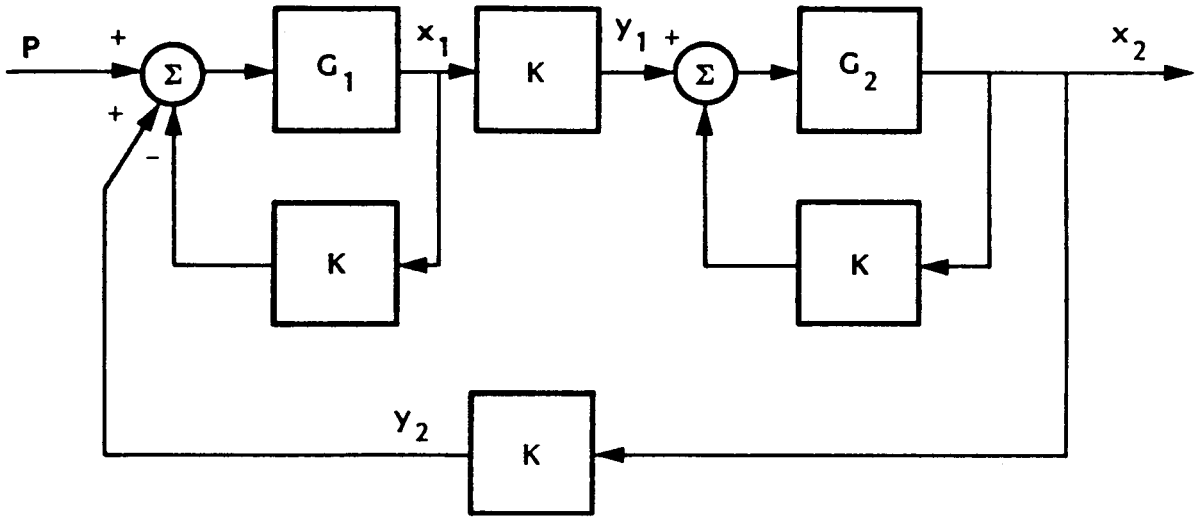

G_1 = MAIN SYSTEM (STRUCTURE)

G_2 = ABSORBER SYSTEM

K = ABSORBER COUPLING PARAMETERS
[SPRING CONSTANTS AND DAMPER VALUES = $(k_2 + sc_2)$]

P = DISTURBANCE INPUT

y_1 = SYSTEM 1 OUTPUT (DEFLECTION)

y_2 = SYSTEM 2 OUTPUT (DEFLECTION)

Figure 4-3. Generalized Multipath Diagram for Absorber Dynamics.

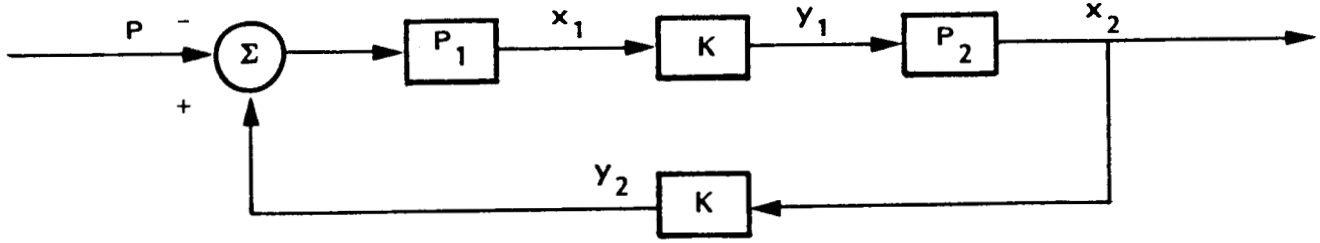

$$P_1 = \frac{G_1}{1 + KG_1} \qquad P_2 = \frac{G_2}{1 + KG_2}$$

$$\frac{x_2}{P} = \frac{K_1 P_1 P_2}{1 - K^2 P_1 P_2} = \frac{K_1 G_1 G_2}{1 + K(G_1 + G_2)} \qquad G_1 = \frac{1}{M_1} \cdot \frac{1}{s^2 + k}$$

$$\frac{x_1}{P} = \frac{P_1}{1 - K^2 P_1 P_2} = \frac{G_1(1 + KG_2)}{1 + K(G_1 + G_2)} \qquad G_2 = \frac{1}{M_2} \cdot \frac{1}{s^2}$$

Figure 4-4. Transfer Function Computation for 2-DOF Absorber System.

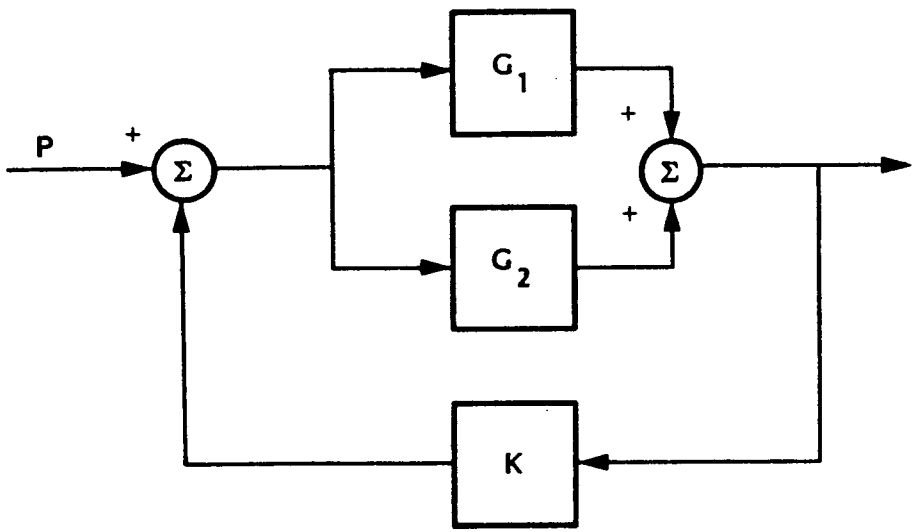

$$K = k_2 + sc_2$$

$$G_1 = \frac{1}{M_1}\left(\frac{1}{s^2 + \omega_o^2}\right) \qquad \omega_o^2 = \frac{M_1}{k_1}$$

$$G_2 = \frac{1}{M_2}\,\frac{1}{s^2}$$

Figure 4-5. Canonical Form for Absorber Roots of 2-DOF Absorber System.

Step 3. Eigenvalue Canonical Form Development: The formation of a canonical form that incorporates absorber effects on system eigenvalues requires determination of the system characteristic equation. This is accomplished by block diagram reduction as shown in Figure 4-4. P_1 and P_2 represent the transfer functions for the structure and absorber respectively with the minor feedback loop incorporated into the expression for the structure. The transfer functions from disturbance input to structural deflection (X_1/P), and disturbance input to absorber deflecton (X_2/P) are developed as shown. The intermediate steps involving P_1 and P_2 illustrate the effects of positive feedback on the outer loop. Substitution of the algebraic relations for P_1 and P_2 in the expressions for the transfer functions and simplifying yields the desired transfer functions in terms of G_1, and G_2. The denominator polynomial of either transfer function is the characteristic equation and contains the required information on system eigenvalues. This expression is linear in the gain K and may be placed in the block diagram form shown in Figure 4-5.

This system has the structure of a simple output feedback control system entailing a single feedback loop, and may be used to synthesize system gains corresponding to absorber parameters. This feedback formulation provides insight to the ability of the absorber to affect system eigenvalues. It should be emphasized that G_2, the transfer function associated with absorber, has the functional form $1/s^2$ and corresponds to the dynamics of the absorber mass without the spring and damper attached. The remaining dynamic elements of the absorber are associated with the feedback loop. The transfer function, G_1, is associated with the structure and has the functional form $1/(s^2 + w_o^2)$ and corresponds to a structural vibration mode. The total system may be viewed as a rigid body mode and a vibration mode that are coupled by an external feedback loop, K.

Absorber Gain Constraints: One additional item requires discussion before proceeding to the control design process; namely, the absorber gain matrix is highly constrained, contains many zero

entries, and repeated elements. This matrix structure leads to a highly constrained output feedback control problem that requires the generalization of feedback control techniques before they can be applied to absorber design. Section 4.5 discusses the problem in detail.

In summary, the simultaneous appearance of system gain elements in multiple loops generates a multipath control problem that severely limits design freedom. This limitation occurs because individual loops cannot be adjusted to meet independent performance specifications. With reference to Figure 4-3, a gain variation in one loop implies simultaneous variation in all loops. The multipath condition exists because the absorber parameters are bidirectional elements that transmit forces in two directions. The absorber parameters operate on the difference of two variables in the system dynamic equations: in the control domain, this implies multiple gain paths. This multiple gain path condition is removed from the formulation by block diagram reduction techniques during development of the root-canonical form thereby rendering the absorber design problem more amenable to control techniques.

4.1.3 Absorber Root Locus

The pole-zero constellation and associated root-locus plot are shown in Figure 4-6. The poles are indicated by x's and the zeros are indicated by o's. The pole frequency at w_o corresponds to the vibration mode of the structure with no absorber attached. A double pole occurs at the origin and corresponds to the absorber mass dynamics. The zeros occur as a result of absorber action and are located at $\pm\ jw_o/(1 + \beta)$ where $\beta = M_1/M_2$ is the ratio of the absorber mass to structural mass. A zero also occurs on the real axis at $-K_2/C_2$ where K_2 is the absorber spring constant and C_2 is the damper value. Zero placement strongly affects the locus behavior, because the closed-loop system poles tend to migrate toward the open-loop system zeros.

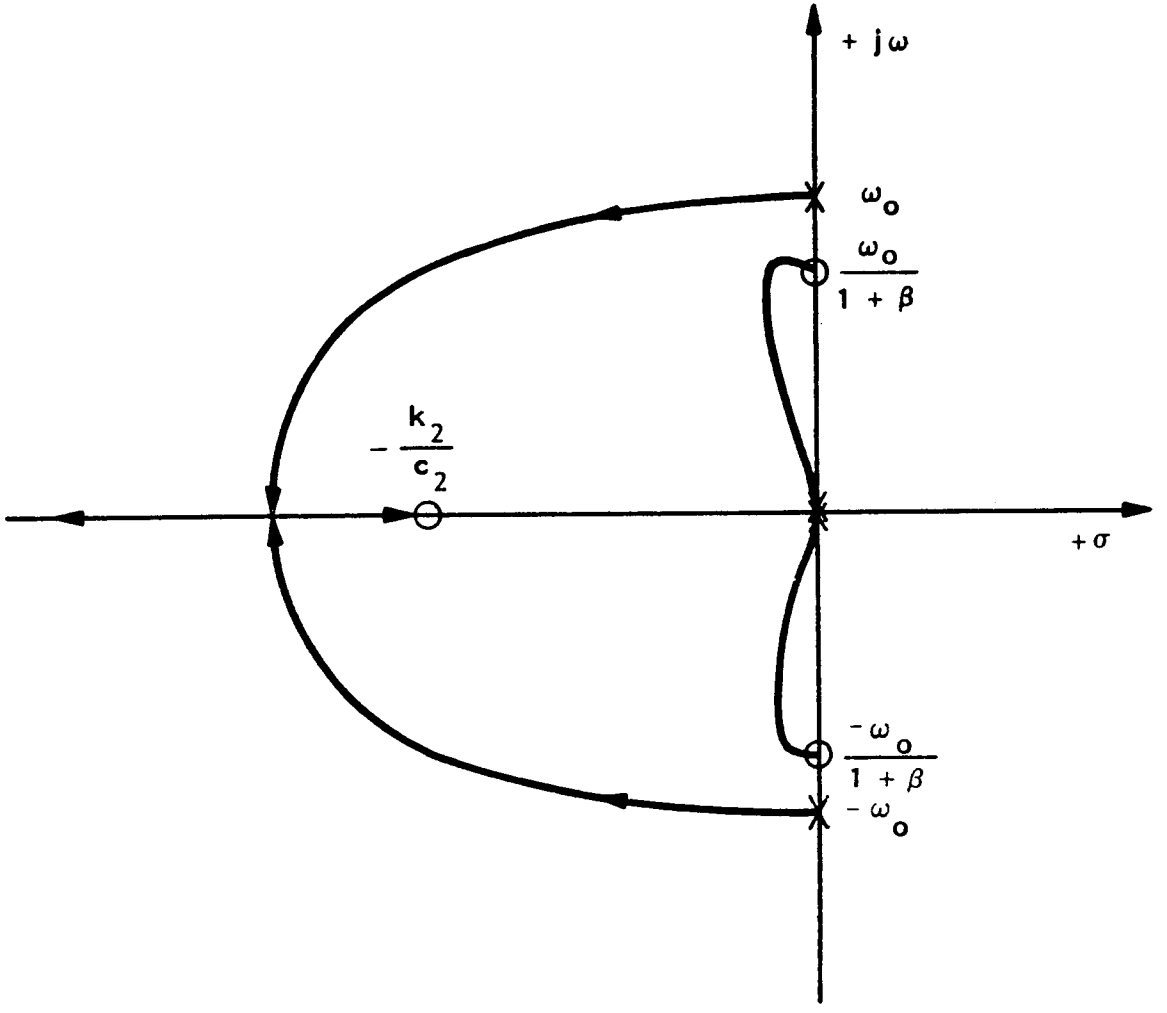

Figure 4-6. Absorber 2-DOF Root Locus Plot.

The root locus exhibits the general properties shown wherein the poles at the origin move toward zeros on the imaginary axis located at $w_o/(1+\beta)$, and the poles on the imaginary axis move toward the real axis. This pattern makes it difficult for one absorber to provide damping for more than one mode. One way to alleviate this situation would be to make the absorber active such that the zero on the real axis would become a complex pair that had an imaginary part approximately equal to the frequency of the modal cluster that required damping. The presence of the complex zero would draw modes of the cluster toward it and thus provide damping.

4.2 Root-Locus Investigation of Absorber Design

This section employs the root-locus to analyze the absorber design process. We study the classical min-max solutions of Timoshenko [10] and Den Hartog [11], and the pole placement procedures employed by Crawley [3-4]. The effect of zero location (damper strength to spring constant ratio) on system performance is also investigated. These studies provide new insight into absorber design.

Illustrative Example: The design example consists of the two degree of freedom system shown in Figure 4-7. The main system parameters are delineated by the subscript, "s", and the absorber parameters are delineated by the subscript, "A". The structural parameters (main system) have been normalized to provide a structural frequency of one radian/sec.

The canonical system that is analyzed with root locus techniques has the structure shown in Figure 4-7. In order to perform a standard gain variation study, the absorber parameters are lumped on the summer output and form the block indicated by $[1 + (c_A/k_A)s]$. The spring constraint, k_A, appears as a variable gain in a separate block. It is this gain that functions as the variable parameter for our root-locus studies. This procedure is equivalent to holding the ratio of c_A/k_A constant; i.e., fixed zero

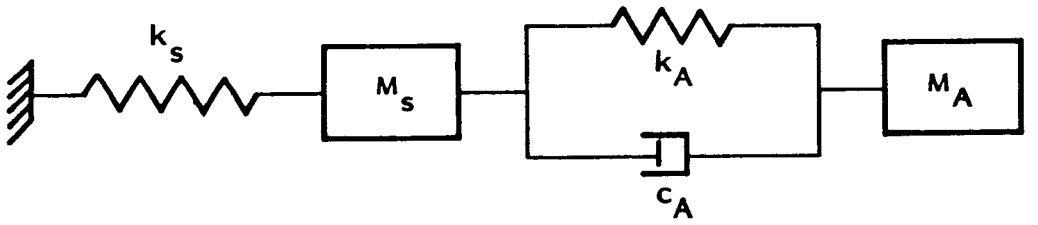

$M_s = 1$ LB
$k_s = 1$ LB/IN. → STRUCTURAL FREQUENCY = 1 RAD/SEC

$M_A = 0.02$ LB

k_A, c_A VARIED – $k_A = 0 \rightarrow 2.6$ LB/IN.

EQUIVALENT SISO SYSTEM FOR ROOT LOCUS

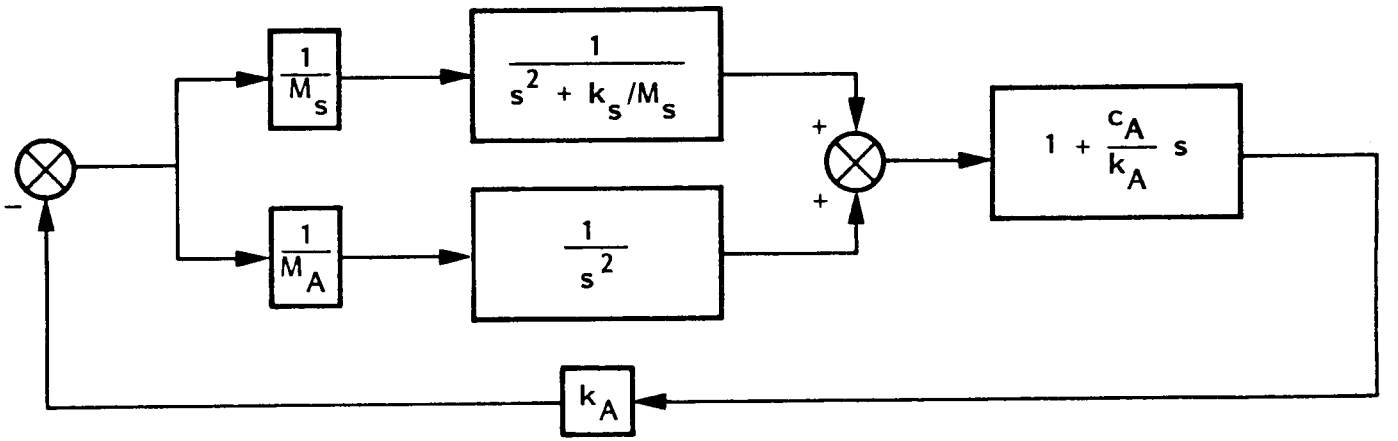

Figure 4-7. Absorber 2-DOF System for Root Locus Analysis.

location, and increasing both the spring constant and damper strength by the identical multiplicative factors.

From a parameter optimization perspective, this root-locus procedure is equivalent to searching the contours of a hypothetical performance criterion along fixed rays. Figure 4-8 illustrates this concept in which the fixed rays emanating from the c_A - k_A origin represent lines of search. These straight lines are equivalent to fixed zero locations on the root locus.

Figure 4-9 depicts the root locus for the illustrative example. The form of the locus corresponds to the general pattern previously shown in Figure 4-6. As the locus is symmetric about the real axis, the locus of the lower half-plane is a mirror image of that of the upper half-plane; accordingly, only the upper half-plane is shown. The area enclosed by the box contains the locus that corresponds to the absorber mass and emanates from the double pole at the origin. This region corresponds to large absorber/system interaction and is of design interest. The remaining portion of the locus leads to high gain designs that ultimately result in absorber lock-up.

Figure 4-10 depicts the expanded region of locus behavior and presents the results of a parametric study on zero location. Recall that zero location is adjusted by variation of the spring constant and relative damper strength. The zero is varied from -20.0 to -2.90 along the real axis. These locations are chosen to bracket the mini-max and pole-placement solutions.

The parametric study provides a general overview of the locus behavior. Each plot has two branches. The upper branch corresponds to the structural mode and proceeds from the imaginary axis with an initial value of 1.0 radian/sec. The lower branch corresponds to the absorber and proceeds from the imaginary axis with an initial value of 0.0 radians/sec. The direction of travel for each branch as the gain increases is as shown. Both roots move into the left half-plane as the gain increases, thus providing increased damping. However an additional increase in gain causes one of the branches to return to imaginary axis thereby reducing damping. The placement of the zero (k_A/c_A ratio) determines which

ROOT LOCUS ANALYSIS

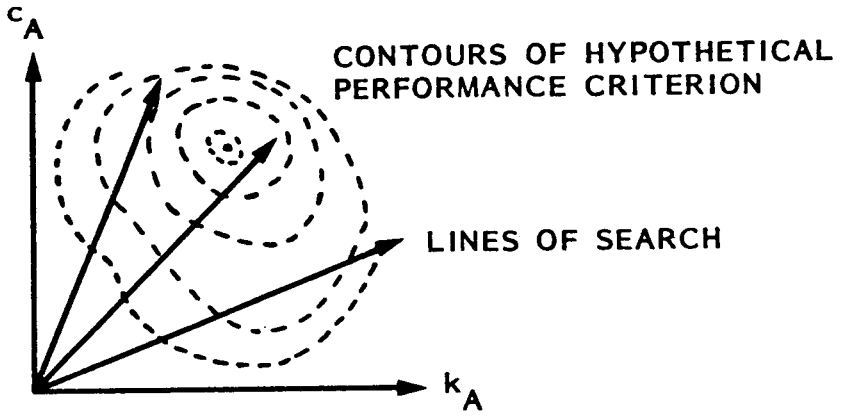

- OBSERVE ROOT LOCUS WITH VARYING k_A AND c_A ALONG PRESCRIBED LINES
- CORRELATE ROOT LOCUS WITH KNOWN OPTIMA FOR 1- AND 2-MODE SYSTEMS

Figure 4-8. Hypothetical Perfomance Criterion Plot for Root Locus Analysis.

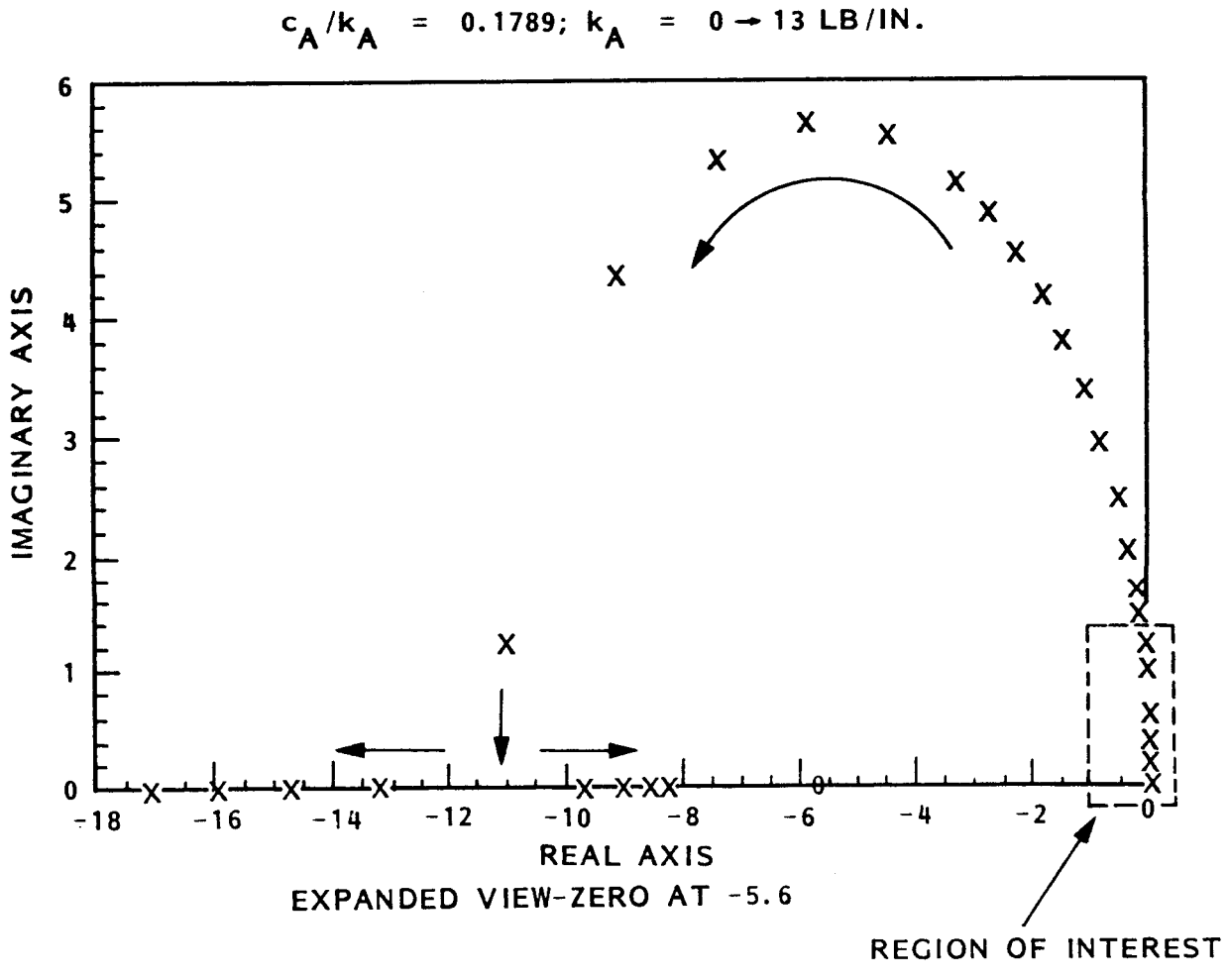

Figure 4-9. Root Locus Expanded View for Minimax Solution.

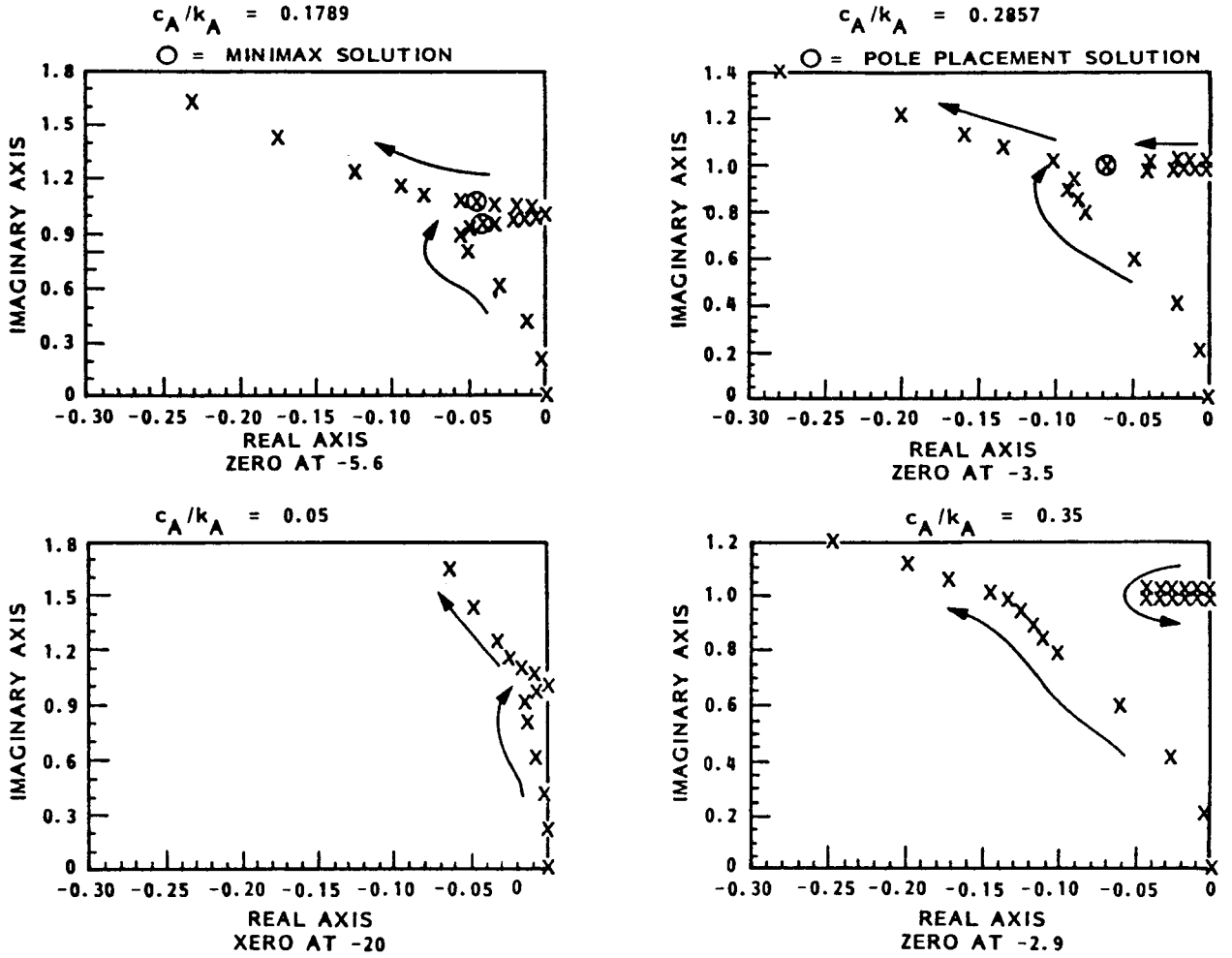

Figure 4-10. Effect of Zero Location on Root Locus of 2-DOF Absorber System.

branch, that associated with structure or that associated with the absorber, returns to the imaginary axis. The zero position strongly influences the left half-plane behavior of each branch. This determines the amount of interaction between the two modes and the ultimate achievable damping for each mode. A good design requires interaction between the two modes such that energy is transferred to the absorber and dissipated across the damping element; i.e., each mode receives a moderate amount of damping. Different optimality criteria achieve these conditions in slightly different manners.

We next consider each plot of Figure 4-10 in detail and proceed clockwise through the charts. Recall that movement of the zero toward the imaginary axis corresponds to increasing the damper strength relative to the spring constraint.

First consider the chart depicting the minimax solution which has a zero at -5.60. The circles indicate roots obtained by application of the classical turning laws [10, 11]. This solution provides maximum interaction between the two modes and leads to the beating phenomenon shown in Figure 4-11. The effect of the zero at this point is to strongly draw the loci into the left-hand plane and thereby produce increased damping. We note that the loci approach each other, but do not intersect.

Next consider the pole placement solution which has a zero at -3.5. Movement of the zero toward the imaginary axis has caused the loci to move further into the left-hand plane and to coalesce. The optimal solution is indicated by the circle enclosing the double pole as shown. The corresponding time response is shown in Figure 4-11. When compared with the pole placement response, we note the absence of the beating phenomenon; i.e., the response decays uniformly to zero.

The next plot has the zero placed at -2.90. A zero this close to the imaginary axis influences that branch of the locus associated with the absorber mass pulling it strongly into the left-hand plane. However, the influence on the structural mode is diminished. The root associated with this mode merely loops back

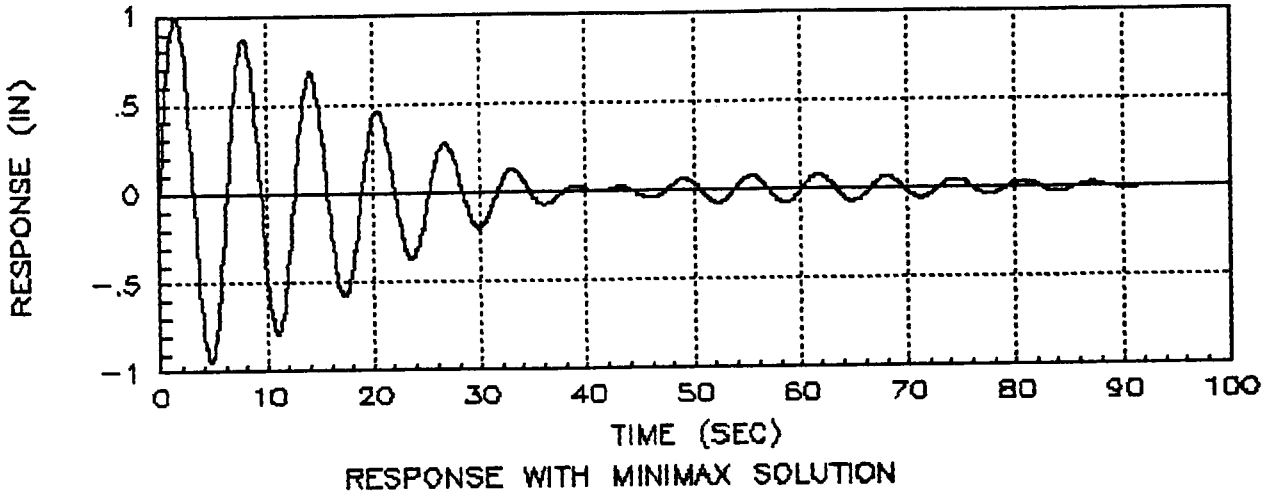

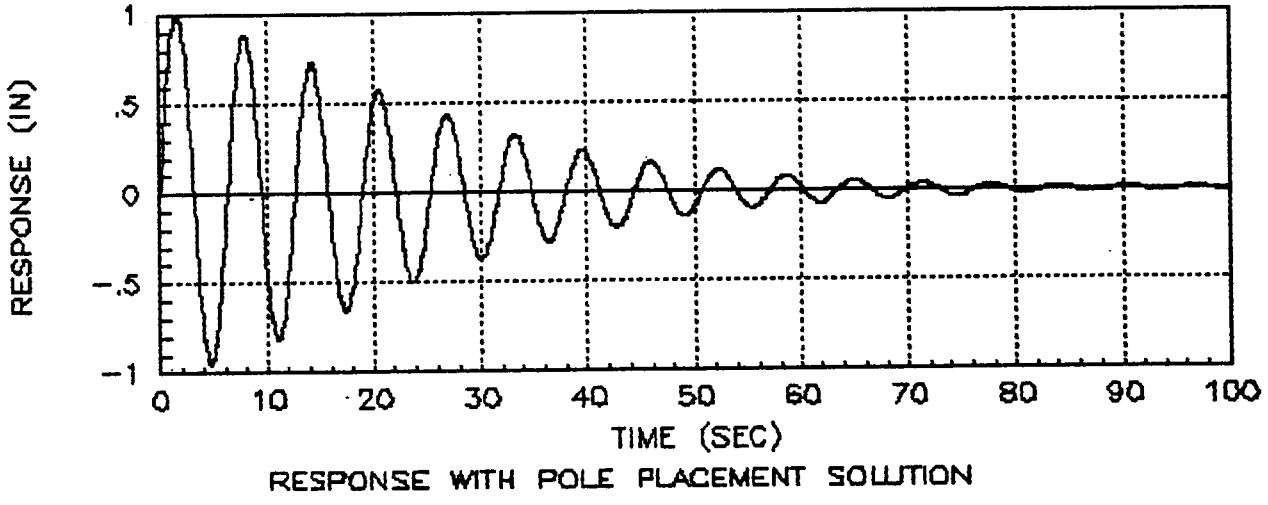

Figure 4-11. Transient Reponse of Structural Mass of 2-DOF Absorber System.

onto itself returning to the imaginary axis. Little interaction occurs between the two modes and performance decreases.

The final plot has the zero placed an extreme distance from the imaginary axis at -20.0; i.e., we have increased the spring constant relative to the damper strength. The zero at this point has reduced influence over the locus branches. Damping and interaction are reduced.

In summary, the root locus is a convenient tool for relating transient response to structural parameters. Movement of the system zero corresponds to adjustment of the spring constant/damper strength ratio. The modal beating effect obtained from classical tuning laws can be analyzed in terms of locus interaction. The method is best applied to two degree of freedom systems that can be analyzed as single input single output (SISO) systems. Subsequent sections deal with the multi-degree of freedom/multi-absorber problem.

4.3 Control Canonical Form for a Finite Element Model

The control canonical form presented in Section 4.1 is developed for a finite element structural model, in preparation for the application of modern control techniques to the multi-DOF, multi-absorber control problem. A simple 2-DOF mass-spring system is analyzed first with an approach which is more direct than that of Section 4.1. The new approach develops the nomenclature for the generalization to the finite element model.

4.3.1 Analysis of the Simple Mass-Spring System

The mass-spring system is shown in Fig. 4-12. The mass, M_S, and spring constant, k_S, define the structure, and M_A, k_A, and c_A define the absorber. The equations of motion for the system are also included in Fig. 4-12.

The control canonical form is obtained by considering the negative of the absorber relative displacement, δ , as the output variable, and the structure inertial displacement and absorber

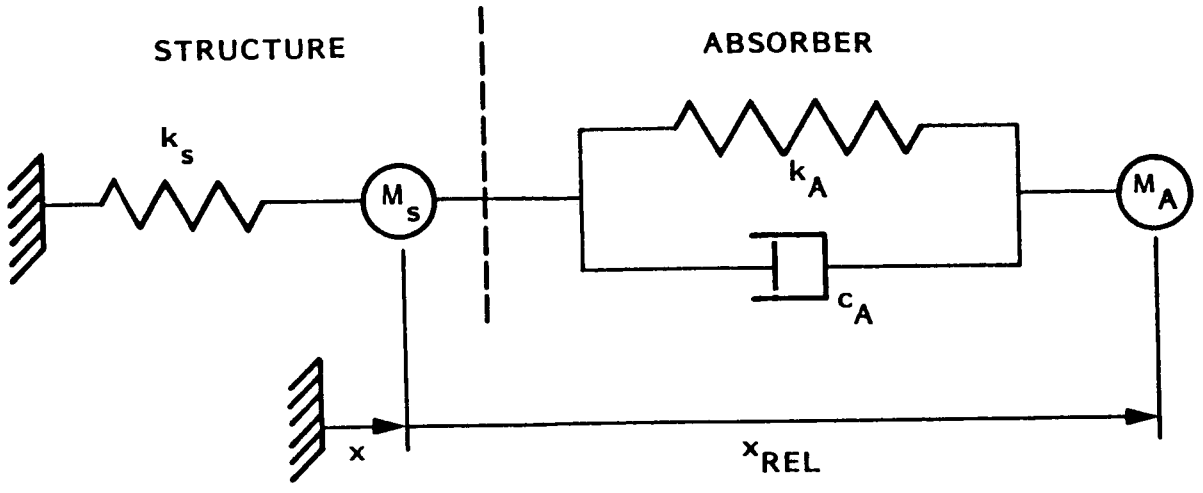

MASS - SPRING SYSTEM DIAGRAM

EQUATIONS OF MOTION

STRUCTURE:

ABSORBER:

$$M_s \ddot{x} = -k_s x + \left[k_A x_{REL} + c_A \dot{x}_{REL}\right]$$

$$M_A (\ddot{x} + \ddot{x}_{REL}) = -\left[k_A x_{REL} + c_A \dot{x}_{REL}\right]$$

COORDINATE TRANSFORMATION:

$$\xi = -(x + x_{REL})$$

$$\delta = -x_{REL}$$

TRANSFORMED EQUATIONS:

$$M_s \ddot{x} + k_s x = -(k_A \delta + c_A \dot{\delta})$$

$$M_A \ddot{\xi} = -(k_A \delta + c_A \dot{\delta})$$

Figure 4-12. Simple Mass-Spring System Equations

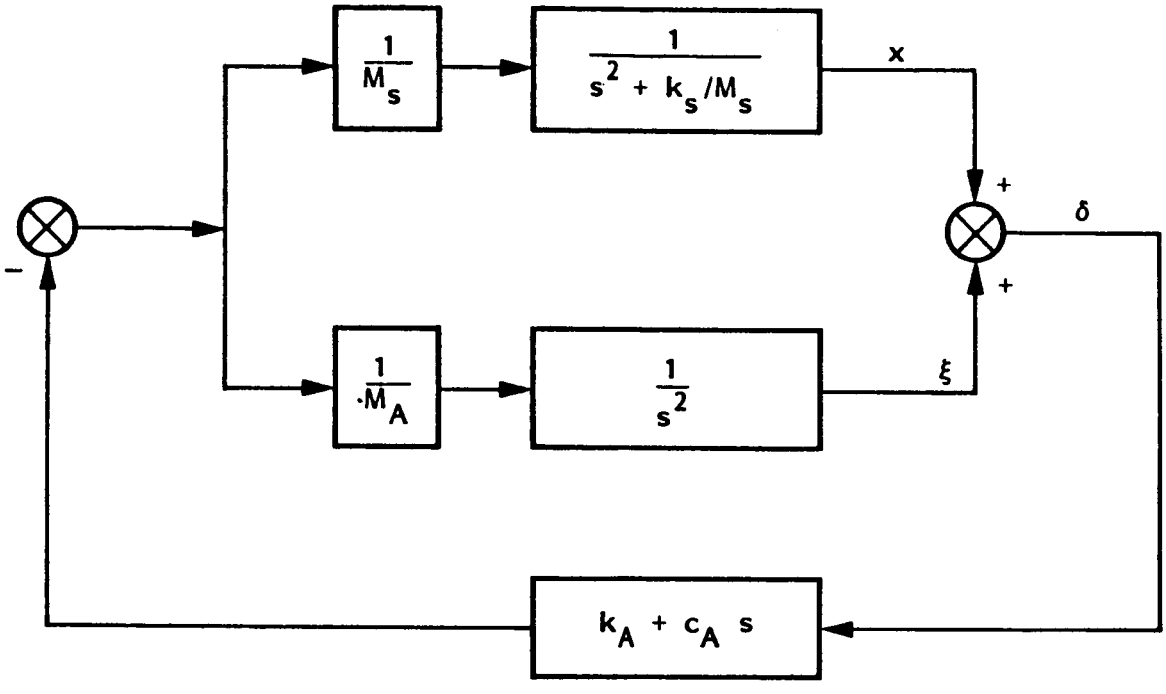

Figure 4-13. Control Canonical Form - Simple Mass-Spring System.

negative inertial displacement, x and ξ , as the state variables. The transformed equations are shown in Fig. 4-12. Note that the transformed equations have essentially decoupled the structure and absorber systems. The control force, applied to both systems, is a function of the relative displacement, $-\delta$, and velocity, $-\dot{\delta}$.

The control canonical form block diagram can be written immediately from the transformed equations in Fig. 4-12, as shown in Fig. 4-13. The input to the structure-absorber system is the absorber control force, u, and the output is the negative of the absorber relative displacement, δ .

4.3.2 Generalization to a Multi-DOF Structure.

The control canonical form for a simple mass-spring system is now extended to the describe the finite element model of a structure with multiple absorbers, Fig. 4-14.

The finite element model (FEM) for a large space structure (LSS) is described by

$$M \ddot{\underset{\sim}{x}} + C \dot{\underset{\sim}{x}} + K \underset{\sim}{x} = \underset{\sim}{R} \qquad (4\text{-}1)$$

where M, C, and K are the mass, damping, and stiffness matrices, respectively, $\underset{\sim}{R}$ is an external force vector, and $\underset{\sim}{x}$ is the vector describing each of the 6 degrees of freedom for all the FEM nodes of the structure.

Eq. (4-1) is transformed to an uncoupled set of differential equations in terms of the natural modes of vibration of the LSS. The transformation is accomplished with a modal transformation matrix Ψ , such that

$$\underset{\sim}{x} = \Psi \underset{\sim}{q} \qquad (4\text{-}2a)$$

The uncoupled equations of motion become

$$\ddot{\underset{\sim}{q}} + 2\Omega Z \dot{\underset{\sim}{q}} + \Omega^2 \underset{\sim}{q} = \Psi^T \underset{\sim}{R} \qquad (4\text{-}2b)$$

where,

$$\Omega^2 = \diagdown\!\!\diagup \omega_i^2 \diagdown\!\!\diagup \qquad (4\text{-}2c)$$

$$2\Omega Z = \diagdown\!\!\diagup 2\, \omega_i\, \zeta_i \diagdown\!\!\diagup \qquad (4\text{-}2d)$$

The ω_i are the natural frequencies of the LSS, and the ζ_i are the modal damping ratios. The columns of Ψ are the eigenvectors of Eq. (4-1).

The objective of the canonical form generalization is the attachment of the absorber dynamics to the FEM of the structure, and expression of the combined system in a form which is identical to that of the spring-mass system, Fig. 4-13. To simplify the formulation, each absorber is restricted to motion along a single degree of freedom, be it a linear or angular displacement. The absorber control force is expressed as a linear function of relative displacement and velocity, and it is added as an external force to the right hand side of Eqs. (4-1) and (4-2b).

The absorbers are placed at nodes of the structure such that absorber motion is parallel to one of the 6 degrees of freedom at a node. The structure displacement corresponding to each absorber is described by

$$x_i = \underset{\sim}{\psi}_i^T \; \underset{\sim}{q}, \qquad i = 1, 2, 3, \ldots, L \tag{4-3}$$

where the $\underset{\sim}{\psi}_i^T$ are rows of Ψ corresponding to the specific x_i.

A consise expression for the absorber locations, x_i, in the state vector, $\underset{\sim}{x}$, is obtained by rearrangement of the modal transformation matrix such that

$$\Psi = \begin{bmatrix} \underset{\sim}{\psi}_1^T \\ \vdots \\ \vdots \\ \underset{\sim}{\psi}_L^T \\ \underset{\sim}{\psi}_{L+1}^T \\ \vdots \\ \vdots \\ \underset{\sim}{\psi}_N^T \end{bmatrix} = \begin{bmatrix} \Psi_A \\ \hline \Psi_R \end{bmatrix} \tag{4-4a}$$

Then,

$$\underset{\sim}{x}^T = [\ x_1 \ \cdots \ x_L \ \vdots \ x_{L+1} \ \cdots \ x_N\ ] = [\ \underset{\sim}{x}_A^T \ \vdots \ \underset{\sim}{x}_R^T\ ] \qquad (4\text{-}4b)$$

where,

$$\underset{\sim}{x}_A = \Psi_A \underset{\sim}{q} \qquad (4\text{-}4c)$$

Likewise, the force on the structure by the absorbers is partitioned so that

$$\underset{\sim}{f} = \begin{bmatrix} \underset{\sim}{f}_A \\ \hline \underset{\sim}{0} \end{bmatrix} \qquad (4\text{-}5)$$

The addition of the absorber force to the structure dynamics, Eqs. (4-2), yields

$$\ddot{\underset{\sim}{q}} + 2\Omega Z \dot{\underset{\sim}{q}} + \Omega^2 \underset{\sim}{q} = \Psi^T \underset{\sim}{R} + [\ \Psi_A^T \ \vdots \ \Psi_R^T\ ] \begin{bmatrix} \underset{\sim}{f}_A \\ \hline \underset{\sim}{0} \end{bmatrix} \qquad (4\text{-}6)$$

$$= \Psi^T \underset{\sim}{R} + \Psi_A^T \underset{\sim}{f}_A$$

The dynamics of the absorbers are expressed as

$$M_A \ddot{\underset{\sim}{\xi}} = \underset{\sim}{f}_A \qquad (4\text{-}7)$$

where $M_A = \{\ m_i\ \}$, $i = 1,\ldots,\ L$ is the matrix of absorber masses, and $\underset{\sim}{\xi}$ is the vector of absorber inertial displacements. The sign convention for $\underset{\sim}{\xi}$ is as described in Section 4.3.1.

The absorber force is expressed as a linear function of the relative absorber displacement and velocity. The relative displacement for a specific absorber is given by $-(\ \xi_i + x_i\ )$, Fig. 4-14,, and the absorber force is given by

$$f_{Ai} = -\ k_i\ (\ \xi_i + x_i\ ) - c_i\ (\ \dot{\xi}_i + \dot{x}_i\ ) \qquad (4\text{-}8a)$$

The force vector for all the absorbers is expressed with the aid of Eq. (4-4b),

$$\underset{\sim}{f}_A = -\ [\ K_A \ \vdots \ C_A\ ] \begin{bmatrix} \underset{\sim}{\xi} + \Psi_A \underset{\sim}{q} \\ \hline \dot{\underset{\sim}{\xi}} + \Psi_A \dot{\underset{\sim}{q}} \end{bmatrix} \qquad (4\text{-}8b)$$

where $K_A = \{ k_i \}$ and $C_A = \{ c_i \}$, i=1,2,...,L.

The structure-absorber equations of motion become

$$\ddot{\underset{\sim}{q}} + 2\Omega Z \dot{\underset{\sim}{q}} + \Omega^2 \underset{\sim}{q} = \Psi^T \underset{\sim}{R} + \Psi_A^T \underset{\sim}{u} \qquad (4\text{-}9a)$$

$$\ddot{\underset{\sim}{\xi}} = M_A^{-1} \underset{\sim}{u} \qquad (4\text{-}9b)$$

$$\underset{\sim}{u} = -[\, K_A \mid C_A \,] \underset{\sim}{y} \qquad (4\text{-}9c)$$

$$\underset{\sim}{y} = \left[\begin{array}{c|c|c|c} \Psi_A & 0 & I & 0 \\ \hline 0 & \Psi_A & 0 & I \end{array}\right] \left[\begin{array}{c} \underset{\sim}{q} \\ \hline \dot{\underset{\sim}{q}} \\ \hline \underset{\sim}{\xi} \\ \hline \dot{\underset{\sim}{\xi}} \end{array}\right] \qquad (4\text{-}9d)$$

For control analysis, Eqs. (4-9) are converted to first order form with the definition,

$$\underset{\sim}{\eta} = \left[\begin{array}{c} \underset{\sim}{q} \\ \hline \dot{\underset{\sim}{q}} \\ \hline \underset{\sim}{\xi} \\ \hline \dot{\underset{\sim}{\xi}} \end{array}\right] \qquad (4\text{-}10)$$

Eqs. (4-9) become

$$\dot{\underset{\sim}{\eta}} = \begin{bmatrix} 0 & I & 0 & 0 \\ -\Omega^2 & -2\Omega Z & 0 & 0 \\ 0 & 0 & 0 & I \\ 0 & 0 & 0 & 0 \end{bmatrix} \underset{\sim}{\eta} + \begin{bmatrix} 0 \\ \Psi_A^T \\ 0 \\ M_A^{-1} \end{bmatrix} \underset{\sim}{u} + \begin{bmatrix} 0 \\ \Psi^T \\ 0 \\ 0 \end{bmatrix} \underset{\sim}{R} \qquad (4\text{-}11a)$$

$$= A \underset{\sim}{\eta} + B \underset{\sim}{u} + E \underset{\sim}{R}$$

$$\underset{\sim}{y} = \begin{bmatrix} \Psi_A & 0 & I & 0 \\ 0 & \Psi_A & 0 & I \end{bmatrix} \underset{\sim}{\eta} = C \underset{\sim}{\eta} \qquad (4\text{-}11b)$$

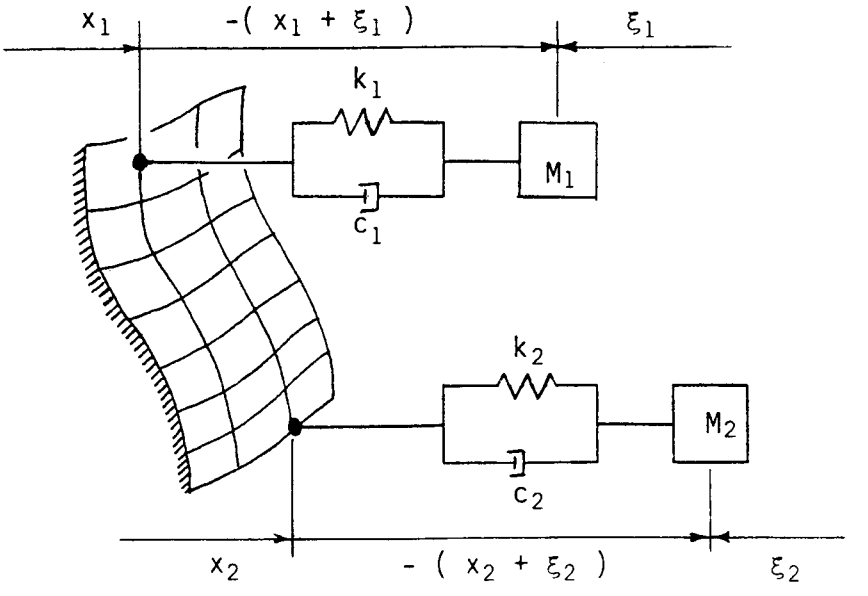

Figure 4-14. Multi-DOF, Multi-Absorber System.

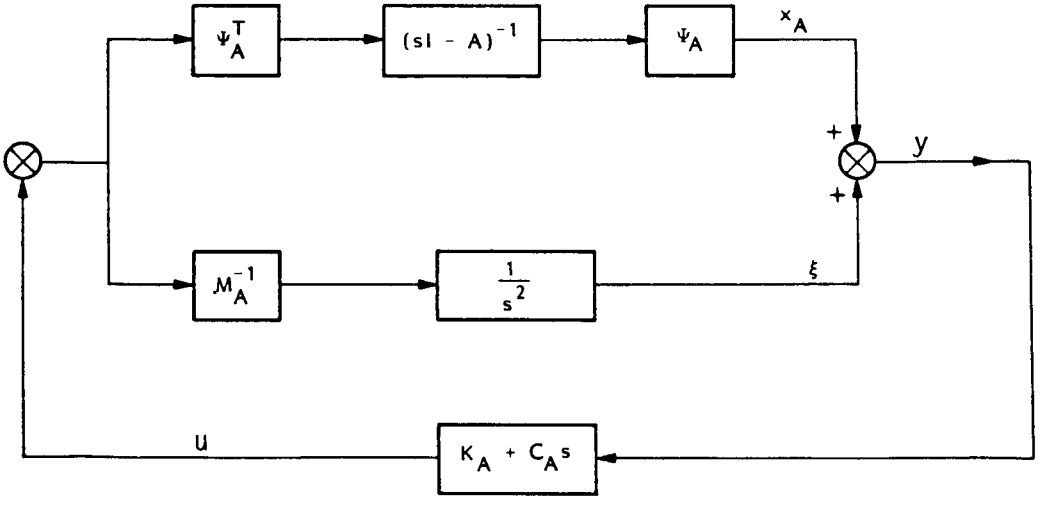

Figure 4-15. Control Canonical Form - Finite Element Structural Model.

$$\underset{\sim}{u} = - [\ K_A \mid C_A\ ]\ \underset{\sim}{y} \qquad (4\text{-}11c)$$

The LSS-absorber system is now expressed in the generalized output feedback canonical form by Eqs. (4-11). A control block diagram for Eqs. (4-11) is presented in Fig 4-15.

4.4 Optimal Output Feedback Formulation

The LSS-absorber system is described by Eqs. (4-11), where the absorber spring and damper constants appear as the output feedback gains, K_A and C_A. The feedback gain matrix,

$$F = [\ K_A \mid C_A\ ] \qquad (4\text{-}12)$$

must be chosen so that the response of the LSS to external disturbances is optimized in some sense.

The goal of the optimization problem is to minimize some perfomance index which penalizes the response - displacement, velocity, or acceleration. The most common performance index applied in linear optimal control theory is the linear quadratic regulator cost functional,

$$J = \int_0^\infty (\ \underset{\sim}{\eta}^T\ Q\ \underset{\sim}{\eta} + \underset{\sim}{u}^T\ R\ \underset{\sim}{u}\ )\ dt \qquad (4\text{-}13)$$

The positive semi-definite matrix Q and positive definite matrix R describe the weighting of the state and control variables in the performance index.

The output feedback form of the performance index is obtained with substitution of Eqs. (4-11c) and (4-12) for $\underset{\sim}{u}$ into Eq. (4-13):

$$J = \int_0^\infty (\ \underset{\sim}{\eta}^T\ [\ Q + C^T F^T R F C\ ]\ \underset{\sim}{\eta}\ )\ dt \qquad (4\text{-}14)$$

The optimal output feedback problem to be solved is

minimize J with respect to F, subject to:

$$\dot{\underset{\sim}{\eta}} = A\,\underset{\sim}{\eta} + B\,\underset{\sim}{u} \qquad (4\text{-}15a)$$

$$\underset{\sim}{u} = -FC\,\underset{\sim}{\eta} \qquad (4\text{-}15b)$$

where the matrices A, B and C are defined in Eqs. (4-11).

4.5 Modern Control Techniques

The linear quadratic regulator problem has been studied extensively, and an exact solution is available for the complete state feedback problem [15]. A sub-optimal solution is also available for the output feedback regulator problem [16].

The performance index, Eq. (4-14), can be expressed in terms of an initial condition vector, and the Lyapunov matrix, P, which is the solution of the Lyapunov equation,

$$(A-BFC)^T P + P\,(A-BFC) + (\,Q + C^T F^T R F C\,) = 0 \qquad (4\text{-}16)$$

Then,

$$J = \underset{\sim}{\eta}_o^T\, P\, \underset{\sim}{\eta}_o \qquad (4\text{-}17)$$

where $\underset{\sim}{\eta}_o$ is the vector of initial conditions. Therefore the performance index, J is an explicit function of the initial state vector.

To eliminate explicit initial condition dependence, J can be minimized over the set of all possible initial conditions. The performance index becomes the expectation of the cost over a uniformly distributed set of initial conditions [17],

$$J = E\,\{\,\underset{\sim}{\eta}_o^T\, P\, \underset{\sim}{\eta}_o\,\} = tr\,[\,P\,] \qquad (4\text{-}18)$$

where tr[] denotes the trace of a matrix. Eq. (4-18) represents an average cost over a set of uniformly distributed initial conditions in state space [17], and provides an upper bound for the

performance cost resulting from any specific initial condition vector.

Solution techniques for the optimal output feedback problem with Eq. (4-18) as the performance index have been examined in the literature [16 - 19]. A sub-optimal solution is presented by Kosut [16], which minimizes the control difference between an optimal state feedback controller, and the equivalent output feedback controller. However, when the observation matrix, C, is not of full rank, as is often the case with a reduced order finite element model, then the solution for the output feedback gain matrix is not unique. In fact, a parametric family of gain matrices is possible [20].

Further complications arise from the constrained structure of the gain matrix, F:

$$F = [\, K_A \mid C_A \,]$$

$$= \left[\begin{array}{cccc|cccc} k_1 & 0 & \cdots & 0 & c_1 & 0 & \cdots & 0 \\ 0 & k_2 & \cdots & 0 & 0 & c_2 & \cdots & 0 \\ \vdots & & & \vdots & \vdots & & & \vdots \\ 0 & 0 & \cdots & k_L & 0 & 0 & \cdots & c_L \end{array}\right] \qquad (4\text{-}19)$$

In general, an optimal output feedback solution such as Kosut's will return a fully populated matrix. Physically, this feedback structure implies that there exists a set of actuators, and a set of sensors such that each actuator obtains information from all the sensors. However, the LSS-absorber problem is similar to a local feedback control problem, in which each actuator only obtains information from a colocated sensor. The LSS problem differs from the local feedback control problem by the fact that the actuator force is applied to both the sensor location on the structure, and the corresponding absorber mass. This leads to the coupled control problem previously discussed in Sec. 4.1.

4.6 Parameter Optimization

The optimal output feedback control problem stated by Eqs. (4-15),(4-16), and (4-18) can be approached with parameter optimization techniques. Numerical optimization algorithms, such as steepest descent or quasi-Newton, vary the elements of the gain matrix, F, until a minimum of the performance index is reached. Only the non-zero elements of F are varied, therefore the result of the optimization is the optimal constrained feedback gain matrix as given in Eq. (4-19).

4.6.1 Statement of the Parameter Optimization Problem

The parameter optimization problem is obtained from Eqs. (4-15), (4-16), and (4-18):

$$\min_{F}\{ J \} = \min \{ \mathrm{tr}[P(F)] \}$$

subject to:

$$A_o^T P + P A_o + Q = 0$$

$$A_o = A - BFC \qquad (4\text{-}20)$$

Note that the explicit weight, R, on the control vector is set to zero, since the control effort is implicitly constrained by the absorber dynamics which are included in the closed loop plant matrix, A_o. The implicit constraint on the control effort is a result of the limitations placed on the control force by the finite absorber mass and the absorber dynamics.

The gradient of J with respect to components of F for the problem stated by Eqs. (4-20) can be computed through the solution of an additional Lyapunov equation for A_o^T [17,21],

$$A_o L + L A_o^T + I = 0 \; . \qquad (4\text{-}21)$$

$$\hat{\nabla} J = - 2 \, \mathrm{col}\{ B^T P L C^T \} \qquad (4\text{-}22)$$

where col{} is a column vector composed of all the elements of the gradient matrix which correspond to non-zero elements of F (e.g., Eq. 4-19). Likewise,

$$\underset{\sim}{v} = \text{col}\{\ F\ \} \tag{4-23}$$

is a vector composed of the spring and damper constants for all the absorbers.

4.6.2 Quasi-Newton Method Description

A quasi-Newton method is chosen to perform the optimization. The quasi-Newton method builds an approximate local quadratic model of the objective function, and proceeds to find the minimum of the model. The method is applicable when an analytic or semi-analytic gradient is available for the objective function, and offers faster convergence than a steepest descent method.

As with most Newton-type optimization methods, the search for the minimum is performed in two steps: (1) choose a search direction, and (2) find the minimum of the function along the search direction. The choice of search direction depends on the method used. For a quasi-Newton method, the search direction is obtained from second derivative information. Consider a hypothetical function W with gradient DW and Hessian (second derivative matrix) D^2W. Then, a local quadratic approximation for W is

$$W(\underset{\sim}{x}) = W(\underset{\sim}{x}_o) + DW(\underset{\sim}{x}_o)\ \delta\underset{\sim}{x} + 1/2\ \delta\underset{\sim}{x}^T\ D^2W(\underset{\sim}{x}_o)\ \delta\underset{\sim}{x} \tag{4-24}$$

A necessary condition for a minimum of W is $DW(\underset{\sim}{x})=0$. The $\delta\underset{\sim}{x}$ which satisfies this condition is

$$\delta\underset{\sim}{x}^T = -[\ D^2W(\underset{\sim}{x}_o)\ ]^{-1}\ DW(\underset{\sim}{x}_o) \tag{4-25}$$

where $\delta\underset{\sim}{x}$ is the new search direction.

Once the search direction is computed, a univariate minimization, often called a line search, is performed to find a minimum of the objective function along the search direction.

The Hessian is approximated from previous function values and gradients. At the first iteration the Hessian is the identity matrix. At subsequent iterations, the Hessian is updated according to the formula given in Ref. [21]. When the Hessian update becomes ill-conditioned a restart is performed, and the Hessian is reset to the identity matrix.

A simplified flow diagram for the quasi-Newton algorithm is presented in Fig. 4-16.

4.6.3 Convergence Criteria

The convergence criteria for the optimization algorithm regulate the accuracy of the solution. The necessary condition for a minimum is

$$\tilde{\nabla} J = 0 \qquad (4\text{-}26)$$

The imposition of this condition alone, however, may place unreasonable convergence requirements on the algorithm. More practical criteria are placed on the change of the performance index, and the spring and damper constants, over consecutive iterations. When the relative difference of the values over an iteration is smaller than specified tolerances, the optimization is stopped. Thus the algorithm is prevented from attempting to satisfy Eq. (4-26) to some tolerance, when the change in spring and damper constants is insignificant for consecutive iterations.

The implemented convergence criteria are

$$(1)\ \left\| \tilde{\nabla} J \right\| < \varepsilon_1$$
$$(2)\ \| \underset{\sim}{v}_{k+1} - \underset{\sim}{v}_k \| \ / \ \| \underset{\sim}{v}_k \| < \varepsilon_2$$
$$(3)\ | J_{k+1} - J_k | \ / \ | J_k | < \varepsilon_3$$

where ε_1, ε_2, ε_3 are specified tolerances.

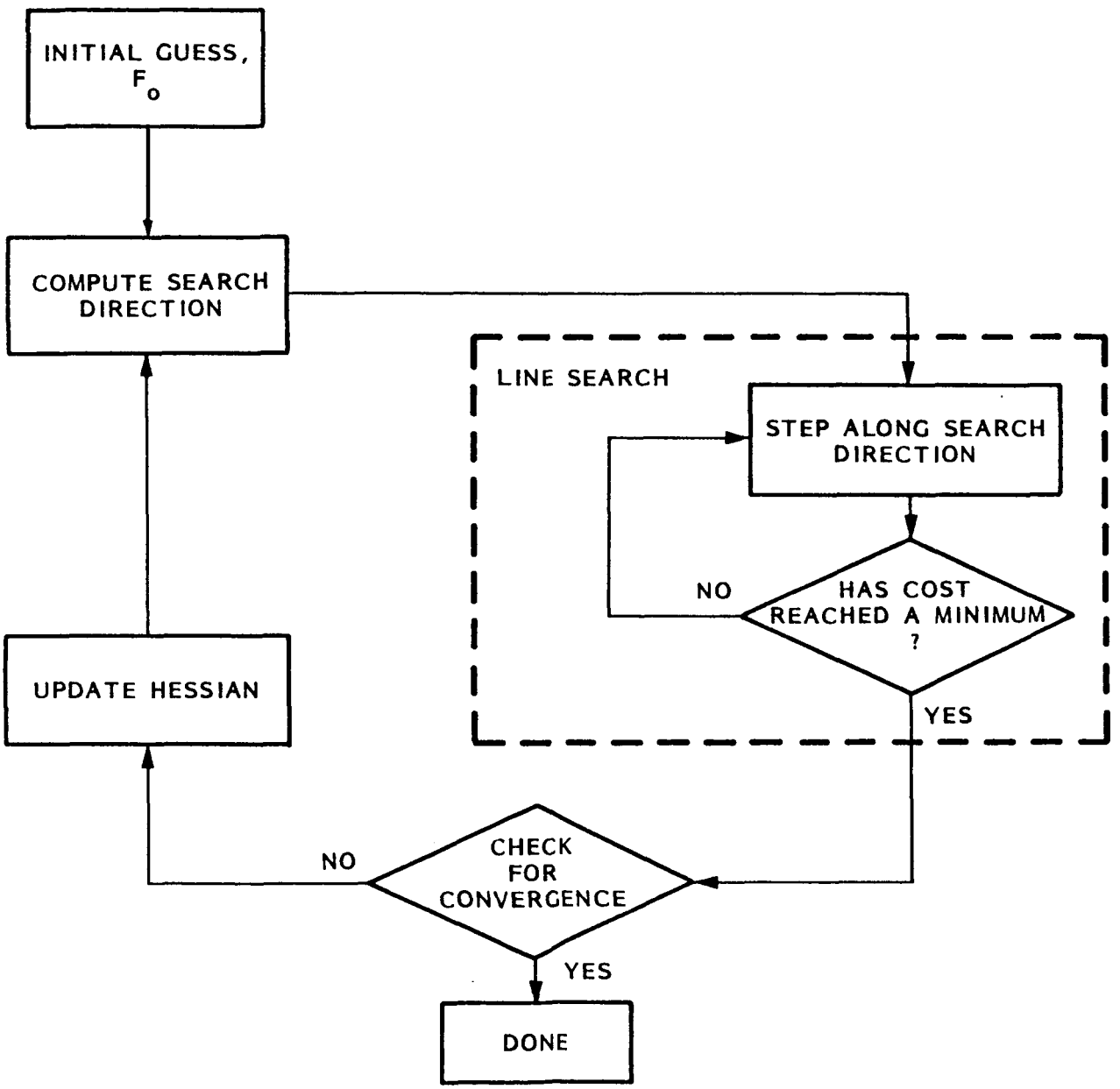

Figure 4-16. Quasi-Newton Algorithm Flow Diagram.

4.6.4 Example Problem

The parameter optimization algorithm is applied to the simple mass-spring system of Fig. 4-12. The system parameters are M_s = 1 lb., k_s = 1 lb/in, M_A = 0.02 lb.

The system equations are

$$\dot{\underset{\sim}{\eta}} = \begin{bmatrix} 0 & 1 & 0 & 0 \\ -1 & 0 & 0 & 0 \\ 0 & 0 & 0 & 1 \\ 0 & 0 & 0 & 0 \end{bmatrix} \underset{\sim}{\eta} + \begin{bmatrix} 0 \\ 1 \\ 0 \\ 50 \end{bmatrix} \underset{\sim}{u} \qquad (4\text{-}27a)$$

$$\underset{\sim}{u} = - \begin{bmatrix} k_a & c_a \end{bmatrix} \begin{bmatrix} 1 & 0 & 1 & 0 \\ 0 & 1 & 0 & 1 \end{bmatrix} \underset{\sim}{\eta} \qquad (4\text{-}27b)$$

with cost weighting matrix,

$$Q = \begin{bmatrix} 1 & 0 & 0 & 0 \\ 0 & 0 & 0 & 0 \\ 0 & 0 & 0 & 0 \\ 0 & 0 & 0 & 0 \end{bmatrix} \qquad (4\text{-}27c)$$

The structural displacement alone is penalized in the cost weighting matrix.

A 3-dimensional plot of J vs. k_a and c_a is presented in Fig. 4-17. The optimization algorithm consistently converges to the values

$$k_a = 0.975 \text{ lb/in}$$
$$c_a = 0.139 \text{ lb-sec/in}$$

for various initial estimates of k_a and c_a.

The algorithm solution is compared to the steady state minimax and pole placement solutions (Sec. 3.2) in Fig. 4-18, along with the corresponding transient responses to an impulse. The steady state minimax response exhibits a smaller amplitude for the second beat (between 40 and 80 seconds) than the parameter optimization

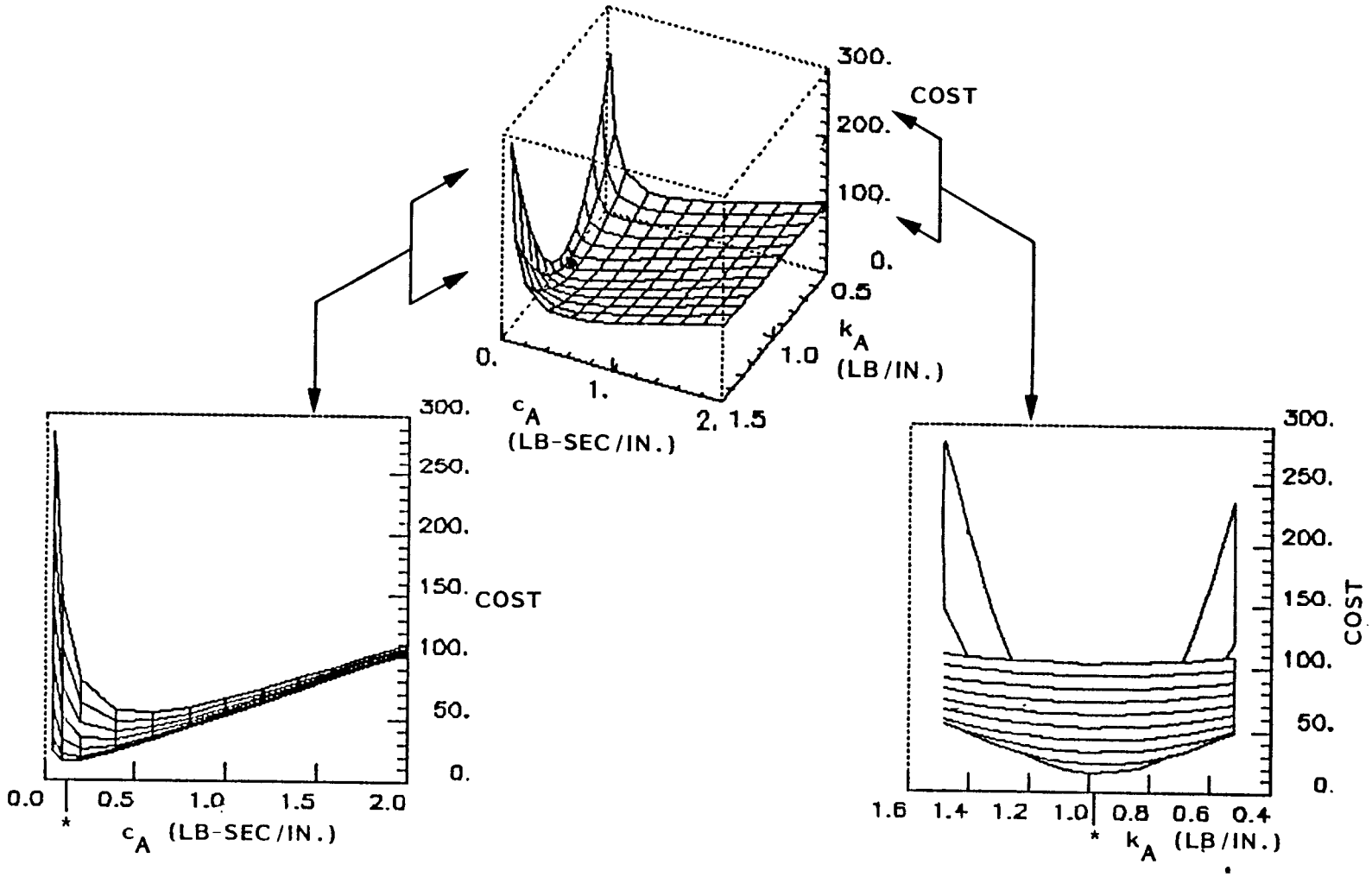

Figure 4-17. Performance Index Plot for Simple Mass-Spring System.

	k_A (LB/IN.)	c_A (LB-SEC/IN.)
ALGORITHM	0.975	0.139
POLE PLACEMENT	0.961	0.137
MINIMAX	0.961	0.086

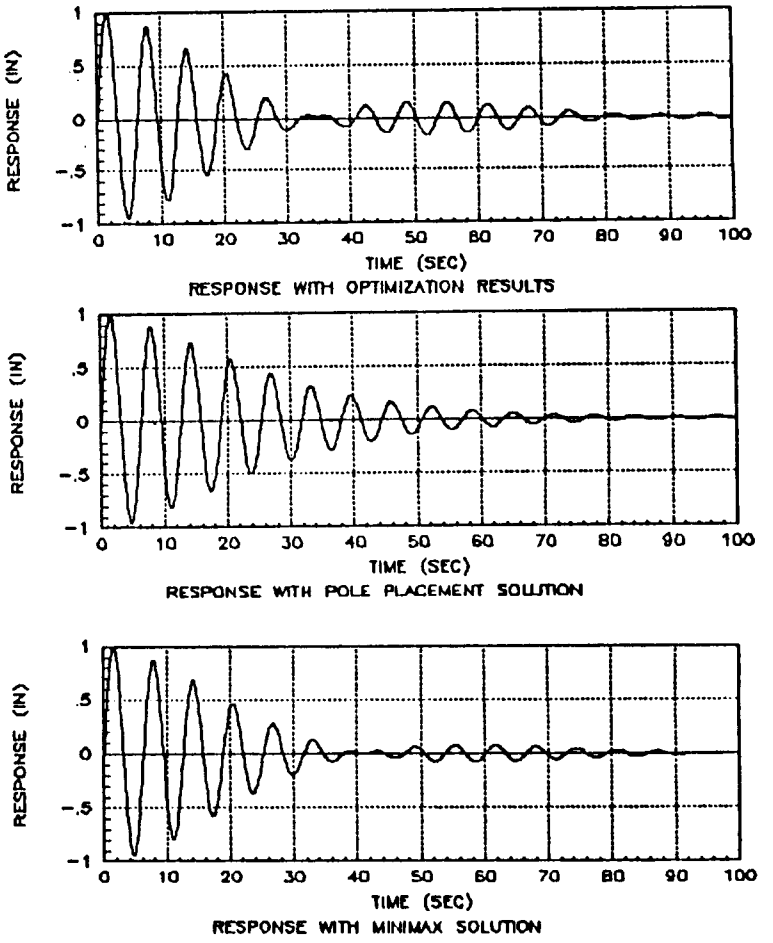

Figure 4-18. Transient Response Comparison for Paramter Optimization Algorithm Solution.

response. However, the parameter optimization response decays to zero amplitude in 35 sec. as compared to 40 sec. for the steady state minimax response. The performance difference between the parameter optimization and steady state minimax solutions is linked to the structure of the performance index for the parameter optimization, which is discussed in the next section.

4.6.5 Comments on the Performance Index

The behavior of the optimization on the sample problem, and also the space station application problems in Section 5, highlights an implicit constraint imposed by the performance index,

$$J = E\{ \underset{\sim}{\eta}_o^T P \underset{\sim}{\eta}_o \} = tr[P] \qquad (4\text{-}30)$$

where, $\underset{\sim}{\eta}_o^T = [\underset{\sim}{q}_o^T \dot{\underset{\sim}{q}}_o^T \underset{\sim}{\xi}_o^T \dot{\underset{\sim}{\xi}}_o^T]$. As discussed in Section 4.5, J is an upper bound for the performance cost resulting from any one specific initial condition vector, say an impulse at a specific location on the structure.

The Lyapunov matrix, P can be sectioned so that

$$P = \left[\begin{array}{c|c} P_q & P_{q\xi} \\ \hline P_{q\xi} & P_\xi \end{array}\right] \qquad (4\text{-}31)$$

Then,

$$J = E\{ [\underset{\sim}{q}_o^T \dot{\underset{\sim}{q}}_o^T] P_q \left[\begin{array}{c} \underset{\sim}{q}_o \\ \dot{\underset{\sim}{q}}_o \end{array}\right] + [\underset{\sim}{\xi}_o^T \dot{\underset{\sim}{\xi}}_o^T] P \left[\begin{array}{c} \underset{\sim}{\xi}_o \\ \dot{\underset{\sim}{\xi}}_o \end{array}\right] \qquad (4\text{-}32a)$$

$$+ (\text{cross-terms in } P_{q\xi}) \}$$

or,

$$J = tr[P_q] + tr[P_\xi] = J_1 + J_2 \qquad (4\text{-}32b)$$

The component J_1 of J represents the cost associated with a disturbance applied directly to the structure. The component J_2 of J represents the cost associated with a disturbance applied to the absorber masses. A disturbance applied to an absorber mass causes absorber motion, and structural excitation. Even though the absorber motion may not be penalized in the cost weighting matrix, Q, the structural excitation will contribute to the perfomance cost J_2. This contribution to J_2 is significant relative to J_1 when the absorber disturbance excites natural modes of the structure-absorber system which are significant components of the structural response.

The energy transmission property of the absorbers may cause mis-tuning, when the transmitted energy excites significant modes of the structure. The removal of this implicit constraint on the performance index, J, and the generalization of the tuning algorithm presents an interesting topic for future study.

4.7 Uncoupled Dynamic Optimization vs. Parameter Optimization.

The uncoupled dynamic optimization formulation provides a simple method of computation of the optimal parameters for several absorbers, by tuning each absorber to a specific mode of vibration. Embedded in the formulation (Sec. 3.6) is the computation of the optimal mass distribution among the absorbers.

The major obstacle, however, which limits the use of the uncoupled dynamic optimization technique on a multi-mode structure with multiple absorbers is the cross-coupling between modes through the absorbers; i.e., the control force of each absorber affects more than one mode, and the displacement and velocity input to each absorber includes more than one mode. The cross-coupling effect is depicted in Fig 4-19, in which a two-mode FEM with two absorbers is shown in control canonical form. Each absorber is assumed to be tuned to one of the modes. The dash lined boxes isolate the 2 absorber-mode systems, while the double-line paths indicate the cross-coupling between mode-absorber systems. The influence coefficients, ψ_{ij}, relate the modal amplitudes to physical

displacements and velocities, and also specify the influence on each of the modes of an input at a physical location.

When the cross-coupling influence coefficients are negligible, the uncoupled dynamic optimization yields the optimal mass distribution and a nearly optimal response. This is the basic assumption of the uncoupled dynamic optimization technique. The parameter optimization algorithm includes the effects of cross-coupling to the extent allowed by the reduced order finite element model.

A comparison of the uncoupled dynamic optimization and the parameter optimization methods of computing the optimal absorber parameters is performed in the next section for several space station application problems.

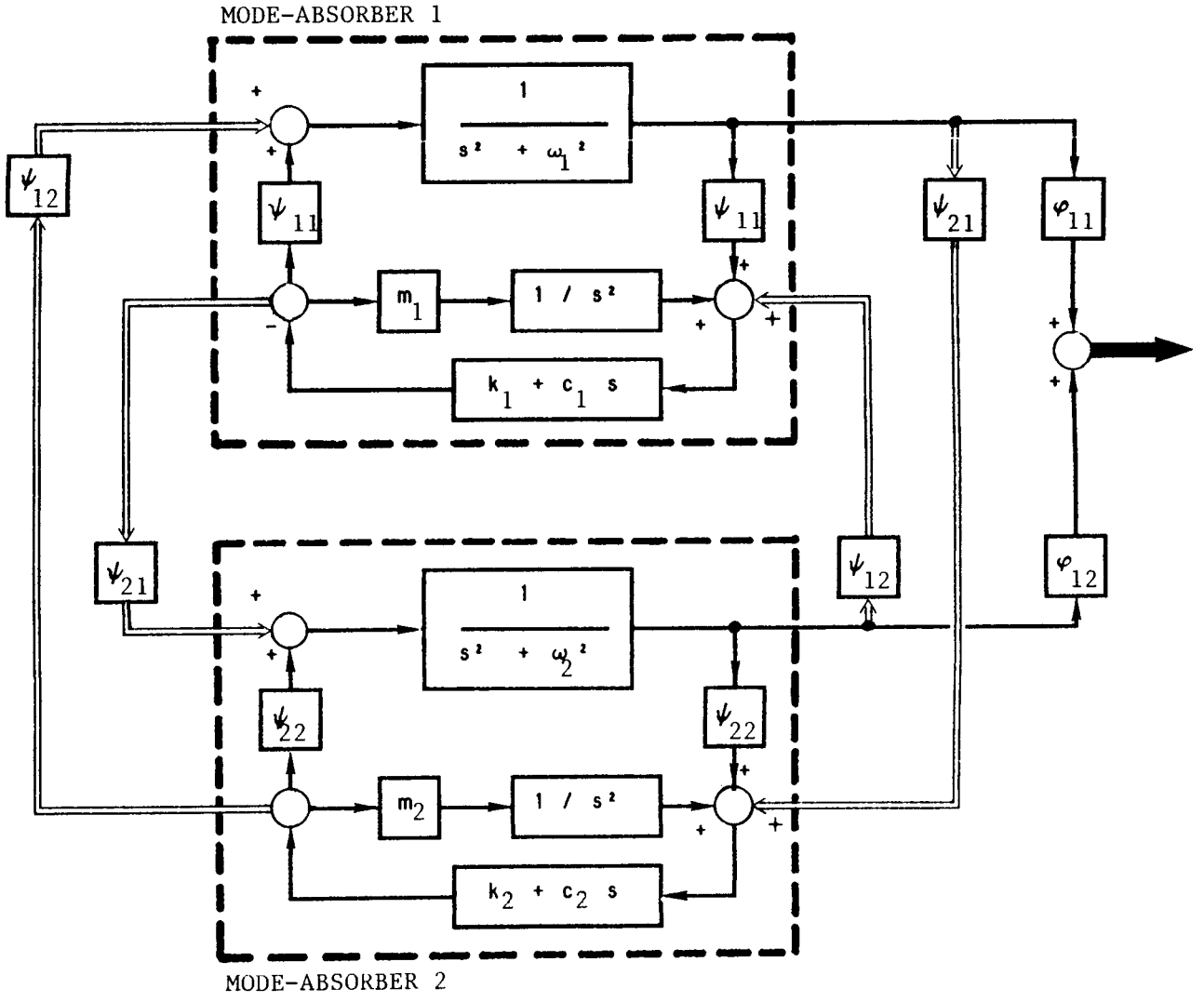

Figure 4-19. Control Canonical Form for 2-Mode, 2-Absorber System.

SECTION 5
SPACE STATION APPLICATIONS

The optimization techniques described in the previous sections are applied to example vibration damping problems on the NASA dual keel configuration Space Station. Two example cases are considered, which evaluate the capabilities of the uncoupled dynamic optimization and the parameter optimization algorithms: (1) micro-g acceleration response at the lab module, and (2) pointing response at a location on the Earth-viewing (lower) payload boom. The disturbance input for both cases is a unit impulse at the habitation module. The force input at this location simulates either a shuttle docking, or crew motion disturbance, depending on the strength of the impulse. The inherent structural damping is assumed to be 0.5%.

In order to examine the performance of the optimization techniques on multi-absorber problems, two absorbers are employed in each of the example problems. The application of two absorbers facilitates the interpretation and expression of the results using two-dimensional plots, and simplifies the interpretation of the dynamic interactions between structure and absorbers.

The results of the example cases provide insight into the optimization techniques, and also quantify some of absorber design parameters, such as spring constants, damper constants and absorber strokes.

5.1 Space Station Finite Element Model

The Space Station finite element model (FEM) describes the dynamics of the IOC version of the Space Station during the phase B evolution as of January, 1986 (Fig. 5-1a). The model is characterized by a 5M erectable truss in the dual keel configuration with the modules placed above the transverse boom. It should be noted that at this writing, a later version of the IOC Space Station configuration has been developed which includes a combination of solar voltaic and solar dynamic power generators on

the transverse boom, and a slightly different module arrangement. Consequently, the model used in the present study does not reflect the latest space station configuration, and the cases studied should be treated as examples only. For the same reason, the construction of the FEM model is not presented in great detail.

The FEM model, shown in Fig. 5-2 without payloads and servicing bays for clarity, employs equivalent beam reperesentations of the 5M erectable truss. The EAL/SPAR finite element code is used. Table 5-1 lists the properties of the model.

Dynamic analysis of the model yields a large number of free-free modes. Primary structural modes are selected by examination of the modal component strain energy rankings and animated mode shape displays. Fig. 5-2 shows side views of the primary modes selected, from a perspective of looking down the Y-axis.

5.2 The Acceleration Response Problem

The stringent micro-g level requirement on the accelerations at the lab module is one of the design drivers which prompted the configuration change from the power tower to the dual keel configuration of the Space Station. The absorber optimization algorithms are applied to minimize the transient lab module acceleration response in the Z-direction (Fig. 5-1b). An arbitrary value for the total absorber mass budget of 1 snail (386 lb.) is assumed.

The spectral composition of the lab module acceleration response is shown in Fig. 5-3. Modes 27, 28, 31 and 40 contribute most significantly to the response. The actual open loop impulse response is shown in Fig. 5-6a.

The two absorbers are located so that the influence of each absorber on a particular mode is maximized (i.e., the absorber is placed at a maximum of the mode shape). The location of the absorbers is shown in Fig. 5-1b. The chosen locations allow both absorbers to influence modes 28, 31, and 40 significantly.

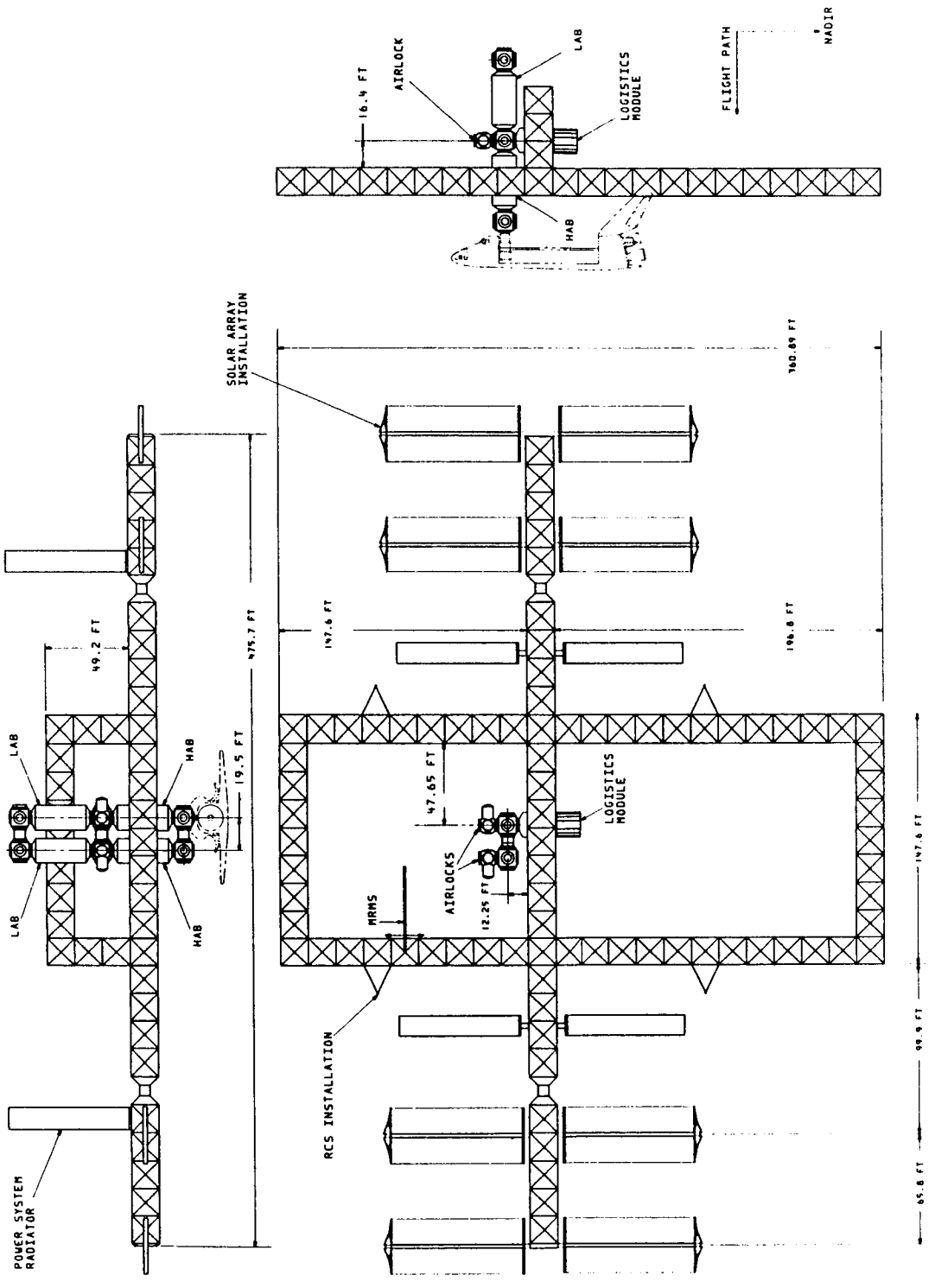

Figure 5-1a. IOC Dual Keel Space Station with 5M Erectable Truss.

C-2

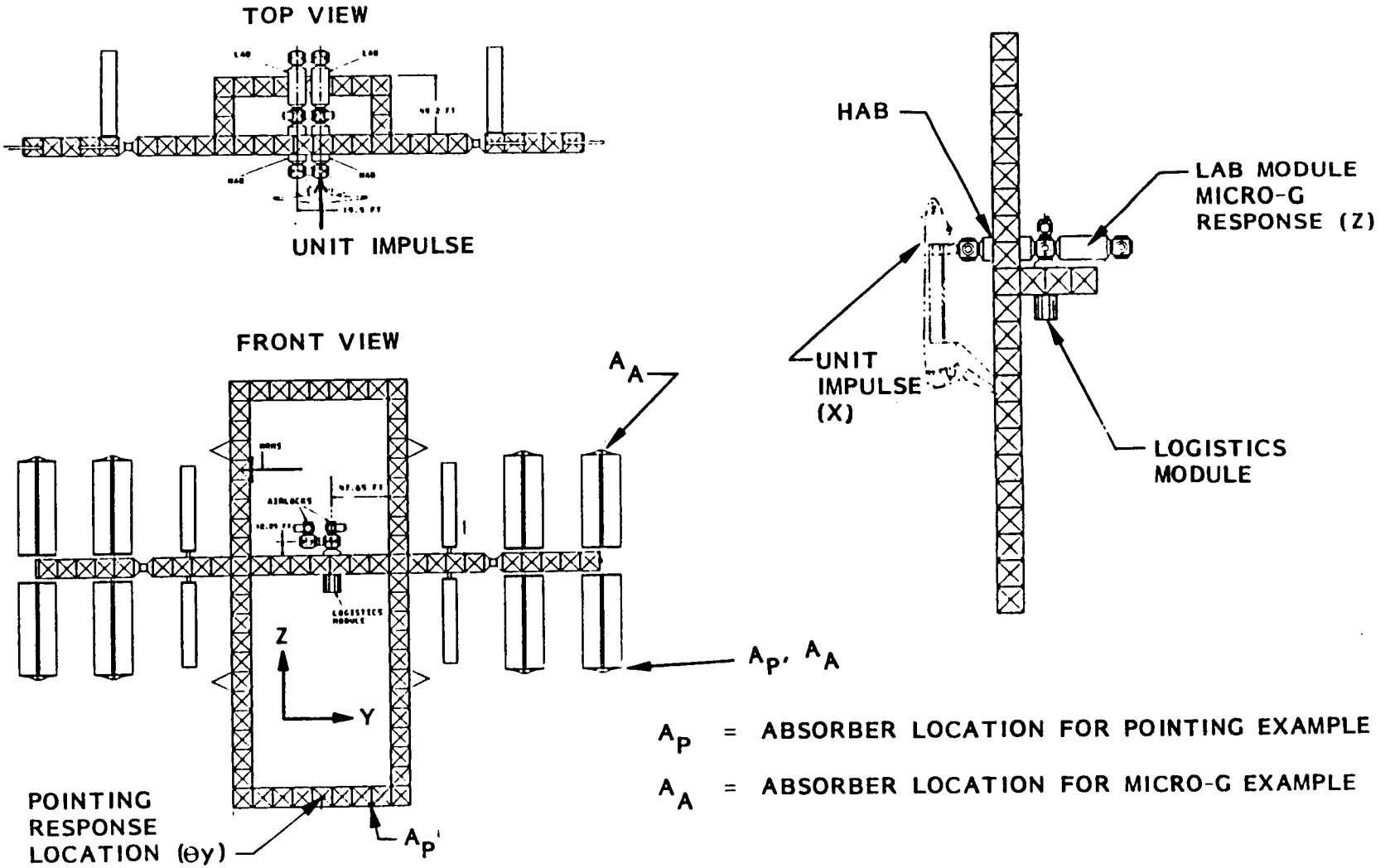

Figure 5-1b. Locations of Force Inputs, Responses, and Absorbers for IOC Dual Keel Example Analyses.

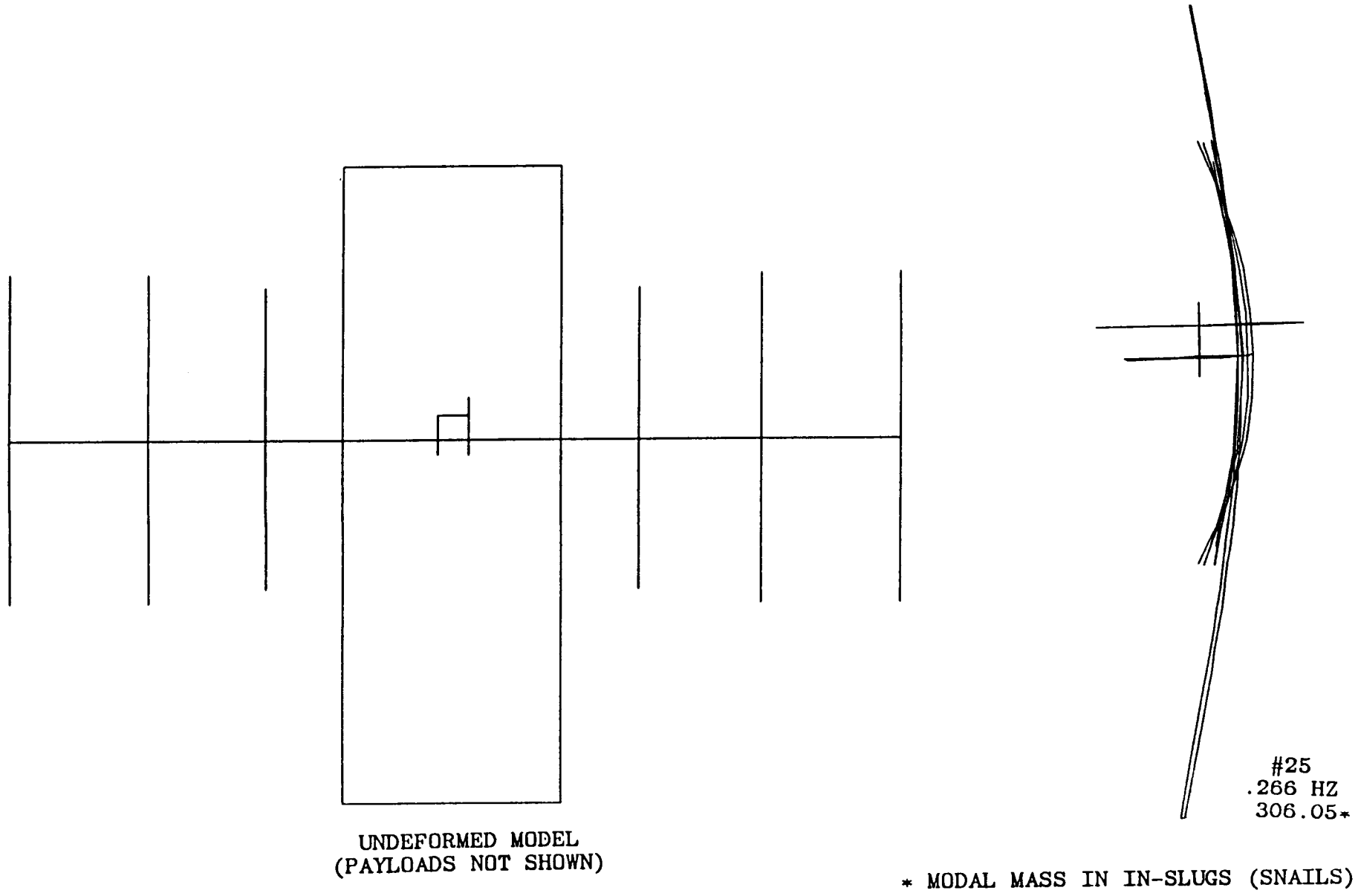

Figure 5-2a. Primary Structural Mode Shapes for IOC Dual Keel. The Frequency (Hz) and Modal Mass (in-slugs) are Indicated Below Each Mode.

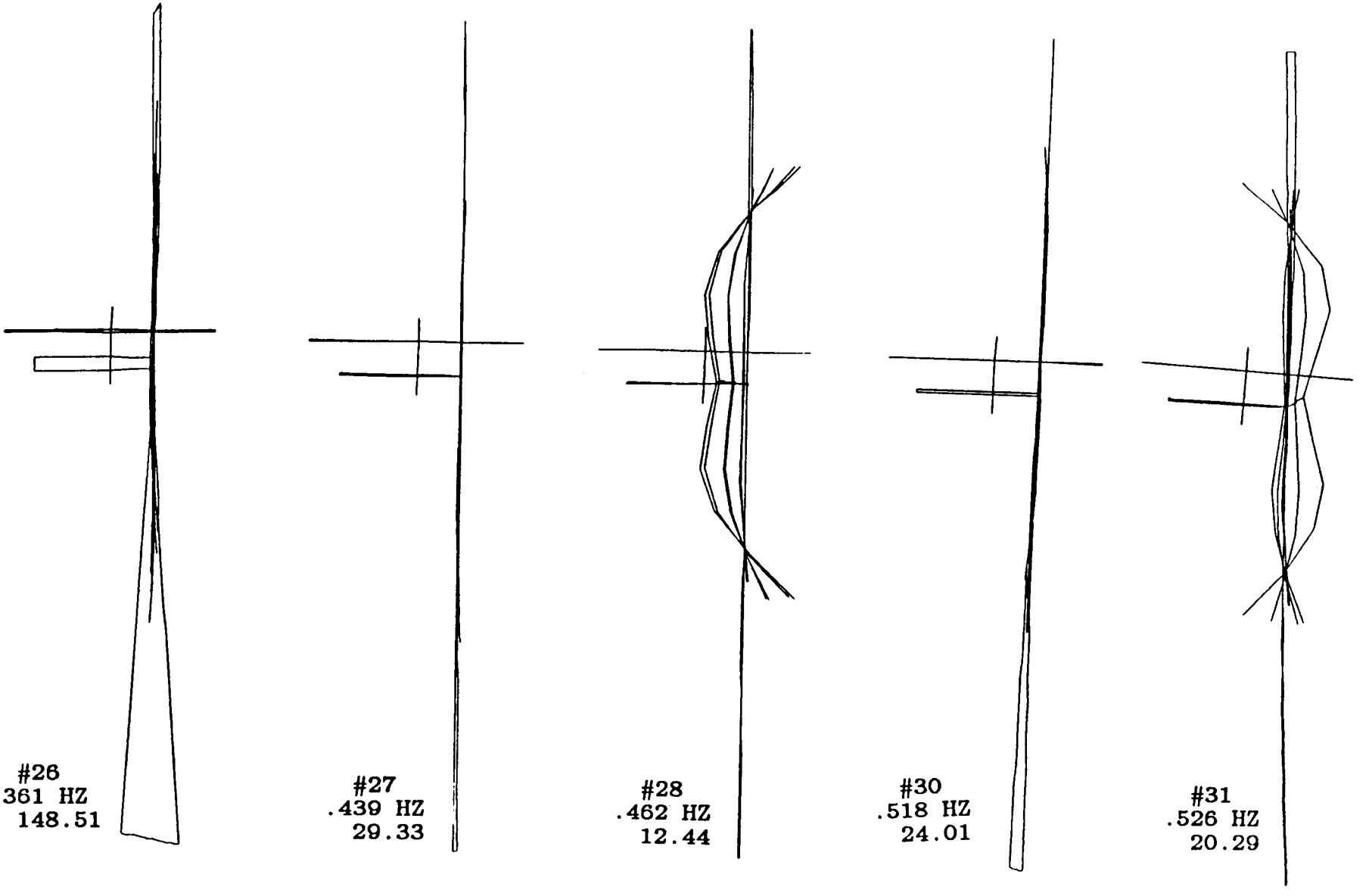

Figure 5-2b. Primary Structural Mode Shapes for IOC Dual Keel. Modes 27, 28 and 31 are In-Plane Modes. Note the Module "Rocking" in Mode 31.

TABLE 5.1. CHARACTERISTICS OF 5M DUAL KEEL FEM MODEL

WEIGHT (LBS): 675,791

INERTIAS (SLUG-FT2):

IXX= 2.25E+08

IYY= 6.82E+07

IZZ= 1.74E+08

5M ERECTABLE TRUSS

EI (LB-IN2): 5.0E+11

GJ (LB-IN2): 1.2E+11

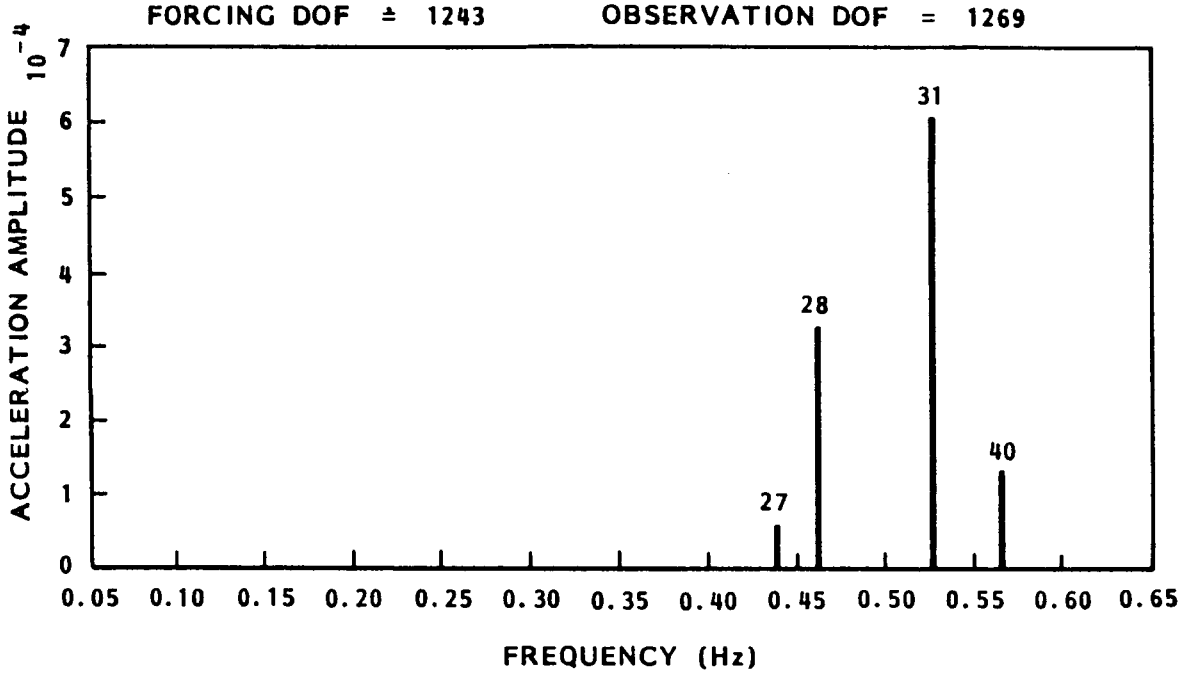

MODES INCLUDED:

MODE	FREQUENCY (Hz)
27	0.4387
28	0.4618
29	0.5052
30	0.5175
31	0.5263
40	0.5656

Figure 5-3. Spectral Composition of Lab Module Z-acceleration Impulse Response.

The techniques described in Sec. 3.7 are employed to examine the degree of coupling introduced through the absorbers for the acceleration response problem. The β_{eff} matrix exhibits a high degree of spatial coupling, as indicated by the relative magnitudes between the diagonal and non-diagonal elements, Fig. 5-4a. The net effect of the spatial and frequency coupling is depicted in Fig. 5-4c, in which the off-diagonal elements of β_{eff} are plotted against the modal frequency ratio. The placement of the plotted points for the acceleration response problem indicates that cross-coupling effects are strong.

5.2.1 Uncoupled Dynamic Optimization Results

For the uncoupled dynamic optimization, an absorber is tuned to each of the dominant modes, 28 and 31. The results of the mass optimization (Eqs. 3-37 through 3-40) are examined graphically in Fig. 5-5, in which the cost J (area under the acceleration response curve) is plotted as a function of the ratio of the absorber mass on mode 28 to the modal mass of mode 28. The optimal mass ratio for the absorber tuned to mode 28 is chosen at the minimum of the curve (Fig. 5-5). The remainder of the 386 lb mass budget is applied to the absorber tuned to mode 31. The two curves in Fig 5-5 illustrate the small error introduced when the area under the response curve is computed by summation of the areas under the individual modal responses, rather than computation of the area under the actual response (modes combined) curve. Both curves have a minimum at $\beta_1 \approx .03$, which agrees with the value obtained from numerical solution techniques (Eq. 3-39). The corresponding value of β_2, applied to mode 31, is 0.031.

Given the absorber mass ratios, the optimal absorber spring and damper constants are computed using the classical steady state tuning laws (Eqs. 3-4 through 3-5e). The computed parameters are listed in Table 5-2.

The acceleration response with the uncoupled dynamic optimization solution is shown in Fig. 5-6c. The response curve includes all the primary station modes listed in Fig. 5-3.

$$\beta_{eff} = \Phi^2 M_A \quad \text{WHERE } \Phi^T M \Phi = I.$$

● MICRO-G CASE

$$\beta_{eff} = \begin{bmatrix} 0.030 & 0.014 \\ 0.047 & 0.031 \end{bmatrix}$$

(a)

♦ POINTING CASE

$$\beta_{eff} = \begin{bmatrix} 0.019 & 0.014 \\ 0.0 & 0.005 \end{bmatrix}$$

(b)

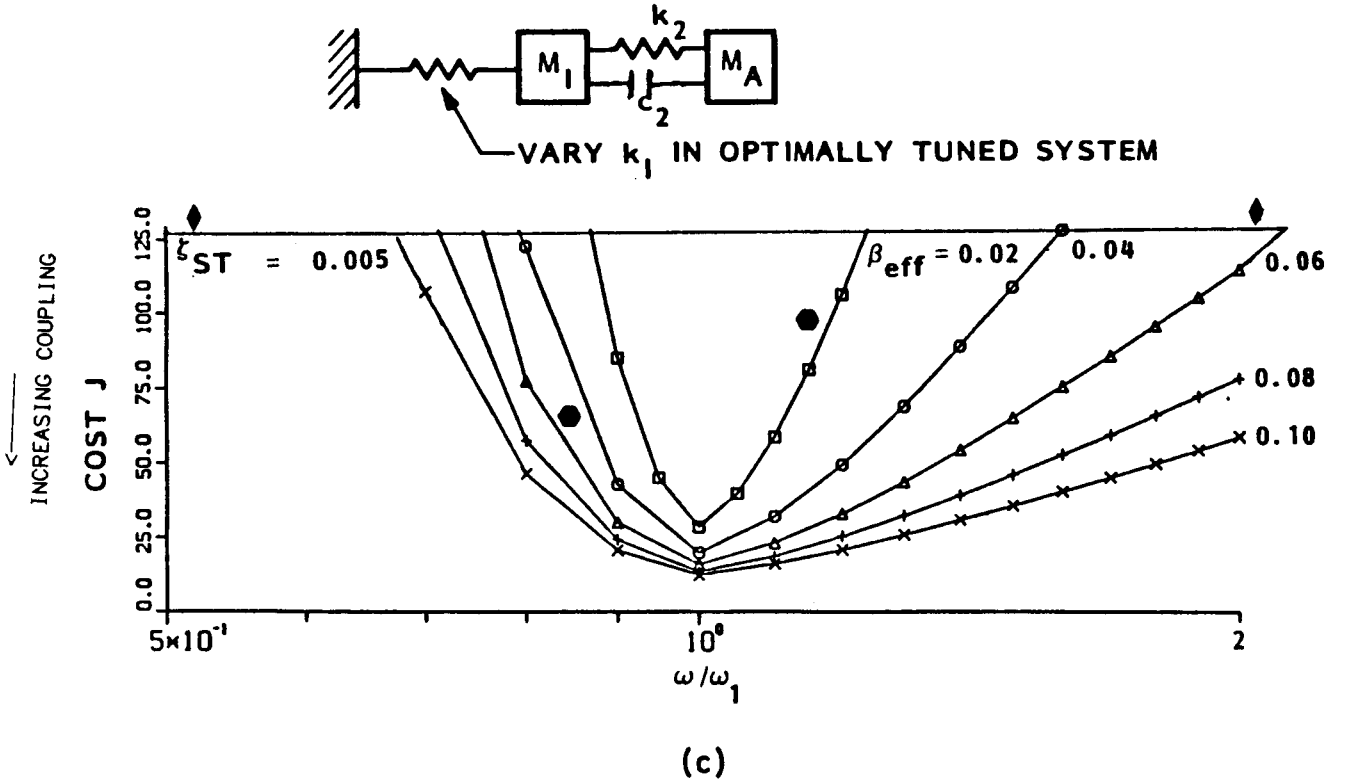

(c)

Figure 5-4. Characterization of Net Effect of Absorber Spatial and Frequency Coupling. The Values for the Pointing Case (Diamonds) are Greater Than 126.0 and are Thus Off the Cost Chart (Uncoupled). The Values for the Micro-Acceleration Case (Hexagons) Indicate a High Degree of Coupling.

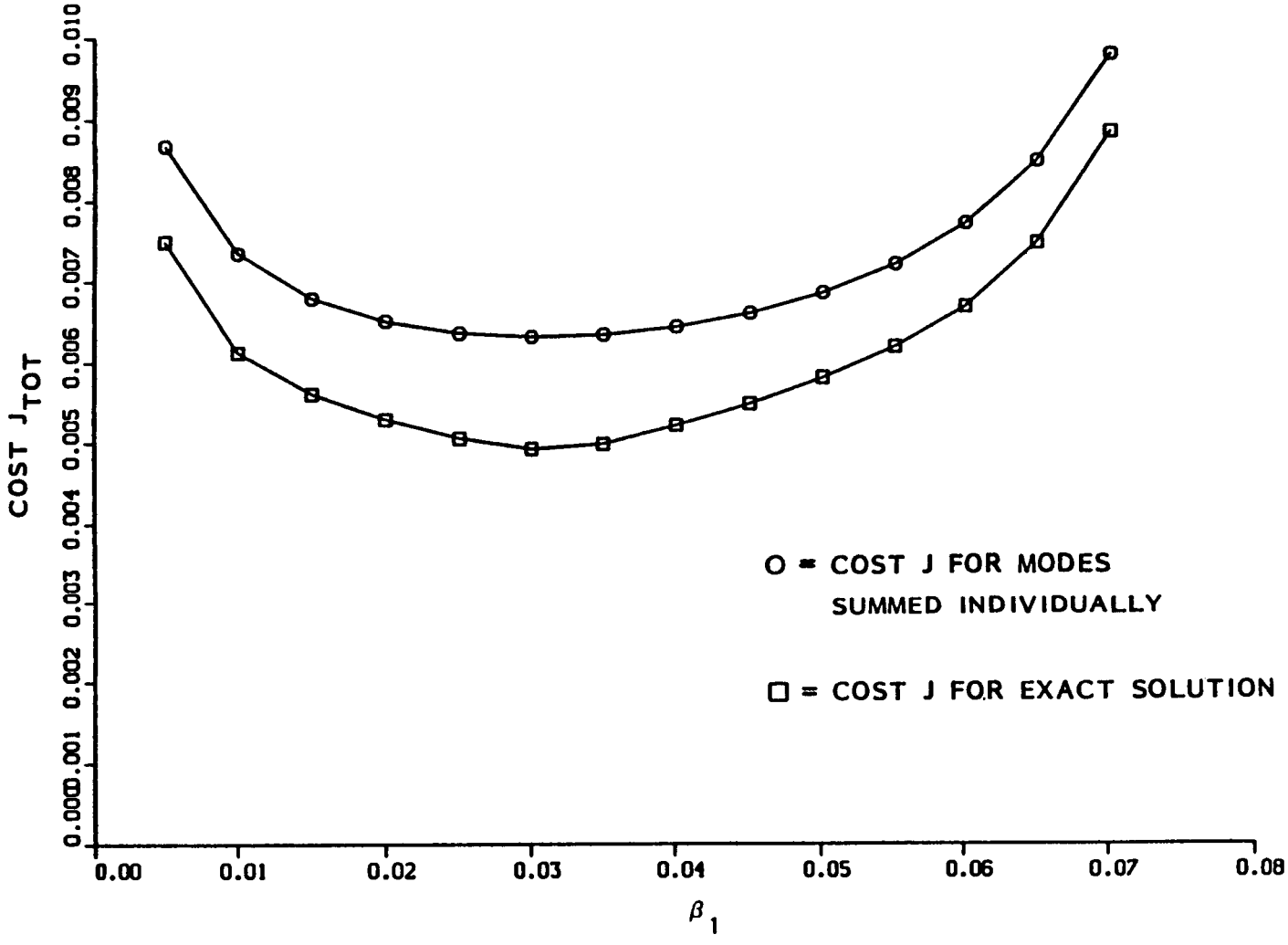

Figure 5-5. Area Under Total Acceleration Response Curve (Cost) Versus the Absorber Modal Mass Ratio for Absorber (1). The Balance of the Absorber Mass Budget is Used for Absorber (2).

ABSORBER	ALGORITHM	MASS (LBS)	SPRING CONSTANT (LB/IN)	DAMPER CONSTANT (LB/IN-SEC)
1	UNCOUPLED OPT.	145	2.98	0.225
	PARAMETER OPT.	145	0.411	0.00224
2	UNCOUPLED OPT.	241	6.43	0.431
	PARAMETER OPT.	241	5.01	1.019

Table 5-2. Absorber Parameters for Acceleration Response Problem.

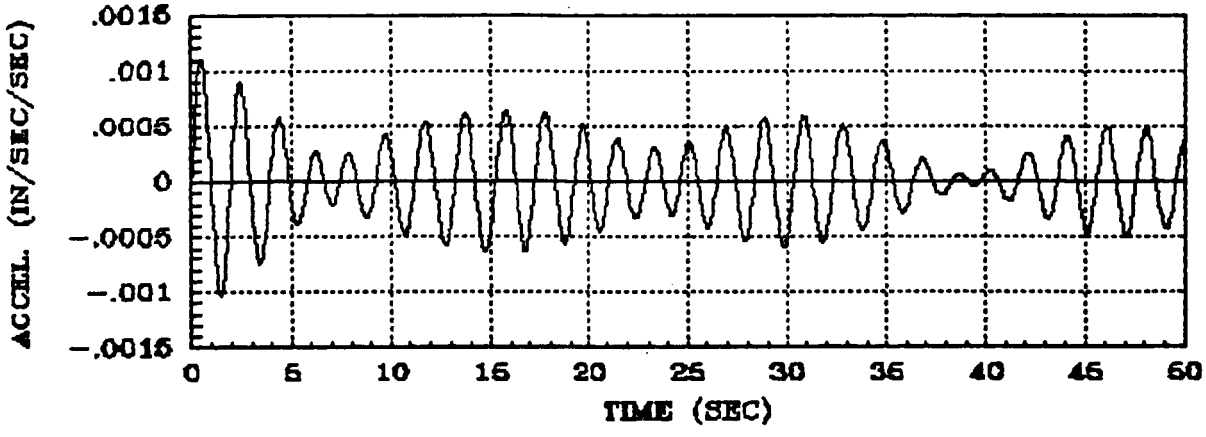

(a) OPEN LOOP RESPONSE

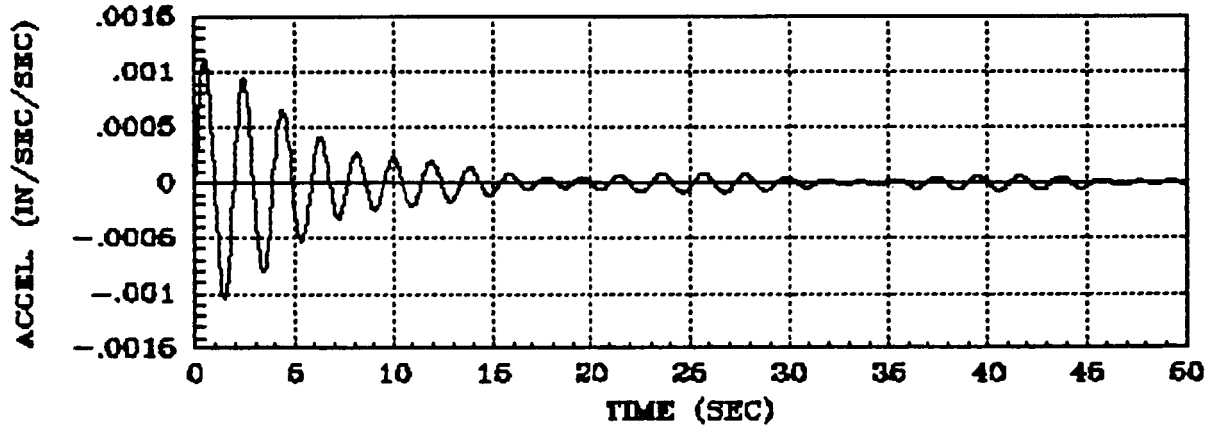

(b) PARAMETER OPTIMIZATION ALGORITHM SOLUTION

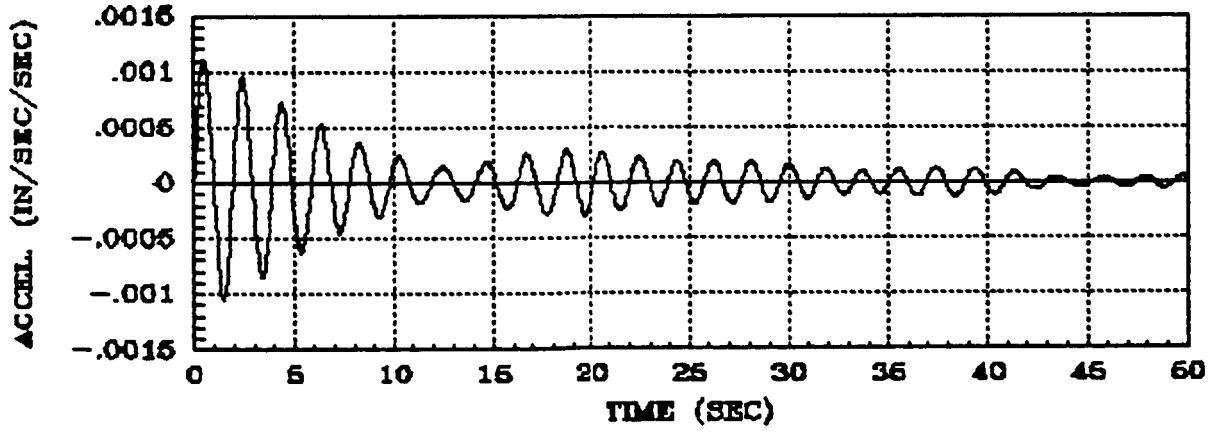

(c) UNCOUPLED DYNAMIC OPTIMIZATION SOLUTION

Figure 5-6. Transient Response For Lab Module Z-Acceleration.

5.2.2 Parameter Optimization Results

The parameter optimization algorithm is applied to a reduced order finite element model of the dual keel space station, which includes the primary vibration modes listed in Fig. 5-3. The cost weighting matrix (Eq. 4-13) penalizes the acceleration response only, in the lab module Z-direction. The dynamic optimization solution (Sec. 5.2.1) provides the absorber masses, and the initial guess for the absorber spring and damper constants.

The parameter optimization solution for the spring and damper constants is listed in Table 5-2. The closed loop frequencies and damping are depicted in Fig. 5-7, in which the frequency shift is highlighted through comparison with the open loop frequencies. The acceleration impulse response is plotted in Fig. 5-6b.

5.2.3 Acceleration Response Case - Discussion

The impulse response results obtained with the parameter optimization and uncoupled dynamic optimization solutions for absorber tuning show the significant amount of damping which can be introduced into the structure by tuned-mass dampers (Figs. 5-6b and c). Both solutions yield a good impulse transient response, although the parameter optimization solution offers a slightly better response than the uncoupled optimization solution.

The frequency content of the impulse responses, Figs. 5-6a, b, and c, is obtained with Fast Fourier Transform (FFT) techniques. The FFT of the impulse responses for the parameter and uncoupled optimization solutions is compared to the open loop response FFT in Fig. 5-8. Both solutions suppress the peak at 0.46 Hz. (near mode 28), but the uncoupled optimization introduces a significant peak near 0.5 Hz which yields a significant contribution to the impulse response.

The damping ratios for the parameter optimization solution are listed in Fig. 5-7, which also illustrates the frequency shift between the open and closed loop systems caused by the attachment

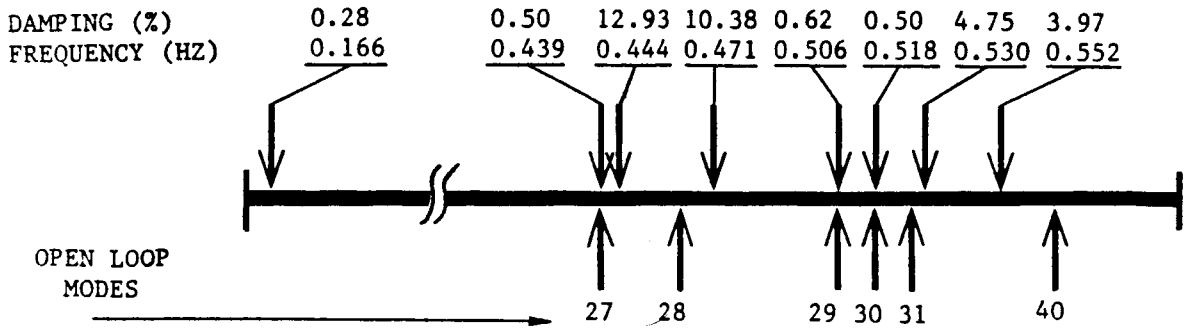

Figure 5-7. Damping Ratios and Closed Loop Frequencies for Parameter Optimization Solution.

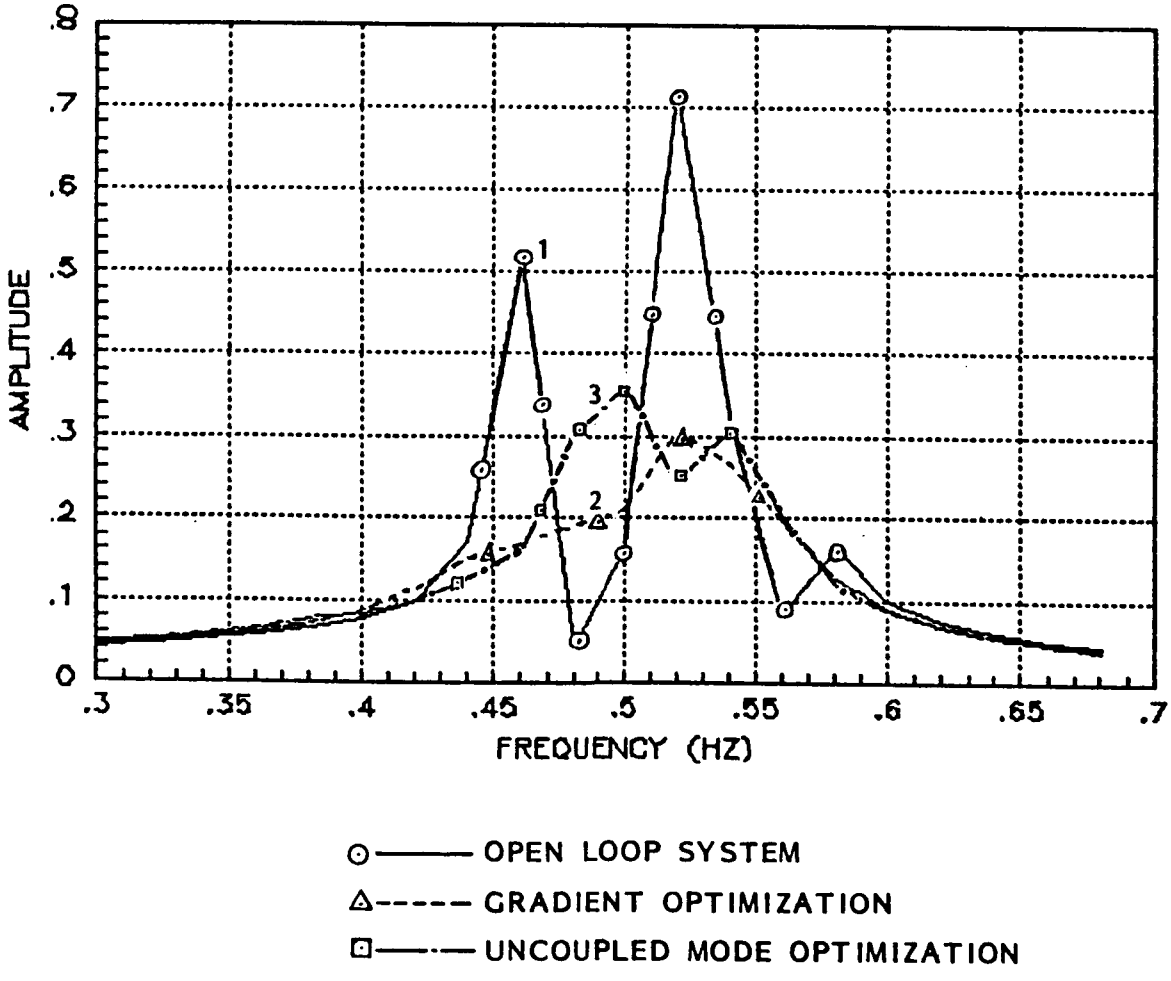

Figure 5-8. FFT of Transient Responses for Acceleration Response Problem.

of the absorbers. Approximately 10% damping is introduced near modes 27 and 28, and approximately 4% near modes 31 and 40.

An interesting feature shown in Fig. 5-7 is the relatively low closed loop frequency at 0.166 Hz, with 0.28% damping - which is less than the 0.5% inherent structural damping! Examination of the absorber parameters for the parameter optimization solution, Table 5-2, reveals that absorber 1 is tuned to very small spring and damper constants. Normally it is difficult to attribute closed loop frequencies to absorbers and structure specifically. However, in this case it is clear that the mode at 0.166 Hz is a direct result of absorber 1, due to the small spring constant which leads to low vibration frequency for the absorber, and the small damping constant.

The parameter optimization algorithm effectively tunes absorber 1 such that it does not affect the structure in the frequency domain of interest (i.e. modes 28 to 40). This behavior indicates possible interference between the absorbers which is allowed by the cross-coupling between absorber locations.

Since absorber 1 is detuned, its allocated mass is inactive. Therefore, it is reasonable to expect that better performance can be obtained by shifting the inactive mass to absorber 2 which provides all of the damping. However, additional test cases in which the mass distribution among the absorbers is varied do not lead to noticeable changes in the response, even when the total mass budget is allocated to absorber 2. A plausible interpretation of these results is that the total mass budget falls in a region where the performance cost is insensitive to total absorber mass. This idea is illustrated for a hypothetical problem in Fig. 5-9.

Further examination of the acceleration response problem with a reduced mass budget (77.2 lbs) verifies the aforementioned hypothesis. Variation of the performance index, J, with the mass distribution is shown in Fig. 5-10 for the reduced mass budget problem. The minimum cost is obtained when all of the mass budget is allocated to absorber 2. The parameter optimization algorithm detunes absorber 1 for mass distributions of approximately 30 to 65%. Since the mass of absorber 1 in that region is inactive, the

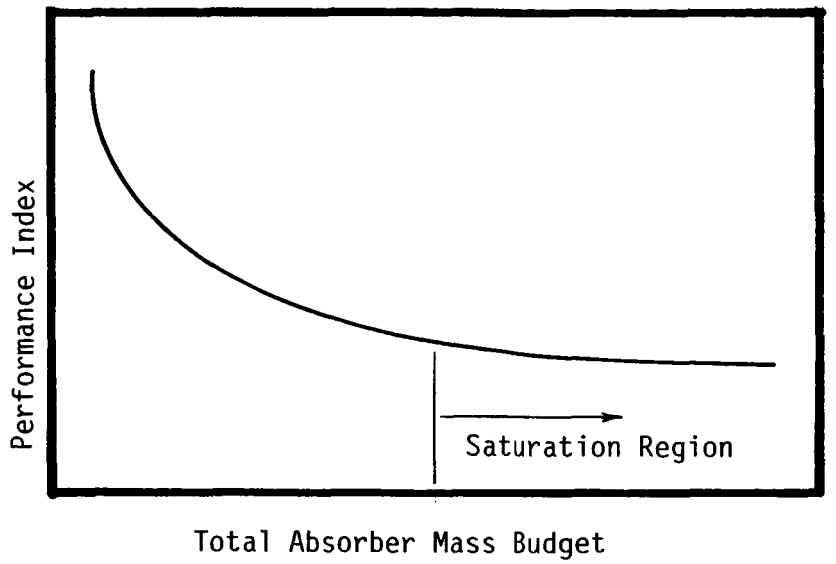

Figure 5-9. Hypothetical Curve of Performance Index vs. Total Absorber Mass Budget.

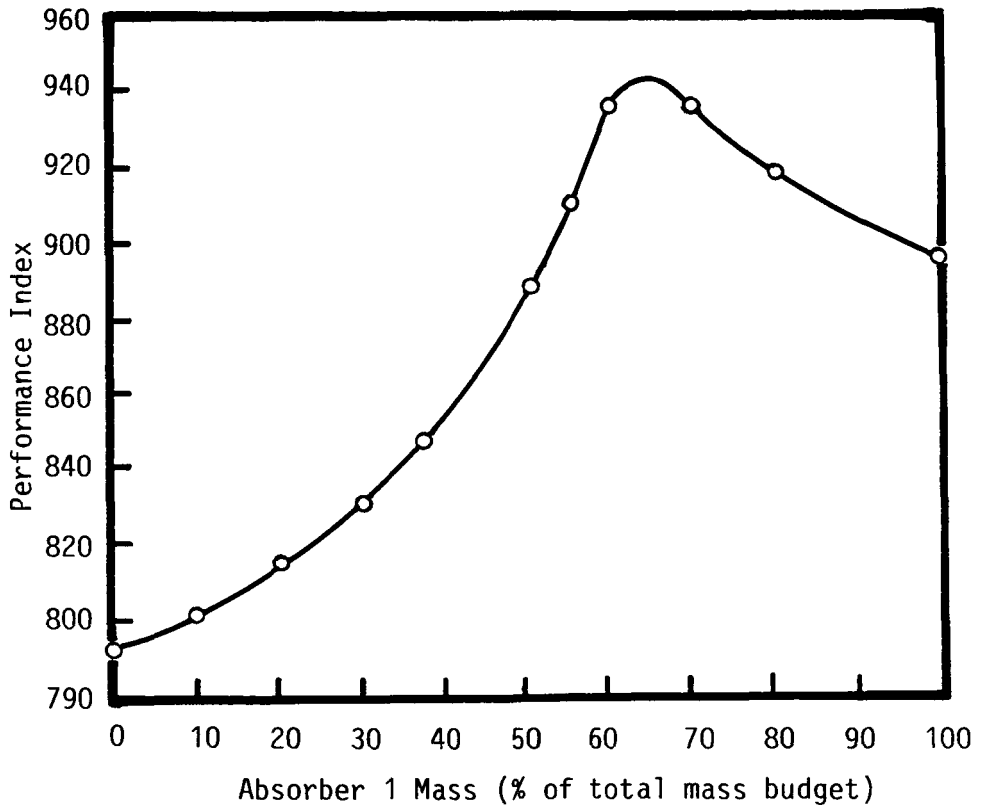

Figure 5-10. Performance Index vs. Absorber Mass Distribution; Acceleration Response Problem With Reduced Mass Budget.

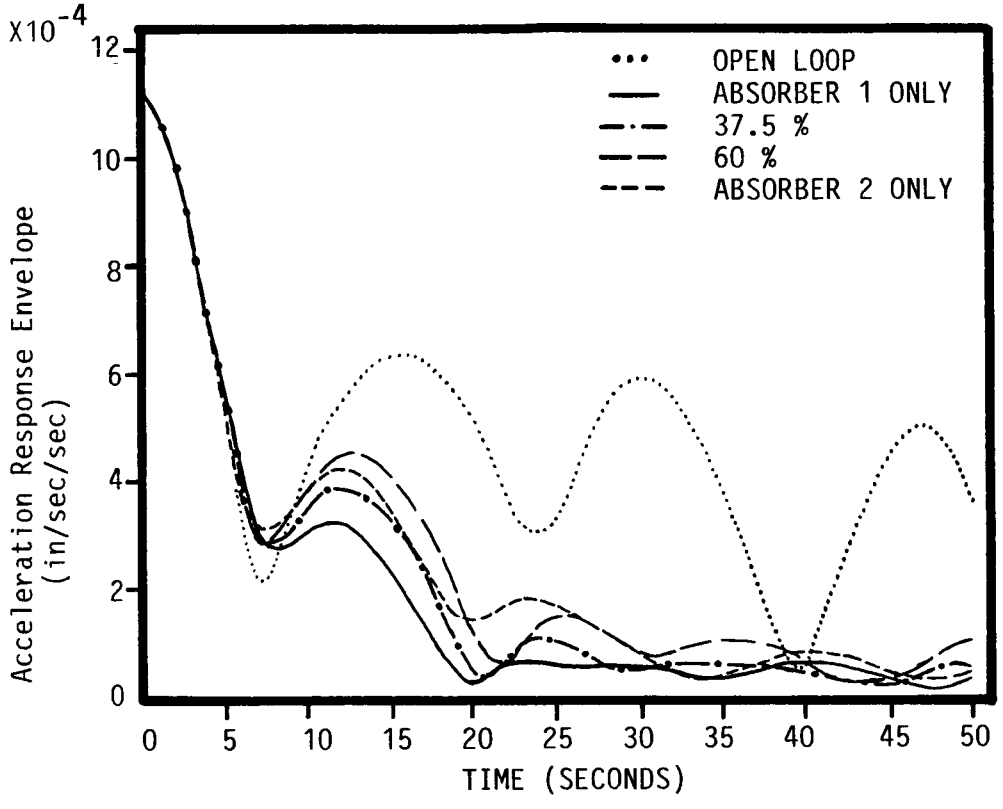

Figure 5-11. Transient Response Comparison for Variations in Absorber Mass Distribution.

cost curve shows the sensitivity of performance cost to the equivalent total absorber mass.

As the mass of absorber 1 increased to values greater than 65% of the total mass budget, the absorber becomes more important and absorber 2 is now gradually detuned. The performance cost decreases as absorber 1 takes control, and absorber 2 becomes ineffective. The performance cost of absorber 1 alone (at 100% in Fig 5-10) is greater than the performance cost of absorber 2 alone (at 0% in Fig 5-10) because of the different locations of the absorbers.

The envelopes of the response curves for the cases of 0, 37, 60, and 100% mass for absorber 1 are compared in Fig. 5-11 for physical evaluation of the performance cost differences depicted in Fig 5-10.

5.3 Payload Pointing Problem

Payloads and experiments mounted on the upper and lower booms may have stringent pointing requirements. To study the application of absorbers to pointing problems involving primary structural modes, the pitch rotation (rotation about the Y-axis) near the center of the Earth-pointing payload boom (Fig. 5-1b) is chosen as an example. Due to the large modal masses of the major system modes, a total absorber mass budget of 6 snails (2316 lbs.) is assumed.

The spectral composition of the pitch response is shown in Fig. 5-12. The corresponding open loop impulse response is shown in Fig. 5-13a. The most significant contribution to the response is by mode 25 at 0.2661 Hz. The next most significant mode is 31 with an amplitude of 28% of that of mode 25.

The absorbers are placed at the maxima modes 25 and 31, Fig. 5-1b. Examination of the β_{eff} matrix, Fig. 5-4b, for the chosen absorber locations, reveals moderate spatial coupling. However, a plot of the values of the off-diagonal terms of β_{eff}, Fig. 5-4c, indicates that the frequencies are far enough apart to provide a net coupling effect which is negligible (none of the points fit on

the chart). Therefore, the pointing problem under analysis is a good example of an uncoupled case.

5.3.1 Uncoupled Dynamic Optimization Results

For the uncoupled dynamic optimization, an absorber is tuned to each of modes 25 and 31. Fig. 5-14 is a graphical representation of the optimization defined by Eq. 3-37 through 3-40, in which the cost J is plotted as a function of the mass ratio of the absorber on mode 25. The remainder of the absorber mass budget is applied to the absorber on mode 31. The error introduced by summation of the areas under the separate modal responses is small. The mininmum cost occurs at $\beta_1 = 0.0193$, which correponds to $\beta_2 = 0.0045$.

Given the absorber mass ratios, the spring and damper constants are computed using the classical steady state tuning laws. The results are listed in Table 5-3.

The pitch response caused by a unit impulse, with absorbers tuned by the uncoupled dynamic optimization solution, is shown in Fig. 5-13c. The response includes all the modes listed in Fig. 5-12.

5.3.2 Parameter Optimization Results

The parameter optimization algorithm is applied to the pitch response problem, with the same absorber mass distribution and locations as for the uncoupled dynamic optimization analysis. The absorber masses, spring constants, and damper constants for the parameter optimization solution are listed in Table 5-3. The closed loop frequencies and damping ratios are shown in Fig. 5-15. The corresponding transient response is shown in Fig. 5-13b.

5.3.3 Payload Pointing Problem - Discussion

The uncoupled dynamic optimization solution provides the best transient response, as evidenced by comparison of Figs. 5-13b and 5-13c. The parameter optimization algorithm tuned absorber 1 succesfully to the high mode (mode 31), but tuned absorber 2

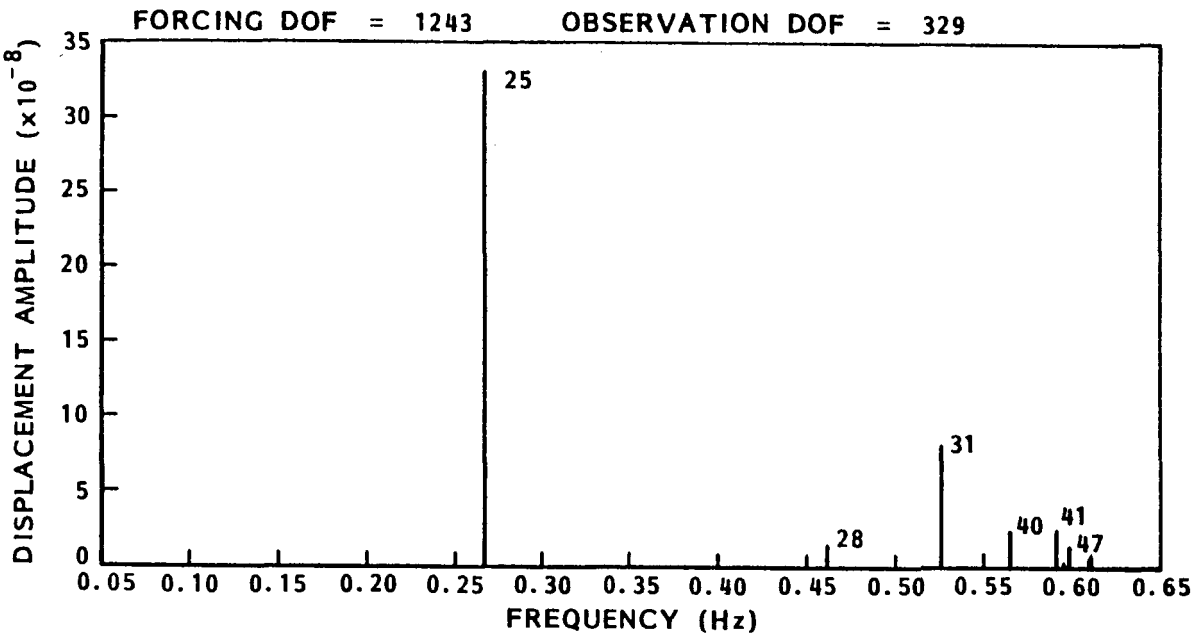

MODES INCLUDED:

MODE	FREQUENCY (Hz)
25	0.2661
28	0.4618
31	0.5263
40	0.5656
41	0.5916
47	0.5991

Figure 5-12. Spectral Composition of Impulse Response; Payload Pointing Problem.

ABSORBER	ALGORITHM	MASS (LBS)	SPRING CONSTANT (LB/IN)	DAMPER CONSTANT (LB/IN-SEC)
1	UNCOUPLED OPT.	2281	15.9	1.66
	PARAMETER OPT.	2281	14.1	3.98
2	UNCOUPLED OPT.	35	0.994	0.0251
	PARAMETER OPT.	35	1.08	0.0625

Table 5-3. Absorber Parameters for Payload Pointing Problem.

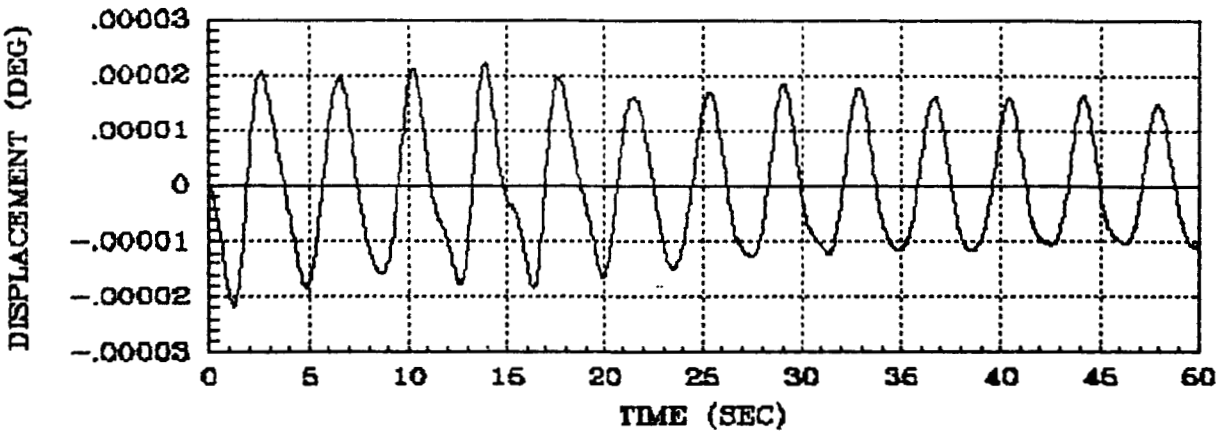

(a) OPEN LOOP RESPONSE

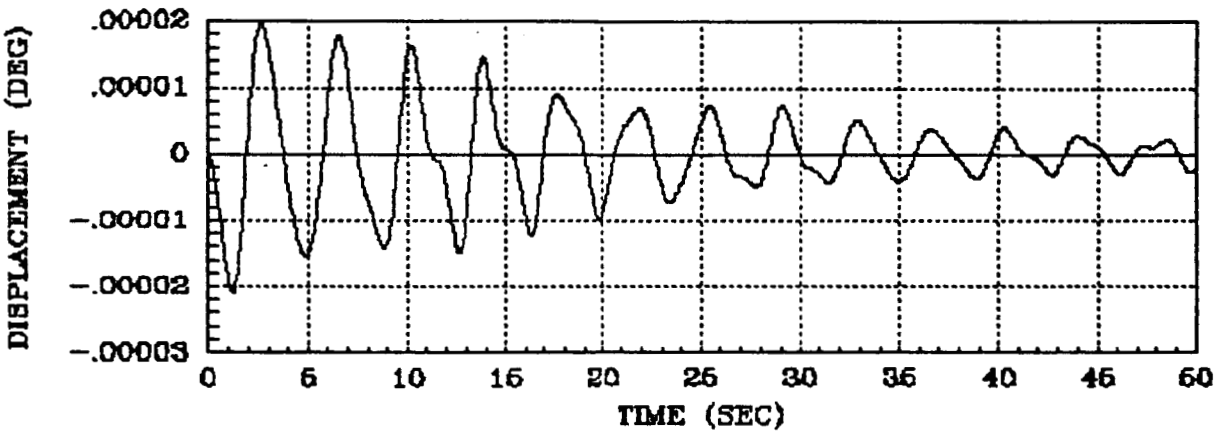

(b) PARAMETER OPTIMIZATION ALGORTIHM SOLUTION

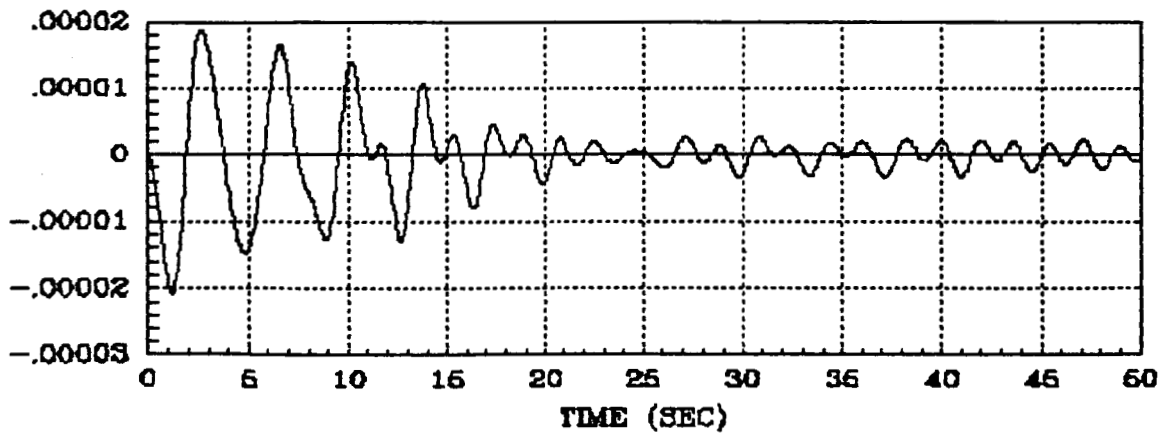

(c) UNCOUPLED DYNAMIC OPTIMIZATION SOLUTION

Figure 5-13. Transient Impulse Response; Payload Pointing Problem.

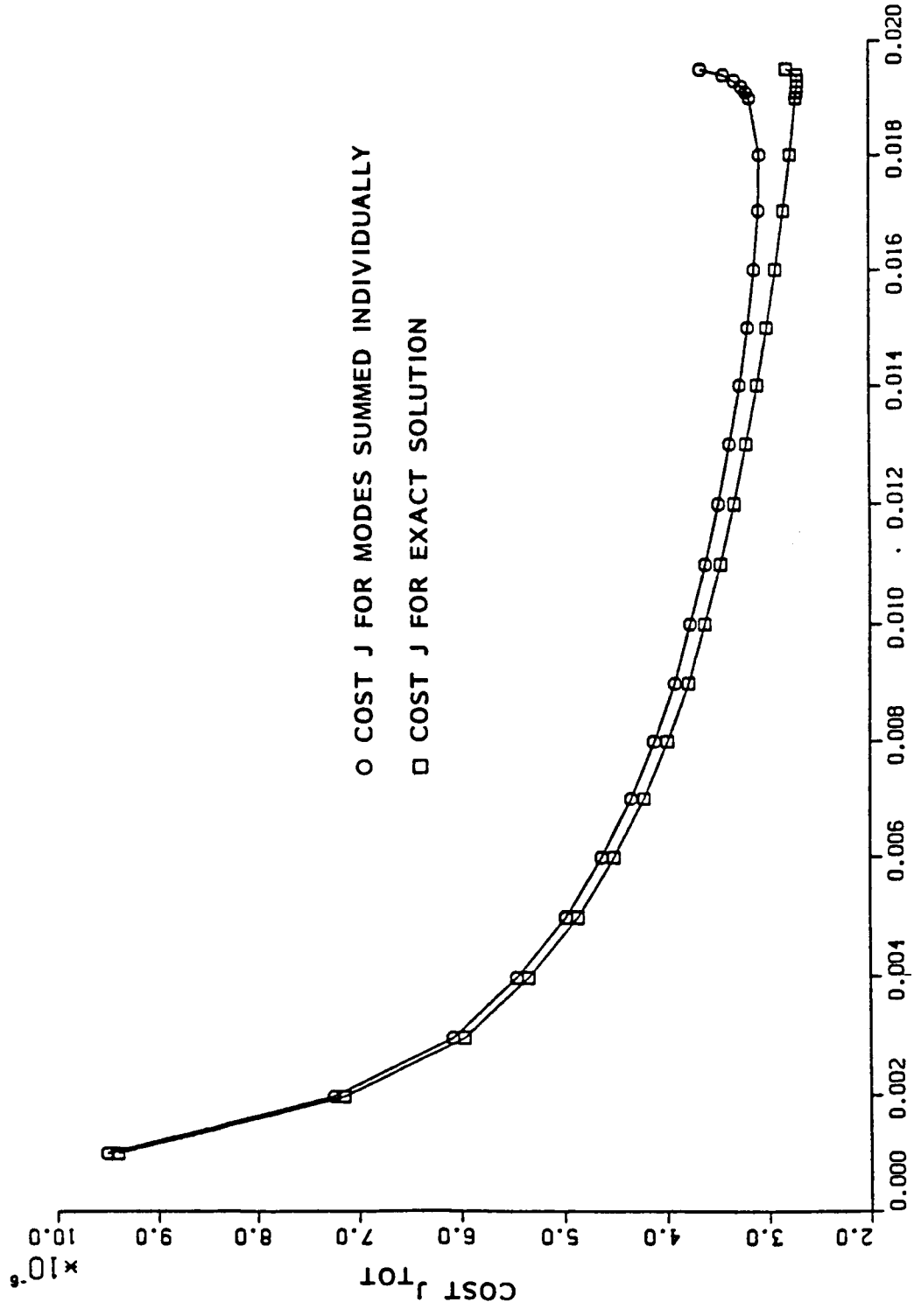

Figure 5-14. Area Under Total Displacement Response Curve (Cost) Versus the Absorber Modal Mass Ratio for Absorber (1). The Balance of the Absorber Mass Budget is Used for Absorber (2).

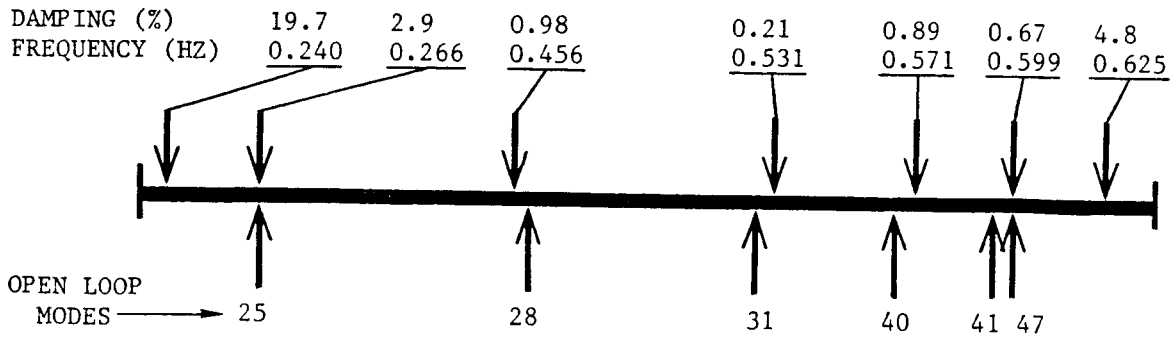

Figure 5-15. Damping Ratios and Closed Loop Frequencies for the Parameter Optimization Solution; Payload Pointing Problem.

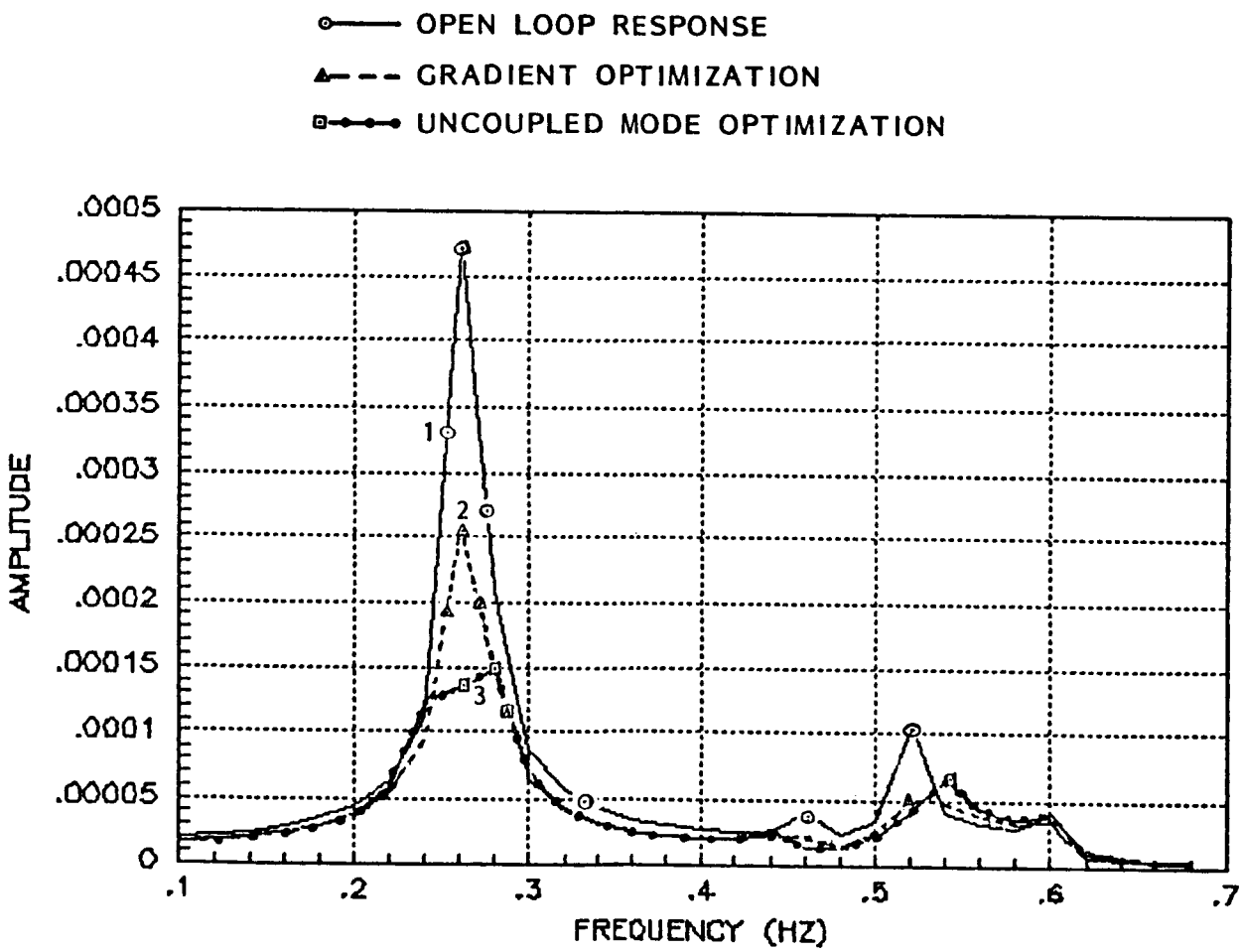

Figure 5-16. FFT of Transient Responses; Payload Pointing Problem.

between modes 25 and 31. Consenquently, the damping achieved in mode 25 is smaller than if the absorber was tuned to mode 25 alone, as was done for the uncoupled optimization solution.

Further examination of the behavior of the parameter optimization algorithm reveals that the contribution of the absorber initial conditions to the performance index, as discussed in Sec. 4.6.5, affects the location of the minimum. The cost, as defined by Eq. (4-32b), associated with the response of Fig. 5-13c is actually higher than the cost associated with the response associated with Fig. 5-13b, even though the former response is clearly better. However, comparison of the partial cost due to structure initial conditions only (the first term in Eq. 4-32b) is smaller for the response with the uncoupled optimization solution than for the response with the parameter optimization solution.

The frequency content and relative amplitudes for the responses of Figs. 5-13a, b, and c is presented in Fig. 5-16 for completeness.

5.4 Absorber Relative Motion

The optimization methods discussed and applied in the previous sections yield absorber masses, and spring and damper constants which reduce some response of a structure caused by an external disturbance. The practical application of the results will raise many hardware design problems, one of which is the absorber relative motion. Large displacements may be impractical, and small displacements and velocities may lead to 'binding' of the absorber.

Absorber displacements and velocities are presented in Figs. 5-17a and b for the tuned absorber of Sec. 5.2.2. The displacement and velocity scales correspond to an impulse of 1 lb-sec. Therefore, for a shuttle docking impulse of 500 lb-sec, a maximum displacement of 0.6 in, and maximum velocity of 1.65 in/sec are reached. For a crew motion disturbance of 25 lb-sec, the maximum displacement and velocity are 0.03 in. and 0.0825 in/sec. The maximum displacement and velocity values show that large relative

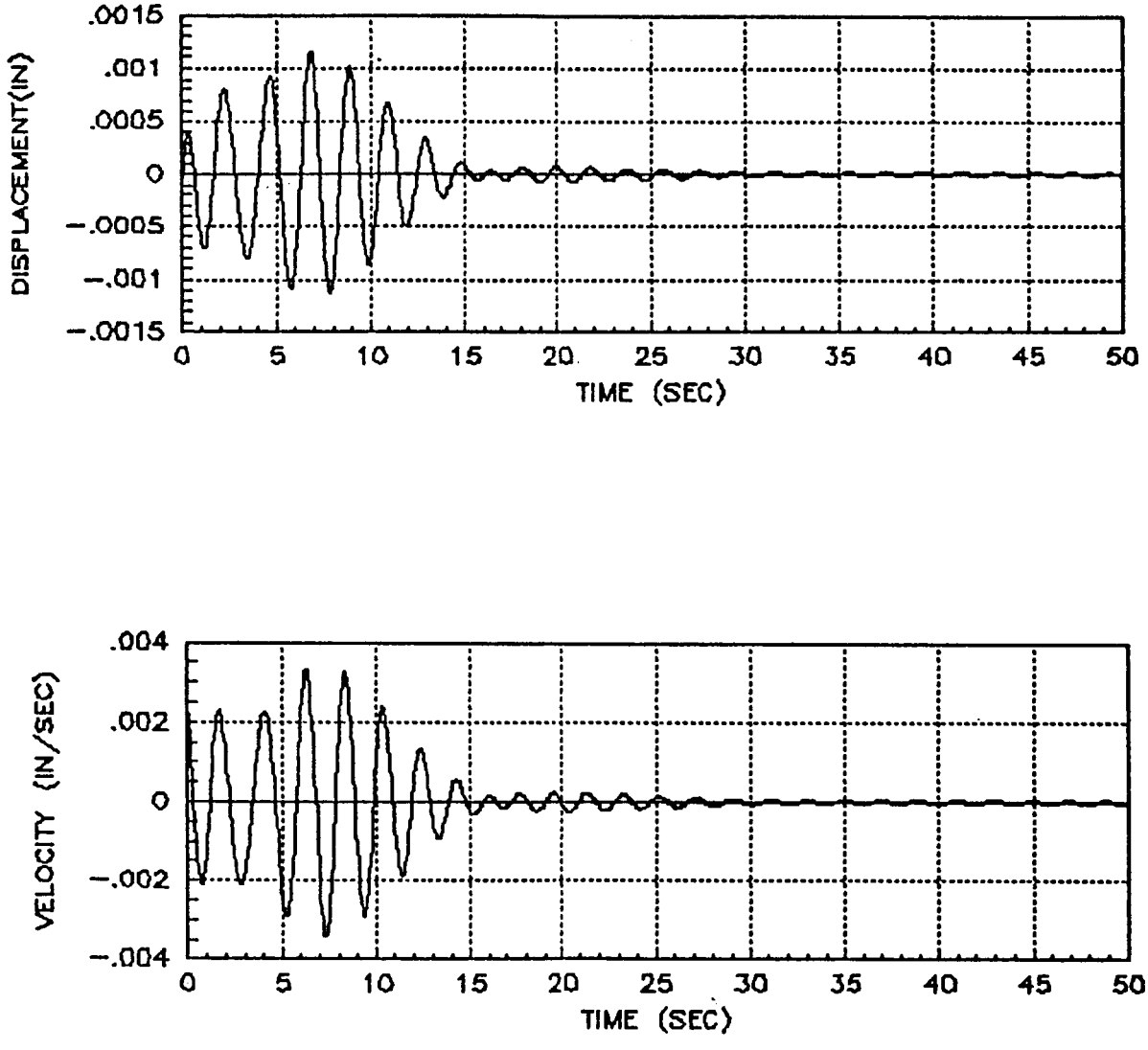

Figure 5-17. Absorber Relative Displacement and Velocity.

motions do not present a design problem, but absorber binding may occur at small displacements and velocities.

5.5 Space Station Applications Summary

The parameter optimization and uncoupled absorber optimization methods are applied to example vibration damping problems on the dual keel configuration space station. The example problems considered are (1) the acceleration response at the lab module, and (2) the pointing response at a location on the lower payload boom. A generic disturbance impulse is applied at the location of the shuttle berthing node. The impulse may simulate either shuttle docking, or crew motion, depending on its magnitude. Two absorbers are tuned to minimize the response in each case.

The parameter optimization and uncoupled optimization solutions both result in satisfactory responses for the acceleration response problem. A slightly better response is obtained with the parameter optimization solution, since cross-coupling effects are taken into account in the formulation of the optimization algorithm.

Examination of the results for the acceleration response reveals that that the total mass budget initially allocated for the two absorbers (386 lbs) falls in the saturation region of the cost vs. total absorber mass curve, i.e., small variations in the total mass budget do not detract from or improve the transient response significantly. Additional test cases with a reduced mass budget (77.2 lbs) demonstrate increased sensitivity of the performance cost to total mass budget.

Variation of the mass distribution among absorbers for both the high and low total mass budget cases shows that the parameter optimization algorithm actually tunes one of the absorbers so that it does not affect the structure in the frequency domain of interest. This is attributed to possible interference between the absorbers through cross-coupling. For the low mass budget problem, detuning switches from absorber 1 to absorber 2 as the mass of absorber 1 is increased.

The payload pointing response example offers a lightly coupled problem. The uncoupled dynamic optimization solution yields a better response than the parameter optimization solution. The parameter optimization solution is restrained by the formulation of the performance index, which penalizes structural excitation caused by disturbances transmitted through the absorbers. The algorithm effectively tunes an absorber away from parameters which would allow energy transmission throught the absorber at significant modes of the closed loop system. This behavior of the algorithm is an interesting topic for further study.

The absorber relative displacement and velocity are examined for the acceleration response case. Displacement and velocity magnitudes for shuttle docking or crew motion are not large, but may lead to absorber binding problems.

SECTION 6
DESIGN PROCEDURES

Design procedures are developed from the analysis and results of Sections 3, 4, and 5. The overall design process is considered and a design procedure is presented. A flow diagram of the design procedure is presented in Fig. 6-1. Each block of the diagram is briefly described in the following paragraphs.

The major focus of this report is the development of algorithms which compute the optimal absorber parameters for a multi-degree-of-freedom system with several absorbers attached. Additional design variables which are considered in the design are absorber locations and total absorber mass budget. Further design constraints result from hardware considerations. Although outside the scope of this report, the hardware design considerations are briefly discussed.

6.1 Vibration Problem Definition

The location and direction of the vibrations to be suppressed are identified. The 'local' vibration problem is influenced by disturbance sources and design requirements.

6.2 Critical Mode Selection

The natural modes of vibration which contribute to the response at the selected locations are identified for the chosen set of disturbance excitations. The relative amplitudes of the various modes in the total response dictate which modes are considered during absorber design.

6.3 Absorber Mass Budget Allocation

The major decision factor for the allocation of total absorber mass concerns the magnitudes of the modal masses corresponding to the modes of vibration to be damped. A mode with a large modal

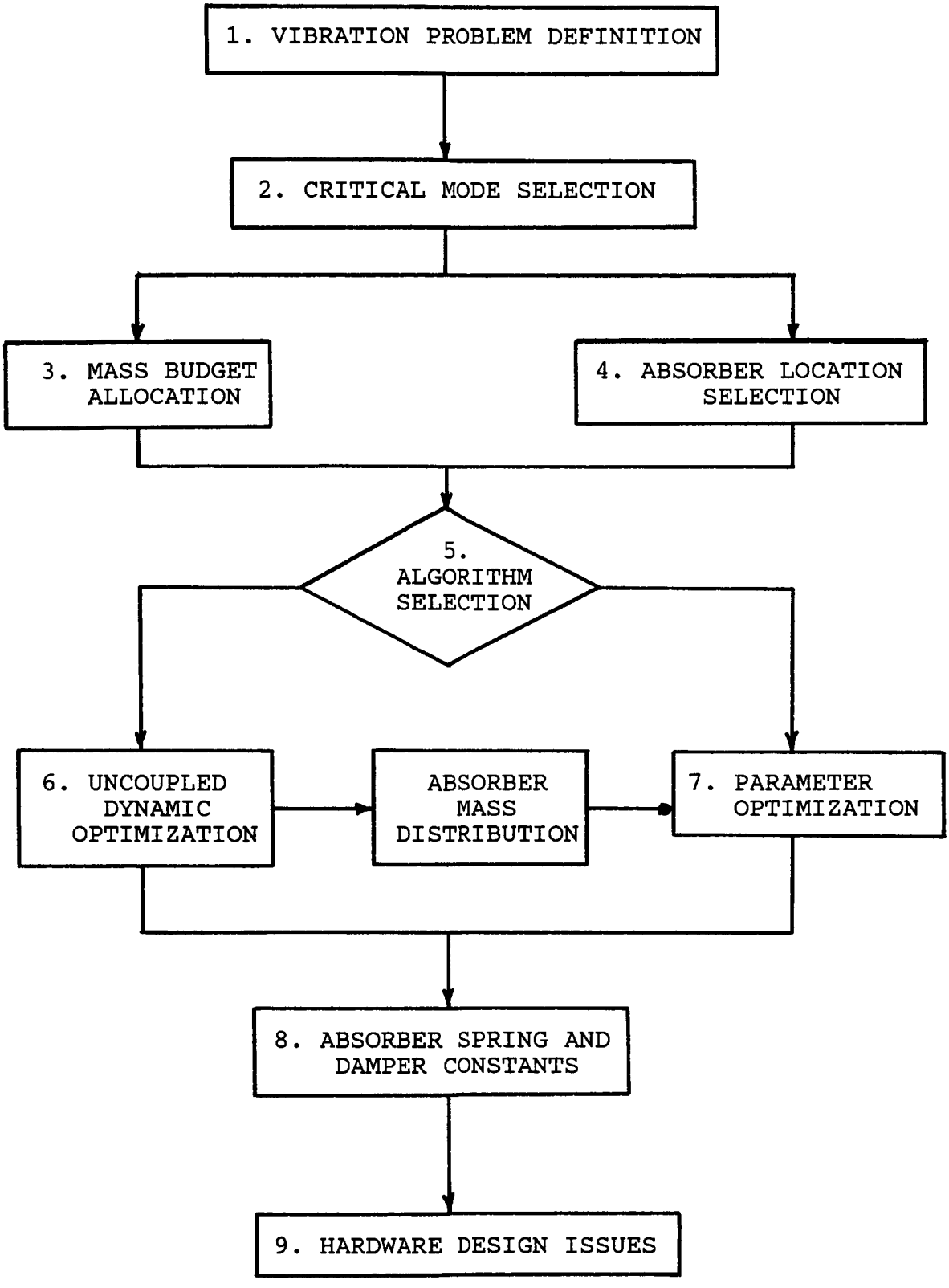

Figure 6-1. Absorber Design Procedure Block Diagram.

mass requires a corresponding larger absorber mass for effective damping than a mode with a smaller modal mass. The total mass budget must be large enough to allow reasonable absorber to modal mass ratios for all the absorbers and modes involved in the problem.

The choice of absorber to modal mass ratio must be sufficiently large to provide effective damping (for example, a 2% ratio provides satisfactory closed loop response for the simple 2-DOF system, Sec. 3.3.3). On the opposite end of the scale, the total absorber mass may be too large. In this case the quality of the closed loop response is insensitive to changes in absorber mass, and a smaller mass can be used (Sec 5.2).

6.4 Absorber Locations

The choice of absorber locations, and the number of absorbers to be used must take into account the spatial coupling through absorber locations, and frequency coupling in the vibration problem. Some rules are:

(1) Place absorbers at a location of maximum amplitude of the mode shape, so that a maximum absorber mass to modal mass ratio is achieved. If absorbers are placed at a location other than the maximum, Eq. (3-26) can be used to compute the additional mass required to achieve the same mass ratio.

(2) When significant absorber coupling (i.e., both spatial and frequency) exists, use one absorber to damp the set of modes coupled by the absorber. Addition of another absorber may cause interference which degrades the response.

6.5 Algorithm Selection

The algorithm selection is influenced by the spatial and frequency coupling through the absorbers. The uncoupled dynamic optimization offers superior results for lightly coupled problems,

and the parameter optimization algorithm yields superior results for strongly coupled problems.

6.6 Uncoupled Dynamic Optimization Algorithm

The uncoupled dynamic optimization algorithm is described in Sec. 3.6. Given absorber locations, the algorithm yields the optimal mass distribution among the absorbers, under the assumption that no spatial coupling is introduced through the absorbers (Sec 4.7). Spring and damper constants for each absorber are computed with the classical tuning laws for a 2-DOF system (Sec 3.2).

6.7 Parameter Optimization Algorithm

The parameter optimization algorithm (Sec 4.6) employs a gradient search method (Quasi-Newton) to find optimal values for the absorber spring and damper constants. The algorithm requires that mass distribution among the absorbers be specified. The initial guess for spring and damper constants may be obtained from the results of the uncoupled dynamic optimization algorithm, or the classical tuning laws for a specified absorber mass distribution.

The optimal mass distribution of the uncoupled dynamic algorithm may also be used, but as demonstrated in Section 5.2 it is not necessarily the best distribution for a strongly coupled problem.

6.8 Absorber Spring and Damper Constants

The output parameters of the design procedure are the absorber spring constants and damper strengths.

6.9 Hardware Design Issues

The final step of the design procedure is shown in Figure 6-1. The consideration of the hardware design issues associated with construction of an absorber with the chosen optimal parameters for

k, c, m; the physical design of the absorber spring and damping elements, is outside of the scope of this study. However, some observations are noted here: Vibration absorbers can add passive damping to a structure through a variety of mechanisms including constrained layer treatments, friction devices, discrete viscous dampers, electromagnetic devices, and fluidic devices. The composite system of the spring and damper should have a net stiffness of k and a net damper strength of c. Ideally, these values would remain constant over the frequency, temperature, load, displacement, and velocity ranges of the operational plant structure.

Two conceptual design examples are shown in Figure 6-2 . Figure 6-2a depicts a large stroke, low frequency design which contains a viscoelastic damping material sandwiched between two plates. Figure 6-2b depicts a small displacement design where the tuning mass is supported only by the viscoelastic material. In this case, the viscoelastic material has both the proper stiffness, k and damping strength, c.

Depending on the requirements of a specific application, the design of the absorber may become highly constrained by hardware issues. For example, viscoelastic materials typically have a loss factor (damping strength) that depends on temperature and frequency. For space applications, there are outgassing problems. For low-stroke applications requiring a very low value of c, the response of devices with moving parts may be dominated by friction and/or stiction effects. A low modal mass, low frequency application may dictate a spring stiffness which is too small to fabricate. Other applications may require stroke lengths that exceed the strain limit for the spring material. A trade study of the various design options available must be conducted in light of the requirements of a specific application. Fortunately, the results of previous sections of this report indicate that near-optimal absorber performance can be obtained in the presence of small variations in the spring stiffness, and even larger variations in the damper strength, especially for larger modal mass ratios.

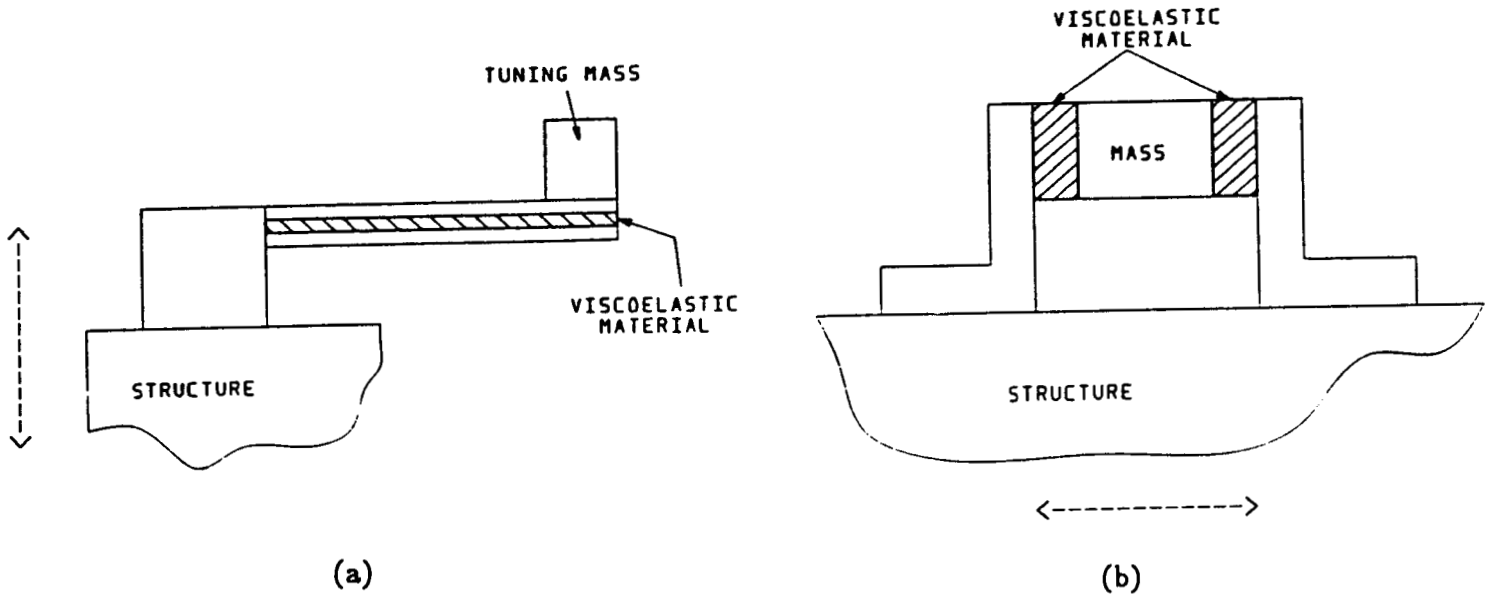

Figure 6-2. Absorber Conceptual Design Examples. Arrows Indicate Direction of Base Motion.

For Space Station applications, the dynamics and the low strain energy involved dictate a low frequency, low stroke, space-qualified design. A possible choice would be a magnetic device with no moving parts. Existing non-structural mass (i.e., the resource modules) on the Space Station could be used to reduce the mass penalty. Ideally, the few absorbers required would be designed with variable stiffness and damping elements so as to permit optimal performance over a range of Space Station dynamic characteristics (i.e., mode shapes) which vary with the distribution of mass during the buildup to a Growth Station.

6.10 Remarks

The design procedure described in the previous paragraphs is an iterative process formulated to interpret insight and visibility into an essentially nonlinear process. The decomposition of the process into several distinct stages allows the application of linear analysis; however, the construction of the design procedure highlights a number of topics which require further investigation. Among these are: the optimization of the number and locations of the absorbers, the incorporation of the absorber masses in the parameter optimization algorithm, and the investigation of tradeoffs between structural mass and absorber mass as means of suppressing vibrations. Further development in these topics will contribute to the refinement of the design procedure.

SECTION 7

CONCLUDING REMARKS

The optimal tuning of multiple tuned-mass dampers for the transient vibration damping of large space structures is investigated. A multidisciplinary approach is used. Structural dynamic techniques are applied to gain physical insight into absorber/structure interaction and to optimize specific cases. Modern control theory and parameter optimization techniques are applied to the general optimization problem. A design procedure for multi-absorber multi-DOF vibration damping problems is presented.

The performance of vibration absorbers designed using classical and other tuning laws is compared using one-mode dynamic models. Based on these results, a performance criterion for the optimal tuning of vibration absorbers for transient response is developed. Classical dynamic models are extended to investigate the effects of absorber placement, existing structural damping, and absorber cross-coupling on the optimal design synthesis. An uncoupled dynamic optimization technique is developed which allocates the absorber mass budget over multiple absorbers.

The control design process for the general optimization problem is formulated as a linear output feedback control problem via the development of a feedback control canonical form. The design variables are expressed as control gains, and the analytical techniques of feedback control theory, both classical and modern, are applied to absorber design. Although active control algorithms are used in the design process, the final remains passive; i.e., an active system is not being designed. The constrained nature of the feedback gain matrix makes the application of established output feedback solution methods difficult; therefore, a nonlinear parameter optimization method is developed and applied to an output feedback formulation of the vibration damping problem.

The complexity of the general optimization problem for multiple vibration absorbers on multi-DOF space structures requires its segmentation into smaller sub-problems. In the present design procedure, the choice of absorber mass, absorber locations, and absorber spring and damper constants are treated as sub-problems. The optimal absorber locations are found to be at the maxima of the eigenvectors of the modes which require damping. The total absorber mass budget is assumed to be constrained by mission requirements. System performance improves as the total absorber mass budget is increased until a saturation point where the addition of absorber mass provides little improvement in performance. Given the total absorber mass budget, the mass distribution among the absorbers is computed using the uncoupled dynamic optimization for cases which involve minimal absorber cross-coupling (i.e., each absorber affects only one mode and vice-versa). For highly coupled cases, trade studies are conducted. Finally, the optimal absorber spring and damper constraints are computed for uncoupled systems using classical tuning laws or computed for coupled systems by applying the parameter optimization algorithm.

The uncoupled dynamic optimization and more general parameter optimization algorithms are applied to two sample problems on the NASA dual keel space station. They are the damping of micro-accelerations in the lab module and the suppression of payload pointing vibrations at the lower boom. Damping levels in the range of 10% - 20% are achieved with two tuned-mass dampers. For these Space Station examples passive dampers increased the damping considerably. The absorber weight penalty associated with the increased damping could be reduced by using existing attached masses or payloads for absorbers.

The potential damping performance gains obtained through the use of tuned-mass dampers on lightly-damped structures merits the further study of the hardware issues associated with these devices. Further study is recommended to investigate the hardware issues and to construct and test hardware concepts. Other recommendations include the further development of constrained optimization techniques and the optimization of combined passive and active control for vibration suppression.

REFERENCES

1. Card, M.F., McComb, H.G., Peebles, S.W., "Preliminary Sizing of Vibration Absorber for Space Mast Structures", NASA TM-84488, May 1982.

2. Juang, J., "Optimal Design of a Passive Vibration Absorber for a Truss Beam", J. Guidance, Control and Dynamics, Nov.-Dec. 1984.

3. Miller, D.W., Crawley, E.F., and Ward, B.A., "Inertial Actuator Design for Maximum Passive and Active Energy Dissipation in Flexible Space Structures", AIAA 26th Structures, Structural Dynamics, and Materials Conference, Part 2, April 1985.

4. Miller, D.W., and Crawley, E.F., "Development of Finite Active Control Elements for Large Flexible Space Structures", M.I.T Space Systems Lab Report #6-85, June, 1985.

5. Rogers, L.C., "PACOSS Contract Status Review", briefing charts from review held at Martin Marietta in Denver, 10-11 April, 1985.

6. Von Flotow, A.H., "Control-Motivated Dynamic Tailoring of Truss-Work Structures", to be presented at the AIAA Guidance, Navigation and Control Conference, August 20-22, 1986.

7. Van de Vegte, J., and Hladun, A.R., "Design of Optimal Passive Beam Vibration Controls by Optimal Control Techniques", ASME J. of Dynamic Systems, Measurement, and Control, December, 1973.

8. Van de Vegte, J., "Optimal Dynamic Absorbers for Plate Vibration Control", ASME J. of Dynamic Systems, Measurements, and Control, December, 1975.

9. Van De Vegte, J. and De Silva, C., "Design of Passive Vibration Controls for Internally Damped Beams by Modal Control Techniques", J. of Sound and Vibrations 45, 1976.

10. Timoshenko, S., Young, D.J. and Weaver, W. Jr., "Vibrations Problems in Engineering", 4th Ed., John Wiley and Sons, New York, 1974.

11. Den Hartog, J.P., "Mechanical Vibrations", 3rd Ed., McGraw-Hill Book Co., New York, 1947.

12. Meirovitch, L., "Elements of Vibration Analysis", McGraw-Hill Book Co., New York, 1975.

13. Hutton, D.V., "Applied Mechanical Vibrations", McGraw-Hill Book Co., New York, 1981.

14. Tipler, P.A., "Physics" Vol. 1, Worth Publishers, Inc., New York, 1976.

15. Kwakernaak, H. and Sivan, R., Linear Optimal Control Systems, John Wiley & Sons, New York, c. 1972.

16. Kosut, R.L., "Suboptimal Control of Linear Time-Invariant Systems Subject to Control Structure Constraints," IEEE Trans. on Automatic Control, Vol. AC-15, No. 5, Oct 1970, pp 557-563.

17. Levine, W.S. and Athans, M., "On the Determination of the Optimal Constant Output Feedback Gains for Linear Multivariable Systems," IEEE Trans. on Automatic Control, Vol. AC-15, No. 1, Feb 1970, pp 44-48.

18. Knapp, C.H. and Basuthakur, S., "On Optimal Output Feedback," IEEE Trans. On Automatic Control, Vol. AC-17, No. 6, Dec. 1972, pp. 823-825.

19. Dabke, R.P., "Suboptimal Linear Regulators with Incomplete State Feedback," IEEE Trans. on Automatic Control, Vol. AC-15, No. 1, Feb. 1970, pp. 120-121.

20. Hegg, D.R., "Extensions of Suboptimal Output Feedback Control with Application to Large Space Structures," J. of Guidance and Control, Vol. 4, No. 6, Nov.-Dec. 1981, pp. 637-641.

21. Vidyasagar, M. and El-Attar, R.A., "Optimal Output Feedback Gains for Linear Control Systems," 21st Symposium on Circuits and Systems, Aug. 14-15, 1978, Ames, Ia.

Standard Bibliographic Page

1. Report No.	2. Government Accession No.	3. Recipient's Catalog No.
NASA CR-4067		

4. Title and Subtitle	5. Report Date
Passive Stabilization for Large Space Systems	April 1987
	6. Performing Organization Code

7. Author(s)	8. Performing Organization Report No.
J. R. Sesak, M. J. Gronet, and G. M. Marinos	

9. Performing Organization Name and Address	10. Work Unit No.
Lockheed Missiles & Space Company, Inc. 1111 Lockheed Way Sunnyvale, CA 94086	11. Contract or Grant No. NAS1-17660
	13. Type of Report and Period Covered
12. Sponsoring Agency Name and Address	
National Aeronautics and Space Administration Washington, DC 20546-0001	Contractor Report
	14. Sponsoring Agency Code 506-43-41-02

15. Supplementary Notes

Langley Technical Monitor: Harold G. Bush
Task Report: Task Assignment No. 4
J.R. Sesak, Program Mgr; M.J. Gronet, Dynamic Analysis;
G.M. Marinos, Control Analysis

16. Abstract

The optimal tuning of multiple tuned-mass dampers for the transient vibration damping of large space structures is investigated. A multi-disciplinary approach is used. Structural dynamic techniques are applied to gain physical insight into absorber/structure interaction and to optimize specific cases. Modern control theory and parameter optimization techniques are applied to the general optimization problem. A design procedure for multi-absorber multi-DOF vibration damping problems is presented.

Classical dynamic models are extended to investigate the effects of absorber placement, existing structural damping, and absorber cross-coupling on the optimal design synthesis. An uncoupled dynamic optimization technique is developed which allocates the absorber mass budget over multiple absorbers in order to optimally damp the transient response.

The control design process for the general optimization problem is formulated as a linear ouput feedback control problem via the development of a feedback control canonical form. The design variables are expressed as control gains, and the analytical techniques of feedback control theory, both classical and modern, are applied to absorber design. A nonlinear parameter optimization method is developed and applied to an output feedback formulation of the vibration damping problem.

The techniques are applied to sample micro-g and pointing problems on the NASA dual keel space station. Damping levels in the range of 10 - 20% are achieved with two tuned-mass dampers. The potential damping performance gains obtained through the use of tuned-mass dampers on lightly-damped structures merits the further study of the hardware issues associated with these devices.

17. Key Words (Selected by Author(s))	18. Distribution Statement
Passive Damping, Discrete Dampers, Optimal Control, Gradient, Optimization, Large Space Systems, Space Station Vibration Absorbers	Unclassified - Unlimited, Subject Category 39

19. Security Classif. (of this report)	20. Security Classif. (of this page)	21. No. of Pages	22. Price
Unclassified	Unclassified	140	A07

For sale by the National Technical Information Service, Springfield, Virginia 22161

NASA-Langley, 1987